ALMA MATER STUDIORUM · UNIVERSITY OF BOLOGNA

School of Science
Department of Physics and Astronomy
Master Degree in Physics

QUANTUM SIMULATION OF NON-ABELIAN LATTICE GAUGE THEORIES

Supervisor:
Prof. Elisa Ercolessi

Submitted by:
Matteo Bergonzoni

Academic Year 2022/2023

Abstract

Lattice gauge theories are powerful tools to describe nature and its interactions, finding applications from the theory of Standard Model to condensed matter physics, but there are still many unresolved issues. The recent development of quantum technologies opens the door to new techniques, such as quantum simulation and quantum computation, which can overcome these difficulties and expand our knowledge of these models. There have already been many studies on Abelian lattice gauge theories, but in this thesis we develop an algorithm to investigate non-Abelian lattice gauge theories with dihedral D_4 and D_3 gauge groups. We describe the gates and the full circuit to prepare the ground state of one and two plaquette systems, given the Hamiltonian and exploiting adiabatic evolution. Then we calculate some relevant observables, such as energy and Wilson loops. All quantum simulations are performed using the open-source Qiskit toolkit. The obtained results are checked against exact diagonalization numerical solutions, with respect to which we find a very good agreement.

Contents

INTRODUCTION

Motivation

Why a gauge theory? Why a lattice gauge theory? And why on a quantum computer?
We refer to as *gauge theory* any physical theory that has redundant degrees of freedom and for this reason it is invariant under a class of transformations, that form the gauge symmetry group. Gauge theories, are powerful tools to describe a broad range of natural phenomena and they find applications from the theory of Standard Model to condensed matter physics. For example gauge theories explain successfully the dynamics of elementary particles: quantum electrodynamics is an Abelian gauge theory with the symmetry group $U(1)$ and has one gauge field, the electromagnetic four-potential, with the photon being the gauge boson. Quantum chromodynamics is a non-Abelian gauge theory with the symmetry group $SU(3)$ and has eight gauge fields (since they have colour charges), with the gluons being the gauge bosons. The whole Standard Model is a non-Abelian gauge theory with the symmetry group $U(1) \times SU(2) \times SU(3)$ and has a total of twelve gauge bosons: the photon, three weak bosons and eight gluons [43]. Gauge theories find applications also in condensed matter physics, for example in spin glasses [42], Chern-Simons theory [11] and superconductivity [53].
The standard approach to study a gauge theory and all its relevant observables is *perturbation theory* [43]. In this approach we consider an Hamiltonian H that is the sum of two components, an unperturbed Hamiltonian H_0 and an interacting (perturbing) Hamiltonian H_{int} representing a weak disturbance to the unperturbed system, such that $H = H_0 + gH_{\text{int}}$, where g is the coupling constant. The idea is to start by studying the unperturbed Hamiltonian H_0 for which a mathematical solution is known, and then add corrections as a power series in the parameter g, and if the coupling constant is small enough we can truncate the series at the first order. This approach is usually possible only if the running coupling is small enough, however, in most gauge theories, like in quantum chromodynamics, there are many interesting questions which are non-perturbative, in particular the explicit forces acting between quarks and antiquarks in a meson. Among non-perturbative approaches to gauge theories, one of the most well established is *lattice gauge theory* [55]. This approach uses a discrete set of spacetime points in such a way that path integrals, and so all required quantities, can be evaluated by stochastic simulation techniques such as the Monte Carlo method. In this approach the gauge theory

is formulated in the Euclidean path-integral formalism, in order to make the integral strictly positive, so that it can be simulated in a computer via Monte Carlo algorithms. Despite being very difficult and demanding, often requiring the use of supercomputers, numerical computations have led to very relevant results. However there are still many unresolved issues, indeed the numerical sign problem prevents the use of Monte Carlo method to study lattice gauge theories, e.g. in presence of fermions at finite chemical potential, at high density and low temperature [41, 54]. Since the theory is Euclidean we also encounter problems when trying to reproduce the real-time dynamics of the model, some quantities, such as conductivity and viscosity, cannot be computed from the Euclidean path-integral. Moreover, the details of the various stages of out-of-equilibrium real-time evolution phenomena, such as heavy-ion collisions, are also out of reach [3, 40].
The recent development of quantum technologies opens the door to new techniques, such as *quantum simulation* and *quantum computation*, which can overcome these difficulties, provide us with new tools of research and expand our knowledge of lattice gauge models. As first proposed by Feynman in 1982 [20], only a quantum device is able to reproduce accurately a quantum system, in particular all its quantum properties that have no classical counterparts and cannot be efficiently simulated on classical simulators or computers. In particular digital quantum computers can be used as universal quantum simulators, i.e. programmable quantum computers are potentially able to calculate the time evolution of many physical models [52]. These suggestions have been made possible by the recent development of quantum control technologies. It must be said, however, that severe limitations persist in the number of qubits and the reliability of gates of currently available quantum computers.
Besides the technical and experimental challenges, in order to realize a quantum simulation of a lattice gauge theory we should be able to overcome some theoretical difficulties. In particular the theory must be formulated in the Hamiltonian approach, keeping time real and continuous while only space is discretized. This is different with respect to what we have in the path-integral approach of usual lattice gauge theory, where we pass to an Euclidean time through a Wick rotation and then we discretize the full Minkowski spacetime. We should also make sure that the theory has a finite-dimensional Hilbert space. In this direction there have already been studies on the quantum simulation of lattice gauge theories [17, 24, 37, 39, 58], especially in the case of an Abelian gauge group. These studies have shown that quantum simulations are intrinsically free of the sign problem and, since they are formulated in the Hamiltonian formalism, it is possible to study the real-time dynamics of the system. The goal of this master thesis is to use the formulation of the Hamiltonian lattice gauge theory with any finite gauge group given in [36], and to implement the quantum gates proposed in [30] in order to realize and analyze a quantum simulation with some finite non-Abelian gauge groups. The aim of this work is not to observe new physics but rather to formulate and verify a simulation of non-Abelian lattice gauge theories. Once this non-perturbative technique is validated, we may have access to regimes not otherwise accessible and new physical phenomena may be observed.

Overview

In chapter 1 we introduce the theoretical framework of lattice gauge theories in the Hamiltonian formalism, starting with the definition of a pure Yang-Mills model in the continuum spacetime, discussing the discretization of the space with a lattice and exploring the quantization of the theory with its Hamiltonian and Hilbert space.
In chapter 2 we introduce the general setting for simulations of a lattice gauge theory on a digital quantum computer, in particular we discuss how to encode the physical degrees of freedom of the model in the simulator, how to reproduce its Hamiltonian dynamics in an evolution gate and how to extract information on physical observables by measurements on the quantum circuit.
In chapter 3 we analyze two specific gauge groups: the dihedral groups D_4 and D_3, in the cases of one and two plaquette lattices. These two groups are interesting because they are the simplest non-Abelian subgroups that can be used to approximate $SO(3)$, and hence $SU(2)$. Through exact and numeric computations we formulate theoretical predictions for the behaviour of some relevant observables like the energy and Wilson loops.
In chapter 4 we implement the quantum circuits required to simulate a lattice gauge theory with D_4 and D_3 gauge groups in the cases of a one and two plaquette lattices, using the Qiskit toolkit. Then the results of the quantum simulation are compared with those obtained in the previous chapter, finding a very good agreement.

Chapter 1

LATTICE GAUGE THEORY

In this chapter we introduce the pure Yang-Mills theory on a lattice. We start by reviewing the usual Yang-Mills theory on a continuum Minkowski spacetime with a generic gauge group G, first in its Lagrangian formulation and then in the Hamiltonian formalism. We give also some hints on how to quantize this model promoting the fields to operator and imposing the canonical commutation rules. In order to regularize the theory we discretize the spatial dimensions and keep time continuous, obtaining in this way a lattice gauge theory where the gauge fields live on the edges of the lattice. We study the structure of the Hilbert space attached to each edge analyzing two possible bases: the group element basis and the representation basis, and in doing so we review the relevant notions on the left and right regular representations and Peter-Weyl theorem. We see how a gauge transformation acts on the total Hilbert space and hence which are the states that are gauge invariant and therefore physical. Then we introduce the Kogut-Susskind Hamiltonian that governs the dynamics of this lattice gauge model, we introduce first its magnetic part and then the electric part. In the electric Hamiltonian we pay particular attention when defining the Laplacian for both compact Lie groups and finite groups. The resulting Hamiltonian is gauge invariant and provides the correct continuum limit. Finally we discuss two useful operators for the study of this model: the vertex operator and the plaquette operator, also mentioning the quantum double model.

1.1 Continuum Yang-Mills theory

In this section we briefly review the Hamiltonian formulation of a Yang-Mills theory in the temporal gauge and defined on a continuum Minkowski spacetime. We start by summarizing some basic concepts of Lie group and Lie algebra theory, introducing in this way the gauge field. We present the Yang-Mills Lagrangian, that describes the dynamics of a model that is symmetric under certain local gauge transformations. Then imposing the temporal gauge to fix a non-physical degree of freedom and performing a Legendre transform we formulate the

Yang-Mills Hamiltonian for a continuum theory. Finally we see how to quantize this theory promoting fields to operators and imposing the canonical commutation rules.

1.1.1 Gauge group

Let's start by reviewing some basic concepts of Lie group theory applied to the context of gauge symmetries. At these first stages we will be interested in compact and simple Lie groups, one example could be $SU(N)$, which has many applications. A Lie group is a group which is also a differentiable manifold, such that the group multiplication and inversion maps are smooth [25]. A Lie group G has an underlying Lie algebra $\mathfrak{g}$. Formally the Lie algebra $\mathfrak{g}$ of a Lie group G is the tangent space of the identity element of G, hence a vector space of the same dimension of the group G. Each element of the group $g \in G$ can be written using the exponential map through some real parameters X^a and the generators T_a of the Lie algebra $\mathfrak{g}$:

$$g = e^{iX^a T_a}, \tag{1.1.1}$$

where the sum over the repeated color index $a = 1, 2, ..., d_G$ is taken for granted, and d_G is the dimension of the group G, or of the corresponding Lie algebra $\mathfrak{g}$, which is then the same. The generators T_a of the Lie algebra $\mathfrak{g}$ satisfy the following commutation rules

$$[T_a, T_b] = i f_{abc} T_c, \tag{1.1.2}$$

where f_{abc} are fully anti-symmetric structure constants and are footprints of the Lie group. In the simple cause of an Abelian group, all these constants are equal to zero, while in a more complex group like $SU(N)$ they are generally different from zero. In order to normalize the generators we require them to satisfy the Killing metric

$$\mathrm{Tr}(T_a T_b) = \frac{1}{2}\delta_{ab}. \tag{1.1.3}$$

Gauge field

At this point we are ready to introduce the main ingredient for a gauge theory, the gauge field. We define a gauge field, or connection, A_μ as an element of the Lie algebra $A_\mu \in \mathfrak{g}$, with $\mu = 0, 1, 2, 3$ that is a tensor index for the spacetime components. Being A_μ an element of the Lie algebra it can be written as a linear combination of the generators:

$$A_\mu = A_\mu^a T_a. \tag{1.1.4}$$

We remark that A_μ is a field and as such it is a function of the spacetime coordinates: $A_\mu(x)$, where $x = (t, \vec{x})$ is a point of Minkowski spacetime $\mathcal{M}$. We will use the Minkowski metric with signature $(-, +, +, +, +)$, and Einstein summation convention, meaning that the sum

over repeated indices is implied.
From the gauge potential A_μ we can construct the field strength, or curvature, $F_{\mu\nu}$ such that

$$F_{\mu\nu} = \partial_\mu A_\nu - \partial_\nu A_\mu - i[A_\mu, A_\nu]. \tag{1.1.5}$$

Also the field strength, being an element of the Lie algebra $\mathfrak{g}$, can be expanded in terms of the Lie algebra generators $F_{\mu\nu} = F^a_{\mu\nu} T_a$.
The gauge field A_μ and the field strength $F_{\mu\nu}$ under a local gauge transformation $g(x) \in G$ transform as follows

$$\begin{cases} A_\mu(x) \to A'_\mu(x) = g(x)A_\mu(x)g(x)^{-1} + ig(x)\partial_\mu g(x)^{-1} \\ F_{\mu\nu}(x) \to F'_{\mu\nu}(x) = g(x)F_{\mu\nu}(x)g(x)^{-1} \end{cases}. \tag{1.1.6}$$

Notice how the gauge transformation of the field strength $F_{\mu\nu}$ is fully determined by the transformation law of the gauge field A_μ, simply using its definition (1.1.5). Non-Abelian gauge fields A_μ transform like the adjoint representation [38].

Matter field

The second ingredient for a gauge theory is a matter field $\Psi(x)$, usually a fermionic one. Matter fields live in the complex vector space V of some representation $\rho : G \to \mathrm{End}(V)$ of the gauge group G. This means that matter fields sit in some vector space of dimension d_ρ, the dimension of the representation. The action of the local gauge transformation $g(x) \in G$ on the matter field $\Psi(x) \in V$ is simply given by $\Psi'(x) = \rho(g(x))\Psi(x)$. In the following we will consider a pure gauge theory, this means that we will neglect the matter field Ψ, considering just the dynamics of the gauge field A_μ. The reader interested in the simulation of gauge theories with scalar or spinor matter fields may refer to [30].

1.1.2 Yang-Mills Lagrangian

Consider a classical field model where only the gauge field $A_\mu(x) \in \mathfrak{g}$ is present and where the system is invariant under local gauge transformations $g(x) \in G$, whose action on the gauge field is given by (1.1.6). The Lagrangian that describes the dynamics of such a theory is the pure Yang-Mills Lagrangian:

$$\mathscr{L}_{\mathrm{YM}} = -\frac{1}{2g^2}\,\mathrm{Tr}(F_{\mu\nu}F^{\mu\nu}). \tag{1.1.7}$$

where g is the coupling constant for the gauge field interaction and the sum over the repeated spacetime indices μ and ν is implied. It is easy to verify that under the gauge transformation (1.1.6) the Yang-Mills Lagrangian (1.1.7) in invariant because of the cyclic property of the trace Tr.

We can also split the field strength $F_{\mu\nu}$ appearing in the Lagrangian (1.1.7) in the chromoelectric field E_i and in the chromomagnetic field B_i, with $i = 1, 2, 3$ (space components) such that

$$\begin{aligned} E_i &= F_{0i}, \\ B^i &= -\frac{1}{2}\epsilon^{ijk} F_{jk}, \end{aligned} \tag{1.1.8}$$

where ϵ^{ijk} is the Levi-Civita symbol. In terms of the fields (1.1.8) the Lagrangian (1.1.7) becomes

$$\mathscr{L}_{\text{YM}} = \frac{1}{g^2} \operatorname{Tr}(E_i E_i - B_i B_i). \tag{1.1.9}$$

1.1.3 Yang-Mills Hamiltonian

Temporal gauge

Now we try to pass to the Hamiltonian formulation of a pure Yang-Mills theory for a generic gauge group G, starting from the Yang-Mills Lagrangian $\mathscr{L}_{\text{YM}}$ (1.1.7). The main issue we have to deal with is gauge invariance, since the Lagrangian (1.1.7) is written with some redundant non-physical degrees of freedom. This is reflected into the fact that if we expand $\operatorname{Tr}(F_{\mu\nu}F^{\mu\nu})$ in terms of the gauge field A_μ it does not contain the term $\dot{A}_0$ (time derivative of the time-component of the gauge field), and so the corresponding conjugate momentum π_0 is identically zero:

$$\pi_0 = \frac{\partial \mathscr{L}_{\text{YM}}}{\partial \dot{A}^0} = 0. \tag{1.1.10}$$

This means that the field A_0 is not dynamical and its equation of motion is a time-independent algebraic equation, which shows that A_0 takes a time-independent constant value. We can isolate A_0 in the Lagrangian (1.1.9), adding a divergence and neglecting second order functions in A_0, that do no not contribute to the equations of motions, in this way we find [31]:

$$\mathscr{L}_{\text{YM}} = \frac{1}{g^2} \operatorname{Tr}(E_i E_i - B_i B_i)\bigg|_{A_0=0} + \frac{1}{g^3} \operatorname{Tr}(A_0 \mathcal{G}), \tag{1.1.11}$$

with $\mathcal{G} = \mathcal{G}^a T_a \in \mathfrak{g}$ defined in terms of its component by

$$\mathcal{G}^a(x) = \partial_i E_i^a(x) + f^{abc} A_i^b(x) E_i^c(x) = D_i E_i^a(x), \tag{1.1.12}$$

where D_μ is the covariant derivative. Given a field F in the representation ρ of the gauge group G, then the covariant derivative of F is

$$D_\mu F_i = \partial_\mu F_i - i A_\mu^a (T_\rho^a)_{ij} F^j, \quad i, j = 1, 2, ..., d_\rho, \tag{1.1.13}$$

where T_ρ^a are the generators of the Lie algebra $\mathfrak{g}$ corresponding to the representation ρ, and d_ρ is the dimension of ρ.

From the expression (1.1.11) we can see that A_0 is a Lagrange multiplier and its equation of motion corresponds to a set of phase space constraints $\mathcal{G}^a(x) = D_i E_i^a(x) = 0$, one for each color index $a = 1, 2, ..., d_G$. These are the non-Abelian analogue of Gauss' law constraint in the Abelian electromagnetic theory. These constraints represent the conditions for a specific configuration to be gauge invariant, and they have to be satisfied by all physical phase space states.
As a gauge fixing condition we can use the temporal gauge in which we fix $A_0 = 0$, then the Lagrangian (1.1.11) becomes

$$\mathscr{L}_{\mathrm{YM}} = \frac{1}{2g^2}(E_a^i E_a^i - B_a^i B_a^i), \tag{1.1.14}$$

where apart from putting A_0 to zero, we have also removed the trace on the color indices using the fact that $E^i = E_a^i T^a$, $B^i = B_a^i T^a$ and the Killing metric (1.1.3). In the last expression, as per our notation, we take for granted the sum over the repeated space index i and the repeated color index a. Notice that the temporal gauge $A_0 = 0$ does not fix completely the gauge freedom, in particular we have a residual gauge invariance under time-independent gauge transformations $g(\vec{x}) \in G$, using the general expression (1.1.6) we can write:

$$A_\mu(x) \to A'_\mu(x) = g(\vec{x})A_\mu(x)g(\vec{x})^{-1} + ig(\vec{x})\partial_\mu g(\vec{x})^{-1}. \tag{1.1.15}$$

Under this gauge transformation we have that $A_0(x) \to A'_0(x) = g(\vec{x})A_0(x)g(\vec{x})^{-1}$, and if we were in temporal gauge $A_0 = 0$, we will remain in the same gauge $A'_0 = 0$.

Legendre transform

In the temporal gauge $A_0 = 0$ one has that $E_i^a = \dot{A}_i^a$, then the momenta π_i conjugate to A_i are

$$\pi_a^i = \frac{\partial \mathscr{L}_{\mathrm{YM}}}{\partial \dot{A}_i^a} = \frac{E_a^i}{g^2}. \tag{1.1.16}$$

The Hamiltonian density $\mathscr{H}_{\mathrm{YM}}$ can be derived using the usual Legendre transform:

$$\mathscr{H}_{\mathrm{YM}} = \pi_a^i \dot{A}_i^a - \mathscr{L}_{\mathrm{YM}} = \frac{g^2}{2}\pi_a^i \pi_a^i + \frac{1}{2g^2}B_a^i B_a^i. \tag{1.1.17}$$

The continuum Yang-Mills Hamiltonian H_{YM} in the temporal gauge is given by

$$H_{\mathrm{YM}} = \int d^4x \left(\frac{g^2}{2}\pi_a^i(x)\pi_a^i(x) + \frac{1}{2g^2}B_a^i(x)B_a^i(x)\right). \tag{1.1.18}$$

As you can see from (1.1.18) the Hamiltonian is made of two pieces, and we will refer to them as electric Hamiltonian H_E and magnetic Hamiltonian H_B respectively, such that $H_{\mathrm{YM}} = H_E + H_B$.

Quantization of gauge fields

To quantize the classical field theory described by the Yang-Mills Hamiltonian (1.1.18) we can promote the gauge fields A_i^a and the conjugate momenta π_i^a to the Hermitian operators $\hat{A}_i^a$ and $\hat{\pi}_i^a$ respectively, acting on an Hilbert space. These operators obey the canonical equal-time commutation rules [21]:

$$\begin{aligned}\left[\hat{A}_i^a(x), \hat{A}_j^b(y)\right]_{x_0=y_0} &= 0,\\ \left[\hat{\pi}_i^a(x), \hat{\pi}_j^b(y)\right]_{x_0=y_0} &= 0,\\ \left[\hat{A}_i^a(x), \hat{\pi}_b^j(y)\right]_{x_0=y_0} &= i\delta_b^a\delta_i^j\delta^3(\vec{x}-\vec{y}).\end{aligned} \tag{1.1.19}$$

This is a situation similar to what we have in a quantum system with the commutation rule $[\hat{x}_i, \hat{p}_j] = i\delta_{ij}$ between the position $\hat{x}_i$ and the momentum $\hat{p}_j$ operators. In that case considering the position representation $\langle x|\psi\rangle = \psi(x)$, we satisfy the commutation rule by imposing that $\hat{x}$ acts multiplicatively and $\hat{p}$ generates the translations. Similarly in the field representation, the Hilbert space is the vector space of wave functionals $\psi[\vec{A}]$ of the configurations of the field $\vec{A}$ at fixed time. In this notation we have $\langle \vec{A}(x)|\psi\rangle = \psi[\vec{A}]$. In order to satisfy the commutation rules (1.1.19), we impose that $\hat{A}_i^a(x)$ acts on $\psi[\vec{A}]$ multiplicatively while $\hat{\pi}_i^a(x)$ is the generator of translations (it is a functional differential operator):

$$\begin{aligned}\hat{A}_i^a(x)\psi[\vec{A}] &= A_i^a(x)\psi[\vec{A}],\\ \hat{\pi}_i^a(x)\psi[\vec{A}] &= -i\frac{\delta}{\delta A_a^i(x)}\psi[\vec{A}].\end{aligned} \tag{1.1.20}$$

Let us notice that the space of wave functionals $\psi[\vec{A}]$ is too large, in the sense that it contains non-physical states. As we saw before, the temporal gauge $A_0 = 0$ has a residual gauge symmetry under local gauge transformations (1.1.15). It can be shown [21] that $\hat{\mathcal{G}}(\vec{x}) = D_i\hat{E}_i(\vec{x})$ is the quantum generator of local infinitesimal time-independent gauge transformations and it commutes locally with the Hamiltonian $[\hat{\mathcal{G}}(\vec{x}), \hat{H}_{\text{YM}}] = 0$. This operator can be used to identify the physical gauge invariant Hilbert space. The physical requirement that states that differ by time-independent gauge transformations, like (1.1.15), be equivalent to each other leads to the demand that we should restrict the Hilbert space to the space of gauge-invariant states, and these states satisfy $\hat{\mathcal{G}}(\vec{x})\,|\psi\rangle = D_i\hat{E}_i(\vec{x})\,|\psi\rangle = 0$. The constraint means that only the states which obey the Gauss' law are in the physical Hilbert space:

$$\mathcal{H}_{\text{phys}} = \left\{|\psi\rangle : \hat{\mathcal{G}}(\vec{x})\,|\psi\rangle = 0\right\}. \tag{1.1.21}$$

In this way in this section we obtained a quantum Yang-Mills gauge theory defined on a continuum Minkowski spacetime; in the following sections we will see how to pass to a Yang-Mills gauge theory defined on a discretized space (lattice) and with a continuous time.

1.2 Lattice regularization

In this section we discuss why we should be interested in the discretization of a continuum gauge theory, as the one presented in the previous section, especially if it cannot be treated with perturbation theory. We define the d-dimensional square lattice used to perform this discretization, and we also describe how to assign to each edge of the model a gauge field (or equivalently a group element).

1.2.1 Introduction to lattice gauge theory

The standard approach to study a gauge theory as the one described in the previous section is perturbation theory, in which the dynamics of the model is studied with perturbative expansions on the coupling constant. These expansions are only meaningful as long as the coupling constant is small, and this is for example the case for Quantum Electrodynamics (QED), the quantum field theory describing the electromagnetic interaction. QED is a gauge theory where the gauge group is $G = U(1)$ and the coupling constant, the electric charge, is weak and many aspects of the dynamics of the model can be treated with perturbation theory. Because of the phenomenon of the screening of the electric charge, increasing the energy, the coupling constant grows and eventually diverges. Fortunately the energy scale at which QED perturbation theory breaks down is huge, far larger than Planck's mass, therefore this divergence is not a real problem [43]. The situation is much different for Quantum Chromodynamics (QCD), the quantum field theory describing the strong interaction between the quarks inside nuclei. QCD is a gauge theory with gauge group $G = SU(3)$ and here the coupling constants diverge in such a way that perturbation theory cannot be applied.
Lattice regularization is the most famous non-perturbative approach to QCD and it was introduced by Wilson [55]. Working on a hypercubic spacetime lattice we are able to remove the ultraviolet divergences, and regularize the theory. Quark fields (matter fields) live on the lattice vertices and gluons (gauge fields) reside on the links between the nearest neighbour vertices. Given this lattice gauge theory, if we work on a Wick-rotated euclidean spacetime, QCD becomes a statistical mechanics model. In the Hamiltonian formulation of this model the time can be kept continuous and real, while we discretize just the space dimensions.

1.2.2 Definition of the lattice

Let us consider a Yang-Mills theory in the temporal gauge on a lattice with a gauge group G and in the Hamiltonian setting. With respect to the continuum gauge theory on the Minkowski $(d+1)$-dimensional spacetime $\mathcal{M}$, in this lattice gauge theory the time variable t is kept continuous, while the space coordinates x_i are discretized, with $i = 1, ..., d$, where d is the dimension of the lattice (in the simulation we will work with $d = 2$). We can in particular

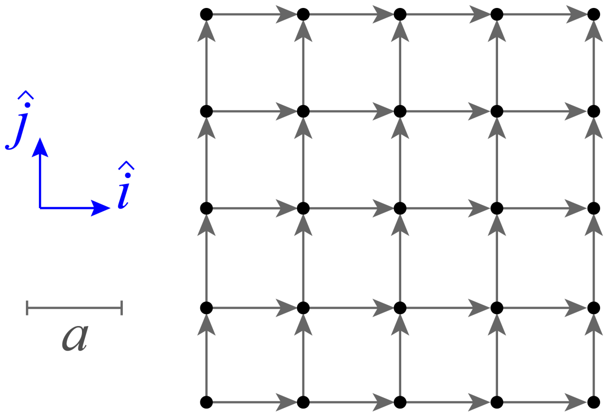

Figure 1.1: The square oriented lattice Λ (1.2.1) for a $d = 2$ dimensional space. The lattice spacing is a, while $\hat{\imath}$ and $\hat{\jmath}$ are two unit vectors that indicate the orientations of the edges. The black dots are the vertices $\vec{x}$, the grey lines are the oriented edges l. For the lattice in the figure we have $L_i = L_j = 4$.

consider a hypercubic oriented lattice Λ, like the one in Fig. 1.1, defined as

$$\Lambda = \left\{ \vec{x} \in \mathbb{R}^d : \vec{x} = \sum_{i=1}^{d} a n_i \hat{\imath}, \quad n_i = 0, 1, ..., L_i \right\}, \tag{1.2.1}$$

where the vertices $\vec{x}$ are points in an Euclidean space $\mathbb{R}^d$, $\hat{\imath}$ is a unit vector in the i-th direction, such that $\hat{\imath} = (0_1, ..., 0_{i-1}, 1_i, 0_{i+1}, ..., 0_d)$, n_i are integer numbers, L_i is the extension of the lattice along the i-th direction and $a > 0$ is the lattice spacing.
We identify the vertices with their space coordinates $\vec{x}$, the set of all vertices is called V. We denote the oriented link (or edge) l by specifying the initial vertex and the unit vector parallel to the link, so for example $l = (\vec{x}, \hat{\imath})$ is the link that goes from $\vec{x}$ to $\vec{x} + a\hat{\imath}$. We denote by l_- the source lattice site at the origin of the segment and by l_+ the target lattice site, as in Fig. 1.2. For example, given the link $l = (\vec{x}, \hat{\imath})$, we have that $l_- = \vec{x}$ and $l_+ = \vec{x} + a\hat{\imath}$. Notice that the orientation of the links is important. The set of all edges is called E.
In a classical configuration of a lattice gauge theory we assign to the vertices the matter fields while to the edges the gauge fields. In particular, on each vertex $\vec{x}$ of the lattice one should put a matter field $\Psi(t, \vec{x})$, but we will consider a pure gauge theory, so in our case there are no matter fields. On the edge $(\vec{x}, \hat{\imath})$ we put the gauge field $A_i(t, \vec{x})$. As we saw in the previous section, gauge fields A_i are elements of the Lie algebra $\mathfrak{g}$, and for this reason using the exponential map (1.1.1) is like we are attaching to each edge a group element $g \in G$. In particular it is possible to prove [53] that at the group element g associated to the link $(\vec{x}, \hat{\imath})$ is

$$g(\vec{x}, \hat{\imath}) = e^{iaA_i(t,\vec{x})}, \tag{1.2.2}$$

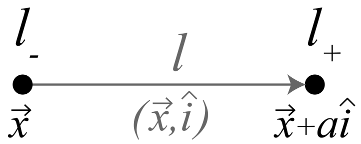

Figure 1.2: Oriented edge $l = (\vec{x}, \hat{i})$. The edge is oriented in $\hat{i}$ direction, it has as origin the vertex $l_- = \vec{x}$ and as target the vertex $l_+ = \vec{x} + a\hat{i}$, where a is the lattice spacing.

where $g(\vec{x}, \hat{i})$ is the group element associated to the link $(\vec{x}, \hat{i})$ and $A_i(t, \vec{x})$ is the spatial component of the gauge field in the direction of $\hat{i}$, evaluated in the point $\vec{x}$ at the time t. The relation (1.2.2) can be derived formally by studying the parallel transport in a vector bundle and defining the comparator for the links of the square lattice, for more details see [53] and [32]. We can notice that the relation (1.2.2) is an exponential map linking a Lie algebra object $A_i(t, \vec{x}) \in \mathfrak{g}$ to a group object $g(\vec{x}, \hat{i}) \in G$.
As we said before links are oriented, and if a link l associated to the group element g_l is traversed in the opposite orientation, then g_l is replaced with its inverse g_l^{-1}.
In the next section we will see how to describe the vector space of each edge as a Hilbert space.

1.3 Hilbert space of a lattice gauge theory

In a quantum lattice gauge theory the space of configuration of each link is a Hilbert space and in this section we discuss the structure of this space and also of the total Hilbert space describing the whole lattice. We analyze two possible bases for the single-link Hilbert space: the group element basis and the representation basis. In order to introduce the second basis we discuss some important results on Peter-Weyl theorem and left and right regular representations. Finally we describe how a gauge transformation acts on the states of the total Hilbert space and therefore how to characterized the physical (gauge invariant) states.

1.3.1 Hilbert space of a single link

In the previous section we saw how a classical configuration for a lattice gauge model is given by a choice of group element $g \in G$ on each lattice link. In the quantum theory the states in the Hilbert space of each link are given by a superposition of the classical configurations. Let's analyze this Hilbert space by distinguishing the case where the gauge group G is a compact Lie group from the case where it is a finite group.

Compact Lie group

Given a compact Lie group G, we attach to each directed link l an Hilbert space $\mathcal{H}^{(l)} = L^2(G)$, that is the space of square integrable functions $\psi : G \to \mathbb{C}$ with respect to left and right invariant Haar measure dg. Given a locally compact group G, a left and right invariant Haar measure on G is a measure dg satisfying the following conditions:

$$\int_G dg f(gh) = \int_G dg f(g) = \int_G dg f(hg), \tag{1.3.1}$$

with $g, h \in G$ and $f : G \to \mathbb{C}$ [27].
Analogously to what happens with $L^2(\mathbb{R}^d)$, where we have the position basis $\{|\vec{x}\rangle\}$, with $\vec{x} \in \mathbb{R}^d$, we can construct a similar basis for the single link Hilbert space $L^2(G)$:

$$\{|g\rangle : g \in G\}, \tag{1.3.2}$$

and we call it *group element* or *position basis*. Since we are considering a Lie group, there are infinite elements inside the group G, and so also the position basis (1.3.2) contains infinite many states. Just as for the usual position basis we have an orthonormality relation also for $\{|g\rangle\}$:

$$\langle g|h\rangle = \delta(g, h), \tag{1.3.3}$$

where $\delta(g, h)$ is a Dirac delta, a distribution, on elements of the group g and h. A generic vector of the Hilbert space $\mathcal{H}^{(l)}$ can be written as a linear superposition (integral) of the position basis states:

$$|\psi\rangle = \int_G dg \psi(g) |g\rangle \,, \tag{1.3.4}$$

where $\psi(g) \in L^2(G)$ is a square integrable function. Whereas in the classical theory we associate a well-defined group element to each link, in the quantum theory is also possible to assign to each link a superposition of group elements, and the weight function $|\psi(g)|^2$ gives us the probability of getting a specific group element g.
The total Hilbert space $\mathcal{H}_T$ for the entire lattice is

$$\mathcal{H}_T = \bigotimes_{l \in E} L^2(G). \tag{1.3.5}$$

A possible basis for the total Hilbert space is $\{\bigotimes_l |g_l\rangle\}$, where $|g_l\rangle$ is a group element basis element for the Hilbert space $\mathcal{H}^{(l)}$ of the single link l.
We emphasise from the outset that the physical (gauge invariant) Hilbert space $\mathcal{H}_{\text{phys}}$ is just a subspace of the total Hilbert space $\mathcal{H}_T$ (1.3.5).

Finite group

If instead of a compact Lie group we are interested in a finite group G, we attach to each directed link l an Hilbert space $\mathcal{H}^{(l)} = \mathbb{C}[G]$, that is the group algebra of G (see appendix

A.2), so the complex vector space spanned by the group element basis $\{|g\rangle\}$, that is defined just as in the Lie group case (1.3.2). Since we are considering a finite group, there is a finite number of elements inside the group G, and so also the position basis (1.3.2) contains a finite number of states. The basis states still satisfy the orthonormality relation (1.3.3), but this time the $\delta(g,h)$ is not a Dirac delta, but simply a Kronecker delta function that returns 1 if $g = h$ and 0 otherwise.
A generic vector of the Hilbert space $\mathcal{H}^{(l)}$ can be written as a linear superposition of the position basis states:

$$|\psi\rangle = \sum_{g\in G} \psi(g)\,|g\rangle\,, \tag{1.3.6}$$

where $\psi(g) \in \mathbb{C}[G]$ and with respect to (1.3.4) we substitute the integral over the Haar measure with the sum over all group elements.
The total Hilbert space $\mathcal{H}_T$ for the entire lattice is

$$\mathcal{H}_T = \bigotimes_{l\in E} \mathbb{C}[G]. \tag{1.3.7}$$

Also for a finite group G, the physical Hilbert space $\mathcal{H}_{\text{phys}}$ is just a subspace of the total Hilbert space $\mathcal{H}_T$ (1.3.7), but before talking about gauge transformations we shall introduce some useful operators.

1.3.2 Left and right translation operators

Left and right operators

Consider the Hilbert space of a single link $\mathcal{H}^{(l)}$, given the group element $g \in G$ we can define the left translation operator L_g, whose action on the group element basis state $|h\rangle$ is

$$L_g\,|h\rangle = |gh\rangle\,. \tag{1.3.8}$$

One can also define the right translation operator R_g, whose action on the group element basis state $|h\rangle$ is

$$R_g\,|h\rangle = |hg^{-1}\rangle\,. \tag{1.3.9}$$

The action of these operators is similar to the one of the translation operator $\exp(ix\hat{p})$ in quantum mechanics, that translates a state by x in the position space. The generator of this translation is the momentum operator $\hat{p}$. We are now interested in finding the analog of the momentum operator (generator of translations) in this group algebra context, because it will be a crucial element for the construction of the electric Hamiltonian.

Generators of left translation

Let us now focus on the case of a compact Lie group G. The left and right translation operators L_g and R_g introduced in (1.3.8) and (1.3.9) can be seen as infinite-dimensional unitary representations of the group G onto the space of $L^2(G)$, known as the *left* and *right regular representations* [58]. Acting on the group element basis it is easy to verify that $L : G \to \mathrm{End}(L^2(G))$, $R : G \to \mathrm{End}(L^2(G))$ and they satisfy

$$L_g L_h = L_{gh}, \quad R_g R_h = R_{gh}, \quad \forall g, h \in G. \tag{1.3.10}$$

These representations are unitary, indeed:

$$(L_g)^{-1} = L_{g^{-1}} = L_g^\dagger, \;\; (R_g)^{-1} = R_{g^{-1}} = R_g^\dagger, \quad \forall g \in G. \tag{1.3.11}$$

Recall that each element g of a Lie group G can be written as the exponential of an element X of the corresponding Lie algebra $\mathfrak{g}$ (1.1.1):

$$g = e^{iX} \in G, \tag{1.3.12}$$

and the Lie algebra element $X \in \mathfrak{g}$ can be written as a linear combination of the generators T_a for some real coefficients X^a, with $a = 1, 2, ..., d_G$ and d_G the dimension of the Lie algebra:

$$X = X^a T_a \in \mathfrak{g}. \tag{1.3.13}$$

We are now interested in finding the regular Lie algebra representation $\mathfrak{L} : \mathfrak{g} \to \mathrm{End}(L^2(G))$ of the Lie algebra $\mathfrak{g}$ that corresponds to L. Using the exponential map (1.3.12), the compatibility of L and $\mathfrak{L}$ implies:

$$L_{e^{iX}} = e^{i\mathfrak{L}(X)}. \tag{1.3.14}$$

You can visualize better this relation in Fig. 1.3. Expanding on the Lie algebra generators T_a (1.3.13) we can see that

$$L_{e^{iX^a T_a}} = e^{iX^a \mathfrak{L}_a}, \tag{1.3.15}$$

where we defined $\mathfrak{L}_a = \mathfrak{L}(T_a)$, the regular Lie algebra representation of the generator T_a of $\mathfrak{g}$. Using the commutation relation (1.1.2) between the generators T_a of the Lie algebra, and the fact that $\mathfrak{L}$ is a Lie representation, we can see that:

$$[\mathfrak{L}_a, \mathfrak{L}_b] = i f_{abc} \mathfrak{L}_c. \tag{1.3.16}$$

The operators $\mathfrak{L}_a$ will play a fundamental role in the definition of the group Laplacian and the electric Hamiltonian, since they are the analog of momentum operators $\hat{p}_i$ in the group algebra.

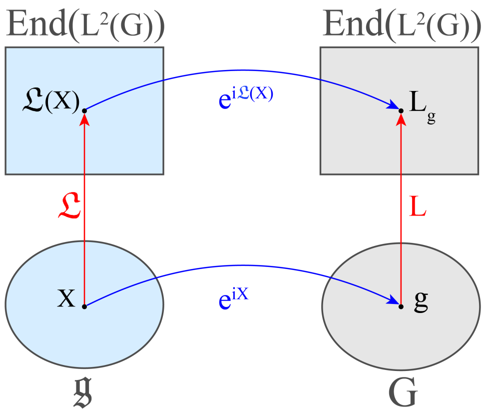

Figure 1.3: Pictorial description of the relation (1.3.14) that ensures the compatibility of L and $\mathfrak{L}$. Given a Lie algebra element $X \in \mathfrak{g}$ via the exponential map (1.3.12) we can associate it a group element $g = e^{iX} \in G$, then the left regular Lie group representation $L : G \to \mathrm{End}(L^2(G))$ associate to g the operator L_g. The same operator can be obtained starting from $X \in \mathfrak{g}$, taking the left regular Lie algebra representation $\mathfrak{L} : \mathfrak{g} \to \mathrm{End}(L^2(G))$ of it, and then applying the exponential map.

1.3.3 Peter-Weyl theorem and representation basis

The representation theory of the left L and right R regular representations leads to the Peter-Weyl theorem, which is a very important theorem for the characterization of the Hilbert space of a single link $\mathcal{H}^{(l)}$, and allows us to introduce a new useful basis for this space. We will give the statement of the theorem for both compact Lie groups and finite groups.

Compact Lie group

Let G be a compact Lie group and $\hat{G}$ the countable set of inequivalent irreducible representations of G labeled by the index j. Then [27, 35]

1. The space $L^2(G)$ of square-integrable functions on G can be decomposed as a sum of representation spaces. More precisely, if V_j is the vector space for the irreducible representation ρ_j, then
$$L^2(G) = \bigoplus_{j\in\hat{G}} V_j^* \otimes V_j, \tag{1.3.17}$$
where V_j^* is the dual of V_j and the direct sum $\bigoplus_j$ is extended to all inequivalent irreducible representations of G.

2. The matrix elements $(\rho_j)_{mn}$ of all inequivalent irreducible representations of G form an orthogonal basis for $L^2(G)$.

3. If $\{|g\rangle\}$ is the orthonormal group element basis for $L^2(G)$, then the *representation basis* $\{|j_{mn}\rangle\}$ satisfies the duality relation:

$$\langle g|j_{mn}\rangle = \sqrt{\frac{d_j}{\mathrm{Vol}(G)}}\rho_j(g)_{mn}, \tag{1.3.18}$$

where d_j is the dimension of the representation ρ_j, hence also of the vector space V_j, while $\mathrm{Vol}(G) = \int_G dg$ is the volume of the group G in the Haar measure.

Finite group

Let G be a finite group and $\hat{G}$ the countable set of inequivalent irreducible representations of G labeled by the index j. Then [35, 49]

1. The group algebra $\mathbb{C}[G]$ can be decomposed as a sum of representation spaces. More precisely, if V_j is the vector space for the irreducible representation ρ_j, then

$$\mathbb{C}[G] = \bigoplus_{j\in\hat{G}} V_j^* \otimes V_j, \tag{1.3.19}$$

where V_j^* is the dual of V_j and the direct sum $\bigoplus_j$ is extended to all inequivalent irreducible representations of G.

2. The matrix elements $(\rho_j)_{mn}$ of all inequivalent irreducible representations of G form an orthogonal basis for $\mathbb{C}[G]$.

3. If $\{|g\rangle\}$ is the orthonormal group element basis for $\mathbb{C}[G]$, then the *representation basis* $\{|j_{mn}\rangle\}$ satisfies the duality relation:

$$\langle g|j_{mn}\rangle = \sqrt{\frac{d_j}{|G|}}\rho_j(g)_{mn}, \tag{1.3.20}$$

where d_j is the dimension of the representation ρ_j, hence also of the vector space V_j, while $|G|$ is the size of the group G, so the number of elements in it.

Some observations

From the point 1 of Peter-Weyl theorem we can see how to decompose the space of square integrable functions $L^2(G)$, that is also the Hilbert space $\mathcal{H}^{(l)}$ attached to a single link l. Two equivalent ways to write the decomposition $V_j^* \otimes V_j$ are

$$V_j^* \otimes V_j \cong \mathrm{End}(V_j) \cong V_j^{\oplus d_j}. \tag{1.3.21}$$

Recall that the space $L^2(G)$ is made of functions on the the group $\psi : G \to \mathbb{C}$. The elements of the position basis $\{|g\rangle\}$ are associated with the Dirac delta distributions like $e_g(h) = \delta(g, h)$, which form a basis of the space $L^2(G)$. The point 2 of Peter-Weyl theorem says us that there exists another possible basis for the space $L^2(G)$, and this basis is made of the matrix elements of all inequivalent irreducible representations of G, hence $(\rho_j)_{mn} : G \to \mathrm{End}(V_j)$, where $j \in \hat{G}$ labels the irreducible representation and m, n label the matrix elements, so they are constrained by $1 \leq m, n \leq d_j$, with d_j the dimension of the representation ρ_j. The function $(\rho_j)_{mn}$ is associated with the Hilbert space state $|j_{mn}\rangle$. The same discussion can be done for the finite group case.
From the point 3 of the Peter-Weyl theorem we see the explicit relation between the group element (or position) basis $\{|g\rangle\}$ and the representation basis $\{|j_{mn}\rangle\}$. Notice how the group element basis $\{|g\rangle\}$ contains $|G|$ elements (in the finite group case), while the representation basis $\{|j_{mn}\rangle\}$ contains $\sum_j d_j^2$ elements. There is a theorem in representation theory that guarantees that these two numbers are the same (A.3.1), as one may expect by two bases of the same Hilbert space.
Both these two bases will play an important role in the following discussion, indeed the group element basis diagonalizes the magnetic part of the Hamiltonian, while the representation basis diagonalizes the electric part of the Hamiltonian.

Decomposition of regular representation

The Peter-Weyl decomposition (1.3.17) allows us to write the left regular representation L_g as [27, 35]

$$L_g = \bigoplus_{j \in \hat{G}} \rho_j(g)^* \otimes \mathbb{I}_j, \tag{1.3.22}$$

where $\mathbb{I}_j$ is the $d_j \times d_j$ identity matrix. An equivalent expression is

$$L_g = \bigoplus_{j \in \hat{G}} \rho_j(g)^{\oplus d_j}, \tag{1.3.23}$$

where the sum is extended to all irreducible representations j of G, with multiplicity equal to d_j. The same decomposition can be done also for the right regular representation R_g:

$$R_g = \bigoplus_{j \in \hat{G}} \mathbb{I}_j \otimes \rho_j(g) \tag{1.3.24}$$

or also

$$R_g = \bigoplus_{j \in \hat{G}} \rho_j(g)^{\oplus d_j}. \tag{1.3.25}$$

Combining the decomposition (1.3.22) and (1.3.24) we obtain:

$$L_g R_h = \bigoplus_{j \in \hat{G}} \rho_j(g)^* \otimes \rho_j(h). \tag{1.3.26}$$

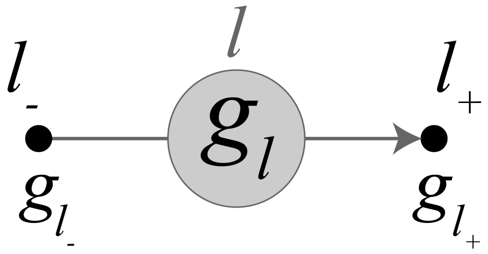

Figure 1.4: In a local gauge transformation we assign to each vertex $\vec{x}$ of the lattice a group element $g(\vec{x})$. The state $|g_l\rangle$ of the link l, in between the sites l_- and l_+, is transformed as $|g_l\rangle \rightarrow |g_{l_-} g_l g_{l_+}^{-1}\rangle$, as in (1.3.28).

1.3.4 Gauge transformation

Gauge transformation operator

Consider now the whole lattice, a local gauge transformation is given by the choice of a group element $g(\vec{x}) \in G$ at every site $\vec{x}$ of the lattice. This transformation acts on the overall Hilbert space $\mathcal{H}_T$ via the operator $\mathcal{G}(\{g(\vec{x})\})$ defined as

$$\mathcal{G}(\{g(\vec{x})\}) = \bigotimes_{(\vec{x},\hat{i})\in E} L_{g(\vec{x})} R_{g(\vec{x}+a\hat{i})} = \bigotimes_{l\in E} L_{g_{l_-}} R_{g_{l_+}}, \tag{1.3.27}$$

where, as per our notation, l_- and l_+ represent respectively the source and the end of the edge l. The decomposition of the operator (1.3.27) in the representation spaces can be found using the expression (1.3.26). The action of the local gauge transformation operator $\mathcal{G}(\{g(\vec{x})\})$ on a single link l state is simply the following (Fig. 1.4):

$$\mathcal{G}(\{g(\vec{x})\})\,|g_l\rangle = |g_{l_-} g_l g_{l_+}^{-1}\rangle\,, \tag{1.3.28}$$

or in the other notation $l = (\vec{x}, \hat{i})$, $l_- = \vec{x}$ and $l_+ = \vec{x} + a\hat{i}$:

$$\mathcal{G}(\{g(\vec{x})\})\,|g(\vec{x},\hat{i})\rangle = |g(\vec{x})g(\vec{x},\hat{i})g(\vec{x}+a\hat{i})^{-1}\rangle\,. \tag{1.3.29}$$

The reason why a local gauge transformation is represented by the operator (1.3.27) is that it provides the correct continuum limit, and now we will show why.
Consider a Lie group G and the expression (1.2.2) for the the group element $g_l = g(\vec{x},\hat{i})$ associated to the link $l = (\vec{x},\hat{i})$ in terms of the gauge field $A_i(\vec{x})$ and neglecting the time dependence of the gauge field. Expanding the exponential in (1.2.2) for small lattice spacing a we have: $g(\vec{x},\hat{i}) = 1 + iaA_i(\vec{x}) + o(a^2)$. Using this expansion and the fact that $g(\vec{x}+a\hat{i})^{-1} =$

$g(\vec{x})^{-1} - a\partial_i g(\vec{x})^{-1} + o(a^2)$ we can see that the transformation (1.3.29) implies:

$$\begin{aligned} g(\vec{x},\hat{\imath}) \to g'(\vec{x},\hat{\imath}) &= g(\vec{x})g(\vec{x},\hat{\imath})g(\vec{x}+a\hat{\imath})^{-1} \\ &= g(\vec{x})g(\vec{x}+a\hat{\imath})^{-1} + iag(\vec{x})A_i(\vec{x})g(\vec{x}+a\hat{\imath})^{-1} + o(a^2) \\ &= 1 + ia\left[g(\vec{x})A_i(\vec{x})g(\vec{x})^{-1} + ig(\vec{x})\partial_i g(\vec{x})^{-1}\right] + o(a^2) \qquad (1.3.30) \\ &= 1 + iaA_i'(\vec{x}) + o(a^2), \qquad (1.3.31) \end{aligned}$$

where in (1.3.30) we recognize the transformation law (1.1.15) of the gauge field A_i' under a local time-independent gauge transformation. From the expression (1.3.31) we verify that in the continuum limit, $a \to 0$, we have $g'(\vec{x},\hat{\imath}) = \exp[iaA_i'(\vec{x})]$, and so that the operator (1.3.29) reproduces the correct transformation law (1.1.15) of the gauge field A_i.

Gauge invariant Hilbert space

In order to be gauge invariant, and so physical, a state of the total Hilbert space $|\psi\rangle \in \mathcal{H}_T$ has to satisfy the so-called Gauss' law constraint:

$$\mathcal{G}(\{g(\vec{x})\})\,|\psi\rangle = |\psi\rangle \quad \forall \{g(\vec{x})\}. \qquad (1.3.32)$$

Clearly not all the states of $\mathcal{H}_T$ satisfy the constraint (1.3.32). The physical gauge invariant Hilbert space then is

$$\mathcal{H}_{\text{phys}} = \{|\psi\rangle : \mathcal{G}(\{g(\vec{x}\})\,|\psi\rangle = |\psi\rangle \;\; \forall\{g(\vec{x})\}\}\,. \qquad (1.3.33)$$

1.4 Lattice gauge theory Hamiltonian

In this section we construct the Kogut-Susskind Hamiltonian, the Hamiltonian for a quantum lattice gauge theory. We examine the two parts of which it is composed: the magnetic Hamiltonian and the electric Hamiltonian. For both we study the continuum limit to be sure that they reproduce the continuum Hamiltonian found in a previous section and also the gauge invariance. Then we pay special attention to the definition of a group Laplacian in the electric Hamiltonian, that in the case of a Lie group is quiet straightforward, while for a finite group there are some ambiguity.

1.4.1 Wilson loop operator

Group element operator

Consider the group element basis $\{|g\rangle\}$ for the single link Hilbert space. One can define the *group element* (or *position*) *operator* $\hat{g}_{mn}$ such that it is diagonal in this basis:

$$\hat{g}_{mn}\,|g\rangle = |g\rangle\,\rho(g)_{mn}, \qquad (1.4.1)$$

where $\rho(g)_{mn}$ is the matrix element in a faithful representation ρ of the group element g. The group element operator $\hat{g}_{mn}$ is not Hermitian, indeed the elements $\rho(g)_{mn}$ are not necessarily real, nor unitary, indeed if one considers the adjoint of the relation (1.4.1):

$$\langle g| (\hat{g}_{mn})^\dagger = \rho(g)^*_{mn} \langle g| , \tag{1.4.2}$$

and looking at the following inner product, combining (1.4.1) and (1.4.2), we can verify that

$$\langle g| (\hat{g}_{mn})^\dagger \hat{g}_{mn} |g\rangle = \rho(g)^*_{mn}\rho(g)_{mn} \langle g|g\rangle \neq \langle g|g\rangle , \tag{1.4.3}$$

while for a unitary operator U one should have $U^\dagger U = \mathbb{I}$.
To solve this problem we can define the matrix operator $\hat{g}$, whose matrix elements are $(\hat{g})_{mn} = \hat{g}_{mn}$, such that

$$(\hat{g})_{mn} |g\rangle = |g\rangle \rho(g)_{mn}. \tag{1.4.4}$$

Being $\hat{g}$ a matrix, when we take its Hermitian conjugate $\hat{g}^\dagger$ one must both transpose its matrix elements (reverse m and n indices) and take the adjoint of them:

$$(\hat{g}^\dagger)_{mn} = (\hat{g}_{nm})^\dagger. \tag{1.4.5}$$

This time if the chosen representation ρ is unitary, so is the operator $\hat{g}$. Indeed we can verify that $\hat{g}^\dagger \hat{g} = \mathbb{I}$ looking at

$$\langle g| \sum_{p=1}^{d_\rho} (\hat{g}^\dagger)_{mp} \hat{g}_{pn} |g\rangle = \sum_{p=1}^{d_\rho} \rho(g)^{*T}_{mp} \rho(g)_{pn} \langle g|g\rangle = \langle g|g\rangle , \tag{1.4.6}$$

where the superscript T indicate the matrix transposition.

Wilson loop operator

Consider the elementary path e passing through an oriented link l of the lattice. There are only two possibilities: either e cross the link in the direction in which the link is oriented, $e \parallel l$, or in the opposite direction, $e \parallel -l$. We can associate to the elementary path e the group element operator $\hat{g}[e]$ defined in this way:

$$\hat{g}[e] = \begin{cases} \hat{g}_l & \text{if } \; e \parallel l \\ \hat{g}_l^\dagger & \text{if } \; e \parallel -l \end{cases} , \tag{1.4.7}$$

where $\hat{g}_l$ is the group element operator for the Hilbert space of the link l, as defined in (1.4.4). Given a global path γ that is the union of many elementary paths e_i, with $i = 1, 2, ..., n$, such that $\gamma = e_1 e_2 ... e_n$, we can define the group element operator associated to this path as

$$\hat{g}[\gamma] = \hat{g}[e_1]\hat{g}[e_2]...\hat{g}[e_n]. \tag{1.4.8}$$

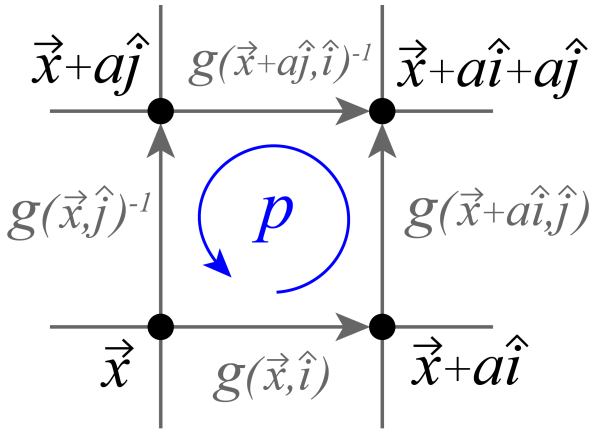

Figure 1.5: Wilson loop operator $\mathrm{Tr}\,\hat{W}_p$ (1.4.10).

If the path $\gamma = e_1 e_2 ... e_n$ is closed we can define the *Wilson loop operator* as

$$\mathrm{Tr}\,\hat{W}[\gamma] = \mathrm{Tr}(\hat{g}[e_1]\hat{g}[e_2]...\hat{g}[e_n]). \tag{1.4.9}$$

For example, if γ corresponds to the boundaries of a plaquette p in a $d = 2$ dimensional lattice as in Fig. 1.5 the corresponding Wilson loop operator is

$$\mathrm{Tr}\,\hat{W}_p = \mathrm{Tr}\Big(\hat{g}(x,\hat{i})\hat{g}(x + a\hat{i},\hat{j})\hat{g}(x + a\hat{j},\hat{i})^\dagger\hat{g}(x,\hat{j})^\dagger\Big), \tag{1.4.10}$$

where $\hat{i}, \hat{j}$ are the two orthogonal unit vector-directions of the square lattice, a is the lattice spacing and by $\hat{g}(\vec{x},\hat{i})$ we mean the group element operator associated to the link that starts in $\vec{x}$ and it is parallel to $\hat{i}$, as per the notation previously introduced.
The Wilson loop operator plays a central role in the construction of the magnetic part of the Hamiltonian for a Yang-Mills theory on a lattice. Wilson loops are also interesting observables to study and measure with a quantum simulation since they are sensitive to topological phase transitions and are order parameters per the confined-deconfined transition [33].

1.4.2 Magnetic Hamiltonian

We define the magnetic Hamiltonian H_B as the sum over all Wilson loop operators of all plaquettes p of the lattice:

$$H_B = -\frac{2}{g^2 a^{4-d}} \sum_p \mathrm{Re}\,\mathrm{Tr}\,\hat{W}_p. \tag{1.4.11}$$

It is possible to prove that the magnetic Hamiltonian (1.4.11) is indeed the spatial discretized version of the magnetic part of the Yang-Mills continuum Hamiltonian H_{YM} (1.1.18) up to $o(a^2)$. To verify this assertion consider a $d = 2$ dimensional square lattice, where the links are oriented parallel to the unit vectors $\hat{i}$ and $\hat{j}$, consider then a plaquette p with origin in the point $\vec{x}$. The expression of the Wilson loop operator $\mathrm{Tr}\,\hat{W}_p$ for the plaquette p is given in the equation (1.4.10). Recall the action (1.4.4) of the group element operator $\hat{g}_l$ on the group element basis $\{|g_l\rangle\}$ of the corresponding link, then the action of the Wilson loop operator $\mathrm{Tr}\,\hat{W}_p$ (1.4.10) on the group element basis is

$$\mathrm{Tr}\,\hat{W}_p = \mathrm{Tr}\Big[g(\vec{x},\hat{i})g(\vec{x}+a\hat{i},\hat{j})g(\vec{x}+a\hat{j},\hat{i})^{-1}g(\vec{x},\hat{j})^{-1}\Big], \tag{1.4.12}$$

where not to be pedantic we have left out the representation ρ through which we should evaluate the trace of the group elements. Now we reintroduce the gauge field A_μ by using the relation (1.2.2) and the fact that $A_j(\vec{x}+a\hat{i}) \simeq A_j(\vec{x}) + a\partial_i A_j(\vec{x})$, we can rewrite (1.4.12) as

$$\mathrm{Tr}\,\hat{W}_p = \mathrm{Tr}\big[\, e^{iaA_i(\vec{x})}e^{ia(A_j(\vec{x})+a\partial_i A_j(\vec{x}))}e^{-ia(A_i(\vec{x})+a\partial_j A_i(\vec{x}))}e^{-iaA_j(\vec{x})}\big]. \tag{1.4.13}$$

Applying twice the Baker–Campbell–Hausdorff formula $e^A e^B = eA + B + \frac{1}{2}[A,B] + ...$ [51] and neglecting all the terms of order $o(a^3)$, that is reasonable in the limit of a small lattice spacing a, the equation (1.4.13) becomes

$$\begin{aligned}\mathrm{Tr}\,\hat{W}_p &= \mathrm{Tr}\Big[e^{ia\left(A_i(\vec{x})+A_j(\vec{x})+a\partial_i A_j(\vec{x})+\frac{ia}{2}[A_i(\vec{x}),A_j(\vec{x})]\right)}e^{-ia\left(A_i(\vec{x})+A_j(\vec{x})+a\partial_j A_i(\vec{x})-\frac{ia}{2}[A_i(\vec{x}),A_j(\vec{x})]\right)}\Big]\\ &= \mathrm{Tr}\Big[e^{ia^2(\partial_i A_j(\vec{x})+a\partial_j A_i(\vec{x})+i[A_i(\vec{x}),A_j(\vec{x})])}\Big].\end{aligned} \tag{1.4.14}$$

We can now introduce in (1.4.14) the field strength F_{ij} (1.1.5) (in its spatial components) , getting to:

$$\begin{aligned}\mathrm{Tr}\,\hat{W}_p &= \mathrm{Tr}\Big[e^{ia^2F_{ij}(\vec{x})}\Big]\\ &= \mathrm{Tr}\left[\mathbb{I} + ia^2F_{ij}(\vec{x}) - \frac{a^4}{2}F_{ij}(\vec{x})F_{ij}(\vec{x})\right],\end{aligned} \tag{1.4.15}$$

where we expanded the exponential for small values of the exponent. The trace is linear, so proceeding terms by terms in the expression (1.4.15): the trace of the identity matrix $\mathbb{I}$ is always a constant and it can be neglected in a Hamiltonian, while for a simple Lie algebra the field strength F_{ij} is traceless in any representation, since $\mathrm{Tr}(F_{ij}) = F^a_{ij}\,\mathrm{Tr}(T_a) = 0$. These considerations leads to rewrite (1.4.15) as

$$\mathrm{Tr}\,\hat{W}_p = -\frac{a^4}{2}\,\mathrm{Tr}[F_{ij}(\vec{x})F_{ij}(\vec{x})]. \tag{1.4.16}$$

We can then use the relation $F_{ij}F_{ij} = 2B_kB_k$ and the Killing metric (1.1.3) to remove the trace, and what we get at the end is

$$\mathrm{Tr}\,\hat{W}_p = -\frac{a^4}{2}B^i_a(\vec{x})B^i_a(\vec{x}) + o(a^6). \tag{1.4.17}$$

If one substitutes the final expression (1.4.17) inside the relation (3.3.18) for the lattice magnetic Hamiltonian H_B we get exactly the same expression that we had for the continuous magnetic Hamiltonian in (1.1.18), as long as we change the discrete sum over the plaquettes $\sum_p$ into an integral $\int d^d x$. Lastly notice that the real part Re in (3.3.18) is needed because the subleading terms in (1.4.17) may not be real.

1.4.3 Electric Hamiltonian

Consider now the electric term in the continuum Yang-Mills Hamiltonian H_{YM} (1.1.18). Upon the quantization the electric term consists of the momentum fields operator $\hat{\pi}^i_a$, that as we saw in (1.1.20), generates the translations on the space of wavefunctionals $\psi[\vec{A}]$. On a lattice we don't have this space, but a tensor product of all group algebra attached to each link. For this reason we may imagine that in a lattice gauge theory the electric Hamiltonian involves the generators of translations on the group algebra. We have already seen that for a single link Hilbert space the left translations on a group G are implemented by the operators L_g (1.3.8). If the group G is a Lie group, we have also seen which are the generators $\mathfrak{L}_a$ (1.3.15) of the translations on the Lie algebra $\mathfrak{g}$. So the operators $\mathfrak{L}_a$ play the role of the momenta $\hat{\pi}^i_a$ in the lattice Hamiltonian. Notice that while the momenta field operators $\hat{\pi}^i_a(x)$ have two indices: the color index a and the spatial component index i, the operators $\mathfrak{L}_a(l)$ have only a color index a, that because the spatial orientation is implicit in the link $l = (\vec{x}, \hat{i})$ to which they belong to. In the light of these considerations, for a Lie gauge group in a lattice the electric term is

$$H_E = \frac{g^2}{2a^{d-2}} \sum_{l \in E} \sum_{a=1}^{d_G} \mathfrak{L}_a(l)^2 \tag{1.4.18}$$

This Hamiltonian provides the correct continuum limit, indeed one can verify that [35]:

$$\mathfrak{L}_a(\vec{x}, \hat{i}) = -a^{d-1} \hat{\pi}^i_a(\vec{x})[1 + o(a)] \tag{1.4.19}$$

Lie group Laplacian

For a Lie group G one can define the Laplacian Δ_l at link l as

$$\Delta_l = \sum_{a=1}^{d_G} \mathfrak{L}_a(l)^2, \tag{1.4.20}$$

where the name "Laplacian" is chosen in analogy with ordinary quantum mechanics, where the square of the momentum operator $\hat{p}$ (or the generator of translation) is indeed the ordinary Laplacian operator. The operator (1.4.20) is also called Laplacace-Beltrami operator on the group manifold G [30]. In terms of the group Laplacian the electric Hamiltonian (1.4.18) becomes:

$$H_E = \frac{g^2}{2a^{d-2}} \sum_{l \in E} \Delta_l \tag{1.4.21}$$

Notice that the definition of the group Laplacian (1.4.20) is possible only if the gauge symmetry has a Lie algebra $\mathfrak{g}$, where the generators $\mathfrak{L}_a$ live. For this reason for a finite group the definition of the Laplacian, and thus the electric term, is more complicated and it will be discussed in the next section.

Group Laplacian in representation basis

Consider a compact Lie group G and its Lie algebra $\mathfrak{g}$. Let ρ_j be a Lie group representation of G, then there exists a corresponding Lie algebra representation $\tilde{\rho}_j$ of $\mathfrak{g}$. These two representations are related by the following relation [27]:

$$\tilde{\rho}_j(X) = -i\,\frac{d}{d\epsilon}\rho_j(e^{i\epsilon X})\bigg|_{\epsilon=0} \quad \forall X \in \mathfrak{g}. \tag{1.4.22}$$

Recall that in the Peter-Weyl decomposition the left translation operator L_g can be written as (1.3.22), and that $\mathfrak{L}_a$ is the regular Lie algebra representation of the generator T_a (1.3.15), using these results and the equation (1.4.22) we can see that

$$\begin{aligned}
\mathfrak{L}_a &= -i\,\frac{d}{d\epsilon}L_{e^{i\epsilon T_a}}\bigg|_{\epsilon=0} \\
&= -i\bigoplus_{j\in\hat{G}}\frac{d}{d\epsilon}\rho_j(e^{i\epsilon T_a})^* \otimes \mathbb{I}_j\bigg|_{\epsilon=0} \\
&= \bigoplus_{j\in\hat{G}}\tilde{\rho}_j(T_a)^* \otimes \mathbb{I}_j \\
&= \bigoplus_{j\in\hat{G}} -\tilde{\rho}_j(T_a)^T \otimes \mathbb{I}_j
\end{aligned} \tag{1.4.23}$$

where in the last line we used the fact that the dual Lie algebra representation is $\tilde{\rho}^* = -\tilde{\rho}^T$, that comes directly from $\rho(g)^* = \rho(g^{-1})^T$ and (1.4.22).
Consider now the Laplacian (1.4.20) for the Hilbert space of a single link, and insert the equation (1.4.23):

$$\begin{aligned}
\Delta = \sum_{a=1}^{d_G}\mathfrak{L}_a^2 &= \sum_{a=1}^{d_G}\bigoplus_{j\in\hat{G}}\tilde{\rho}_j(T_a)^T\tilde{\rho}_j(T_a)^T \otimes \mathbb{I}_j \\
&= \bigoplus_{j\in\hat{G}}\sum_{a,b=1}^{d_G}\delta_{a,b}\tilde{\rho}_j^T(T_a)\tilde{\rho}_j^T(T_a) \otimes \mathbb{I}_j.
\end{aligned} \tag{1.4.24}$$

Recall the definition of the Casimir element as $\Omega = \sum_{a,b} B(T_a, T_b)T_aT_b$, where B is the Killing form [27]. For a compact group the Killing form is proportional to $\delta_{a,b}$, so we recognize that the right-hand side of the equation (1.4.24) is proportional to the Casimir operator on each representation subspace $C(j) = \tilde{\rho}_j(\Omega)^T$. We can then write

$$\Delta = \sum_{j \in \hat{G}} C(j) \mathbb{P}_j, \tag{1.4.25}$$

where $\mathbb{P}_j$ is the projector on the j-th representation subspace V_j:

$$\mathbb{P}_j = \sum_{m,n=1}^{d_j} |j_{mn}\rangle \langle j_{mn}| \tag{1.4.26}$$

Looking at the explicit expression of the projectors is trivial to say that the group Laplacian (1.4.25) is diagonal in the representation basis $\{|j_{mn}\rangle\}$, and therefore the electric Hamiltonian H_E (1.4.18). One can also verify that the projectors $\mathbb{P}_j$ are gauge invariant, and therefore the Laplacian is too. A proof of this result is presented in section 1.4.5 for a finite gauge group, but it is completely equivalent also for a Lie group.

1.4.4 Finite group Laplacian

The expression (1.4.25) for the group Laplacian was found under the assumption that the gauge group G was a compact Lie group, nevertheless we can try to generalize this expression also to the case of finite groups, indeed it is possible to define the representation basis $\{|j_{mn}\rangle\}$ and the projectors $\mathbb{P}_j$ also in the latter case. We define the finite group Laplacian as

$$\Delta = \sum_{j \in \hat{G}} f(j) \mathbb{P}_j, \tag{1.4.27}$$

where $f(j)$ is an arbitrary function of the representation j only and plays the role of the Casimir operator $C(j)$, which in the finite group case is not present. It easy to verify, like for the Lie group Laplacian, that also the finite group Laplacian (1.4.27) is gauge invariant.
Even if the choice of the function $f(j)$ appearing in the finite group Laplacian (1.4.27) remains undetermined we can constraint it with some properties that it should satisfy. The function $f(j)$, representing an energy density, should be positive semi-definite, and it should be zero only for the trivial representation $j = 0$. If the finite group under study can be seen as the discretization of a Lie group, one can also impose that the function $f(j)$ of the finite group approximates the Casimir operator $C(j)$ of the corresponding Lie group.
A method to construct a finite group Laplacian satisfying these requirements has been proposed in [36] and we are going to illustrate it. This method is based on the choice of a generating subset Γ for the group G under study, the construction of the corresponding Cayley graph (G, Γ) and then the definition of the Laplacian Δ of this graph. Let's examine this procedure in details.

Generating subset

Given a finite group G, let choose a generating subset $\Gamma \subset G$ that satisfies the following properties:

1. Γ is a set of generators of the group G. That means that every element of the group G can be written as the product of one or more elements of the generating subset Γ.
2. Γ is invariant under inversion of group element (symmetric), $\Gamma = \Gamma^{-1}$, that means that $\forall k \in \Gamma, \;\; k^{-1} \in \Gamma$.
3. Γ is invariant under conjugation, $\Gamma = g\Gamma g^{-1}$, that means that $\forall k \in \Gamma, g \in G \;\; gkg^{-1} \in \Gamma$. In other words Γ is the union of conjugacy classes of G.
4. Γ does not contain the identity element $e \notin \Gamma$.

The reasons why we require these properties will be clear proceeding in the discussion. Notice that the previous constraints are not sufficient to make the choice of such a subset Γ unique, each possibility produces a different theory. This means that the group G of gauge symmetry does not fix completely the theory, several models with different energetic eigenvalues (especially in the electric Hamiltonian) are possible and can be considered through the choice of different generating subset Γ.

Cayley graph

Consider a finite group G and a subset $\Gamma \subset G$. We can define the Cayley graph (G, Γ) as the graph where the vertices are the elements of the group G, while two vertices (group elements) are linked by an edge if from one we can reach the other by a right multiplication of an element of the generating set Γ. In other words, given the vertices $g, h \in G$ we connect them with an edge if and only if there exists $k \in \Gamma$ such that $h = gk$, or equivalently if $g^{-1}h \in \Gamma$. In the figures Fig. 1.6a and Fig. 1.6b you can see two examples of directed Cayley graphs. The four conditions that we imposed on the generating subset Γ guarantee some interesting properties for the corresponding Cayley graph (G, Γ). First, the fact that Γ contains the generators of the group ensures that there are no isolated sub-graphs in the graph. The fact that Γ is symmetric means that if there is a directed edge connecting the vertex g to h, there is also a directed edge connecting h to g. In the following we will consider these two directed edges as a unique undirected edge. Finally the fact that $e \notin \Gamma$ exclude the presence of self-loops around each vertex. These properties cause the Cayley graph (G, Γ) to be simple, without multiple edges and loops.

Adjacency matrix

Given a graph with n vertices we define the $n \times n$ adjacency matrix A as the matrix that indicate whether pairs of vertices are adjacent or not in the graph. In particular we have that the matrix

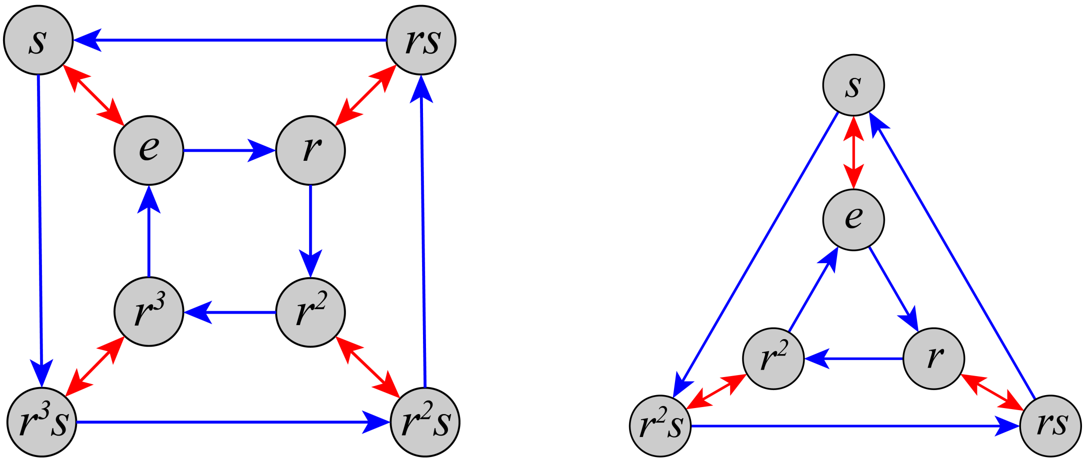

(a) Directed Cayley graph of $(D_4, \{r, s\})$. For more information about this group see the section 3.1.

(b) Directed Cayley graph of $(D_3, \{r, s\})$. For more information about this group see the section 3.2.

Figure 1.6: Two examples of directed Cayley graph. Each vertex represents an element of the group, D_4 or D_3. A directed blue link connecting the vertex g to the vertex h means that $gr = h$, while a directed red link connecting the vertex g to the vertex h means that $gs = h$.

element A_{ij} is 1 if the vertices i and j are connected by an edge, while it is 0 otherwise. For the Cayley graph (G, Γ) the matrix elements of the adjacency matrix A are

$$A_{gh} = \begin{cases} 1 & \text{if } g^{-1}h \in \Gamma \\ 0 & \text{otherwise} \end{cases} = \sum_{k \in \Gamma} \delta(g^{-1}h, k). \tag{1.4.28}$$

We can see the adjacency matrix A as an operator on the group algebra $\mathbb{C}[G]$. Given a function $f : G \to \mathbb{C}$, that assigns a complex number to each group element, one can define the action of the adjacency matrix on this function as

$$Af(g) = \sum_{h \in G} A_{gh} f(h). \tag{1.4.29}$$

A convenient way to see the action of the adjacency matrix A on the group algebra function f is the following: consider a graph with $|G|$ vertices, the adjacency matrix A is a $|G| \times |G|$ matrix, while f is a column vector of $|G|$ elements, where the g-entry is given by $f_g = f(g)$. The product of the two is Af, while $Af(g)$ (1.4.29) is g-th entry of the product vector Af. Given the adjacency matrix (1.4.28) for the graph (G, Γ) we can see that

$$Af(g) = \sum_{k \in \Gamma} f(gk). \tag{1.4.30}$$

Consider now the right regular representation R_g and its action on a generic function $\psi : G \to \mathbb{C}$ of the group algebra, it is possible to prove that

$$R_g\psi(h) = \psi(hg). \tag{1.4.31}$$

This can be easily shown considering the action of R_g on a group element basis state $|h\rangle$ (1.3.9), and then a generic state $|\psi\rangle$ (1.3.6) for $\psi \in \mathbb{C}[G]$ such that

$$R_g |\psi\rangle = \sum_{h\in G} \psi(h)R_g |h\rangle = \sum_{h\in G} \psi(h) |hg^{-1}\rangle = \sum_{h\in G} \psi(hg) |h\rangle , \tag{1.4.32}$$

and from that we verify the expression (1.4.31). Using the results (1.4.31) and (1.4.30), we can write

$$A = \sum_{k\in\Gamma} R_k. \tag{1.4.33}$$

One can verify that for any $g \in G$ the adjacency matrix A and the right translation operator R_g commute, indeed

$$\begin{aligned} AR_g &= \sum_{k\in\Gamma} R_k R_g = \sum_{k\in\Gamma} R_{kg} \\ &= \sum_{k\in\Gamma} R_{(gkg^{-1})g} = \sum_{k\in\Gamma} R_{gk} = R_g A, \end{aligned} \tag{1.4.34}$$

where we used the fact that Γ is closed under conjugation and so the element gkg^{-1} is inside Γ as well as k. Recall that from the Peter-Weyl decomposition we can write the right regular representation as in (1.3.25), therefore on a specific representation space V_j, the right regular representation is an irreducible representation $R|_{V_j} = \rho_j^{\oplus d_j}$ and from (1.4.34) it commutes with the adjacency matrix A. Given these two hypothesis we can then apply the Schur's lemma and say that the adjacency matrix is proportional to the identity on each representation subspace V_j (spanned by $\{|j_{mn}\rangle : 1 \leq m, n \leq d_j\}$), such that

$$A = \sum_{j\in\hat{G}} a(j)\mathbb{P}_j, \tag{1.4.35}$$

where $a(j)$ is a function of the representation j only and $\mathbb{P}_j$ is the projector on the V_j subspace defined in (1.4.26). Using the decomposition (1.3.25) we can also write A as

$$A = \sum_{k\in\Gamma} R_k = \bigoplus_{j\in\hat{G}} \sum_{k\in\Gamma} \rho_j(k)^{\oplus d_j} \tag{1.4.36}$$

Taking the trace of the expressions (1.4.35) we see that $\operatorname{Tr} A = \sum_j a(j)d_j^2$, while from the trace of the expression (1.4.36) we have $\operatorname{Tr} A = \sum_j d_j \sum_k \chi_j(k)$, where $\chi_j(k) = \operatorname{Tr}\rho_j(k)$ is the character function of the j-th representation. Comparing these two traces we derive the explicit expression of the eigenvalues $a(j)$ of the adjacency matrix, that are

$$a(j) = \frac{1}{d_j} \sum_{k \in \Gamma} \chi_j(k). \tag{1.4.37}$$

The adjacency matrix (1.4.35) with eigenvalues (1.4.37) is a key ingredient for the Laplacian of the graph (G, Γ).

Laplacian of a graph

There are various way in which one can introduce a discrete Laplacian Δ for a graph, differing by sign and scale factor, we present the traditional definition [13]. Given the graph (G, Γ) and a function $\psi : G \to \mathbb{C}$, we define the Laplacian Δ as

$$\Delta\psi(g) = \sum_{k \in \Gamma} [\psi(g) - \psi(gk)], \tag{1.4.38}$$

where to compute the Laplacian of the function ψ in the vertex g we are taking the difference between ψ evaluated in g and ψ evaluated in a nearest-neighbor vertex gk with $k \in \Gamma$, then we sum over all nearest neighbours.
It is not difficult to see that the graph Laplacian (1.4.38) for a simple graph as (G, Γ) has the matrix form:

$$\Delta = D - A, \tag{1.4.39}$$

where D is the degree matrix and A is the adjacency matrix (1.4.28) of the graph. The degree matrix D is a $|G| \times |G|$ diagonal matrix, with $|G|$ representing the number of vertices in the graph. The matrix element D_{gg} is the degree of the vertex g, i.e. the number of edges that it is connected to. In our case we have that $D_{gg} = |\Gamma|$. Therefore, putting together the expressions (1.4.39) and (1.4.35), we can write the graph Laplacian as

$$\Delta = \sum_{j \in \hat{G}} f(j) \mathbb{P}_j, \tag{1.4.40}$$

where $f(j)$ is defined by

$$f(j) = |\Gamma| - \frac{1}{d_j} \sum_{k \in \Gamma} \chi_j(k). \tag{1.4.41}$$

This is the expression of the finite group Laplacian on the Hilbert space $\mathbb{C}[G]$ of a single link that we will use inside the electric Hamiltonian (1.4.21) obtaining:

$$H_E = \frac{g^2}{2a^{d-2}} \sum_{l \in E} \sum_{j \in \hat{G}} f(j) \mathbb{P}_j(l). \tag{1.4.42}$$

1.4.5 Kogut-Susskind Hamiltonian

The Hamiltonian of a pure Yang-Mills theory on a lattice is called Kogut-Susskind Hamiltonian [28], putting together the electric (1.4.42) and magnetic (1.4.11) terms we see that it is given by

$$H_{\mathrm{KS}} = \frac{g^2}{2a^{d-2}} \sum_{l \in E} \sum_{j \in \hat{G}} f(j) \mathbb{P}_j(l) - \frac{2}{g^2 a^{4-d}} \sum_p \operatorname{Re} \operatorname{Tr} \hat{W}_p, \tag{1.4.43}$$

where the function $f(j)$ is the the Casimir operator $C(j)$ for a compact Lie group, while it is the function (1.4.41) for a finite group. The electric term H_E is diagonal in the representation (momentum) basis $\{|j_{mn}\rangle\}$ while the magnetic term H_B is diagonal in the group element (position) basis $\{|g\rangle\}$.

Different parametrization

For what concerns the coupling constants, in the expression (1.4.43) of the Kogut-Susskind Hamiltonian there is the coupling g that we had in the continuum limit (1.1.18) together with dimensional corrections with the lattice spacing a. In the following chapters we often use different parametrizations for the coupling.
One possibility is to define two independent coupling constants: $\lambda_E = g^2/2a^{d-2}$ for the electric Hamiltonian and $\lambda_B = 1/g^2 a^{4-d}$ for the magnetic Hamiltonian. Using these two couplings the expression (1.4.43) becomes:

$$H_{\mathrm{KS}} = \lambda_E \sum_{l \in E} \sum_{j \in \hat{G}} f(j) \mathbb{P}_j(l) - 2\lambda_B \sum_p \operatorname{Re} \operatorname{Tr} \hat{W}_p. \tag{1.4.44}$$

In order to visualize better both the electric ($\lambda_B = 0$) and the magnetic limit ($\lambda_E = 0$) one can use the following parametrization of the coupling constants

$$H_{\mathrm{KS}} = \lambda \sum_{l \in E} \sum_{j \in \hat{G}} f(j) \mathbb{P}_j(l) - 2(1-\lambda) \sum_p \operatorname{Re} \operatorname{Tr} \hat{W}_p \tag{1.4.45}$$

where $\lambda \in [0,1]$ and $\lambda = \lambda_E/(\lambda_E + \lambda_B)$. In this way, a part from a multiplicative factor J, we are able to reproduce any combinations of the two coupling constants, $\lambda_E = J\lambda$ and $\lambda_B = J(1-\lambda)$.

Gauge invariance

We can prove that the Kogut-Susskind Hamiltonian (1.4.43) is gauge invariant, indeed both the electric and the magnetic Hamiltonians are gauge invariant. Let us prove this.
Let's start by considering the magnetic Hamiltonian H_B (1.4.11). This Hamiltonian is the sum of Wilson plaquette operators $\operatorname{Tr} \hat{W}_p$ (1.4.10), so in order to prove gauge invariance it is sufficient to prove that for any plaquette p the gauge transformation operator $\mathcal{G}_p = \otimes_{l \in p} L_{g_{l_-}} R_{g_{l_+}}$

(1.3.27) for that specific plaquette commutes with the corresponding Wilson loop operator $\mathrm{Tr}\,\hat{W}_p$. The action of gauge transformation $\mathcal{G}_p$ is shown in Fig. 1.7. The commutation relation can be easily checked on the group element basis $|g_1, g_2, g_3, g_4\rangle$ of the plaquette p. Indeed, one has:

$$\begin{aligned}
\mathrm{Tr}\,\hat{W}_p\mathcal{G}_p\,|g_1,g_2,g_3,g_4\rangle &= \mathrm{Tr}\,\hat{W}_p\,|g_{v_1}g_1g_{v_2}^{-1}, g_{v_2}g_2g_{v_3}^{-1}, g_{v_4}g_3g_{v_3}^{-1}, g_{v_1}g_4g_{v_4}^{-1}\rangle \\
&= \mathrm{Tr}\left[g_{v_1}g_1g_2g_3^{-1}g_4^{-1}g_{v_1}^{-1}\right]|g_{v_1}g_1g_{v_2}^{-1}, g_{v_2}g_2g_{v_3}^{-1}, g_{v_4}g_3g_{v_3}^{-1}, g_{v_1}g_4g_{v_4}^{-1}\rangle \\
&= \mathrm{Tr}\left[g_1g_2g_3^{-1}g_4^{-1}\right]|g_{v_1}g_1g_{v_2}^{-1}, g_{v_2}g_2g_{v_3}^{-1}, g_{v_4}g_3g_{v_3}^{-1}, g_{v_1}g_4g_{v_4}^{-1}\rangle\,,
\end{aligned} \tag{1.4.46}$$

where we omitted the representation ρ through which we should evaluate the trace of the group elements, and in (1.4.46) we used the cyclic property of the trace. Similarly we have:

$$\begin{aligned}
\mathcal{G}_p\,\mathrm{Tr}\,\hat{W}_p\,|g_1,g_2,g_3,g_4\rangle &= \mathrm{Tr}\left[g_1g_2g_3^{-1}g_4^{-1}\right]\mathcal{G}_p\,|g_1,g_2,g_3,g_4\rangle \\
&= \mathrm{Tr}\left[g_1g_2g_3^{-1}g_4^{-1}\right]|g_{v_1}g_1g_{v_2}^{-1}, g_{v_2}g_2g_{v_3}^{-1}, g_{v_4}g_3g_{v_3}^{-1}, g_{v_1}g_4g_{v_4}^{-1}\rangle\,.
\end{aligned} \tag{1.4.47}$$

Comparing the expressions (1.4.46) and (1.4.47) we see that the operators $\mathcal{G}_p$ and $\mathrm{Tr}\,\hat{W}_p$ commute. This means that the Wilson plaquette operator $\mathrm{Tr}\,\hat{W}_p$ is gauge invariant and the magnetic Hamiltonian as well.
Let us now verify if the projector operators $\mathbb{P}_j$ (1.4.26), and hence the Laplacian Δ (1.4.27) and also the electric Hamiltonian H_E (1.4.21) are gauge invariant or not.
Let consider the Hilbert space $\mathcal{H}^{(l)}$ of a single link, a state $|j_{mn}\rangle$ of the representation basis and the action of the gauge transformation L_gR_h, as in (1.3.27):

$$L_gR_h\,|j_{mn}\rangle = \sqrt{\frac{d_j}{|G|}}\sum_{k\in G}\rho_j(k)_{mn}L_gR_h\,|k\rangle \tag{1.4.48}$$

$$\begin{aligned}
&= \sqrt{\frac{d_j}{|G|}}\sum_{k\in G}\rho_j(g^{-1}kh)_{mn}\,|k\rangle \\
&= \sqrt{\frac{d_j}{|G|}}\sum_{k\in G}\sum_{p,q=1}^{d_j}\rho_j(g^{-1})_{mp}\rho_j(k)_{pq}\rho_j(h)_{qn}\,|k\rangle \\
&= \sum_{p,q=1}^{d_j}\rho_j(g^{-1})_{mp}\rho_j(h)_{qn}\,|j_{pq}\rangle\,,
\end{aligned} \tag{1.4.49}$$

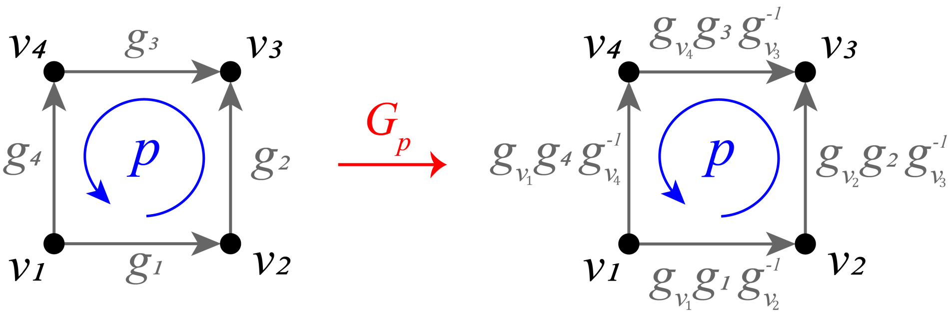

Figure 1.7: Action of the gauge transformation $\mathcal{G}_p$ (1.3.27) on a single plaquette p.

where in (1.4.48) and (1.4.49) we used the duality relation (1.3.20). The gauge transformation $L_g R_h$ transforms the projector $\mathbb{P}_j$ (1.4.26) as:

$$
\begin{aligned}
(L_g R_h)\mathbb{P}_j(L_g R_h)^\dagger &= \sum_{m,n=1}^{d_j} (L_g R_h) \left|j_{mn}\right\rangle \left\langle j_{mn}\right| (L_g R_h)^\dagger \\
&= \sum_{m,n=1}^{d_j} \sum_{p,q=1}^{d_j} \sum_{r,s=1}^{d_j} \rho_j(g^{-1})_{mp} \rho_j(h)_{qn} \rho_j(g^{-1})^*_{mr} \rho_j(h)^*_{sn} \left|j_{pq}\right\rangle \left\langle j_{rs}\right| \\
&= \sum_{m,n=1}^{d_j} \sum_{p,q=1}^{d_j} \sum_{r,s=1}^{d_j} \rho_j(g)_{rm} \rho_j(g^{-1})_{mp} \rho_j(h)_{qn} \rho_j(h^{-1})_{ns} \left|j_{pq}\right\rangle \left\langle j_{rs}\right| \\
&= \sum_{p,q=1}^{d_j} \sum_{r,s=1}^{d_j} \delta_{r,p} \delta_{q,s} \left|j_{pq}\right\rangle \left\langle j_{rs}\right| \\
&= \sum_{p,q=1}^{d_j} \left|j_{pq}\right\rangle \left\langle j_{pq}\right| = \mathbb{P}_j,
\end{aligned}
\tag{1.4.50}
$$

that proves that the projector $\mathbb{P}_j$ is gauge invariant, hence the Laplacian Δ (1.4.25) and the electric Hamiltonian H_E (1.4.21) as well.

1.5 Plaquette and vertex operators

In this sections we introduce two useful objects that we will use in the following: the vertex operator and the plaquette operator, looking also at their commutation relations. The vertex operator can be used to define a gauge transformation, while the plaquette operator is particularly useful to introduce plaquette states, as we will see in section 3.3.1. These two operators

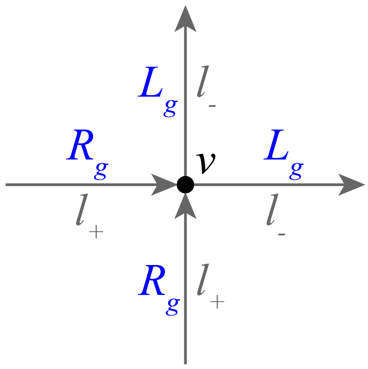

Figure 1.8: Graphical representation of the vertex operator A_v^g (1.5.1). Given a group element $g \in G$ and a vertex v of the lattice, the vertex operator A_v^g acts on the Hilbert spaces of the links connected to v, with the operator L_g if v is the source of the corresponding link ($v = l_-$), and with R_g if v is the target of the corresponding link ($v = l_+$).

can be used also to discuss the quantum double model, a model related to the lattice gauge theory we are interested in.

1.5.1 Vertex operator

Consider a vertex v of the lattice Λ (1.2.1) and a group element $g \in G$, we define the *vertex operator* A_v^g as

$$A_v^g = \bigotimes_{v=l_-} L_g(l) \bigotimes_{v=l_+} R_g(l). \tag{1.5.1}$$

In other words the vertex operator A_v^g (1.5.1) acts on the Hilbert spaces of the oriented edges l connected to the vertex v, with the left translation operator L_g (1.3.8) if the vertex is the source of the link $v = l_-$, with the right translation operator R_g (1.3.9) if the vertex is the target of the link $v = l_+$. A pictorial representation of the operator is shown in Fig. 1.8.

Gauge transformation

We can use the vertex operators to write the gauge transformation operator $\mathcal{G}(\{g_v\})$ (1.3.27) as

$$\mathcal{G}(\{g_v\}) = \bigotimes_{v \in V} A_v^{g_v}, \tag{1.5.2}$$

where we assign a group element g_v to each site v of the lattice, and the tensor product is extended to all vertices V.

1.5.2 Plaquette operator

Consider an oriented plaquette p of a square lattice and a group element $g \in G$, we define the *plaquette operator* B_p^g as

$$B_p^g = \sum_{g_1,g_2,g_3,g_4 \in G} \delta(g, g_1 g_2 g_3^{-1} g_4^{-1}) \mathbb{P}_{g_1}(l_1) \mathbb{P}_{g_2}(l_2) \mathbb{P}_{g_3}(l_3) \mathbb{P}_{g_4}(l_4), \tag{1.5.3}$$

where $\mathbb{P}_g(l)$ is the projector $|g\rangle\langle g|$ in the Hilbert space of the link l, while l_1, l_2, l_3, l_4 are the four edges of the plaquette p, as shown in Fig. 1.9. It easy to see that the plaquette operator is a projector with eigenvalues 0 and 1, indeed $(B_p^g)^2 = B_p^g$. The action of the plaquette operator B_p^g consists in selecting those states that have a group element g assigned to the plaquette p. In other words a state $|g_1, g_2, g_3, g_4\rangle$, in order not to be annihilated by this projector, must have the product of the group elements g_l associated to each edge l equal to g, so $g = g_1 g_2 g_3^{-1} g_4^{-1}$. Notice that links crossed in the opposite direction with respect to their orientation appear with the inverse of their group element. Using the plaquette operator (1.5.3) we can write the Wilson loop $\mathrm{Tr}\, \hat{W}_p$ (3.3.30) for a single plaquette as

$$\mathrm{Tr}\, \hat{W}_p = \sum_{g \in G} B_p^g \chi_F(g), \tag{1.5.4}$$

where χ_F is the character of the faithful representation F.
The plaquette operator can be generalized to a generic closed path γ that surround more than one plaquette. In this case we have:

$$B_\gamma^g = \sum_{g_1,g_2,\ldots,g_m} \delta\left(g, \prod_{l \in \gamma} g[l]\right) \bigotimes_{l \in \gamma} \mathbb{P}_{g_l}(l), \tag{1.5.5}$$

where the path γ contains m edges, $g_1, g_2, \ldots, g_m$ are the group elements associated to the links of the path γ, while $g[l]$ is equal to g_l if the path γ is parallel to the link l, while it is equal to g_l^{-1} if γ is anti-parallel to l.

1.5.3 Commutation relations

Let us now consider the commutation rules between the operators that we have just introduced. Given two group elements $g, h \in G$ and two vertices $v, u \in V$, the vertex operators A_v^g and A_u^h commute whenever they are applied on different vertices, $v \neq u$. In order to prove that notice that A_v^g and A_u^h, besides the trivial case, have at most one edge in common, in that case they act one with the left L_g and one with the right R_h regular representation, and these operators commute, as you can easily see from their expressions (1.3.22) and (1.3.24). So we have that

$$[A_v^g, A_u^h] = 0 \quad \text{if} \;\; v \neq u. \tag{1.5.6}$$

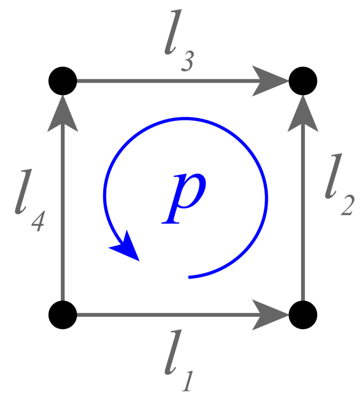

Figure 1.9: An oriented plaquette p with its 4 oriented links l_1, l_2, l_3, l_4.

The situation is different if the vertex operators A_v^g and A_u^h act on the same vertex, $v = u$, in this case we have

$$A_v^g A_v^h = A_v^{gh}, \tag{1.5.7}$$

that can be easily proven using the definition of A_v^g (1.5.1) and the property (1.3.10) of the operators L_g and R_g.
For what concerns two plaquette operators B_p^g and B_q^h defined on two different plaquettes $p \neq q$, with $g, h \in G$, if they do not share any edge it is obvious that they commute, but also with one link in common, we can easily prove that they commute:

$$[B_p^g, B_q^h] = 0 \quad \text{if } \ p \neq q. \tag{1.5.8}$$

Two plaquette operators defined on the same plaquette p satisfies the relation:

$$B_p^g B_p^h = \delta(g,h) B_p^g, \tag{1.5.9}$$

because the plaquette operator is a projector. A vertex operator A_v^g on the vertex v, which is not the origin of a plaquette p, commutes with the plaquette operator B_p^h. If instead the vertex v is the origin of the plaquette p we have:

$$A_v^g B_p^h = B_p^{ghg^{-1}} A_v^g. \tag{1.5.10}$$

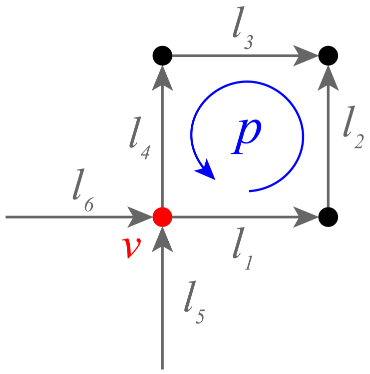

Figure 1.10: Graphical representation of the action of the vertex operator A_v^g and plaquette operator B_p^h, with the vertex v at the origin of the plaquette p (1.5.10).

This result can be proved considering a system like the one in Fig. 1.10, and the definitions (1.5.1) and (1.5.3) of the operators A_v^g and B_p^h respectively:

$$
\begin{aligned}
A_v^g B_p^h =& L_g(l_1)L_g(l_4)R_g(l_5)R_g(l_6) \sum_{g_1,g_2,g_3,g_4\in G} \delta(h, g_1g_2g_3^{-1}g_4^{-1})\cdot \\
&\cdot \mathbb{P}_{g_1}(l_1)\mathbb{P}_{g_2}(l_2)\mathbb{P}_{g_3}(l_3)\mathbb{P}_{g_4}(l_4) && (1.5.11)\\
=& \sum_{g_1,g_2,g_3,g_4\in G} \delta(h, g_1g_2g_3^{-1}g_4^{-1}) \left|gg_1\right\rangle \left\langle g_1\right| \mathbb{P}_{g_2}(l_2)\mathbb{P}_{g_3}(l_3)\cdot \\
&\cdot \left|gg_4\right\rangle \left\langle g_4\right| R_g(l_5)R_g(l_6) && (1.5.12)\\
=& \sum_{g_1,g_2,g_3,g_4\in G} \delta(h, g^{-1}g_1g_2g_3^{-1}g_4^{-1}g) \left|g_1\right\rangle \left\langle g^{-1}g_1\right| \mathbb{P}_{g_2}(l_2)\cdot \\
&\cdot \mathbb{P}_{g_3}(l_3) \left|g_4\right\rangle \left\langle g^{-1}g_4\right| R_g(l_5)R_g(l_6) && (1.5.13)\\
=& \sum_{g_1,g_2,g_3,g_4\in G} \delta(ghg^{-1}, g_1g_2g_3^{-1}g_4^{-1})\mathbb{P}_{g_1}(l_1)\mathbb{P}_{g_2}(l_2)\mathbb{P}_{g_3}(l_3)\mathbb{P}_{g_4}(l_4)\cdot \\
&\cdot L_g(l_1)L_g(l_4)R_g(l_5)R_g(l_6) && (1.5.14)\\
=& B_p^{ghg^{-1}} A_v^g, && (1.5.15)
\end{aligned}
$$

where in the expression (1.5.11) we used the fact that $L_g\mathbb{P}_{g_l} = L_g \left|g_l\right\rangle \left\langle g_l\right| = \left|gg_l\right\rangle \left\langle g_l\right|$, in (1.5.13) we change variable in the sum $g_1 \to gg_1$ and $g_4 \to gg_4$, while in (1.5.14) we used $\mathbb{P}_{g_l}L_g = \left|g_l\right\rangle \left\langle g_l\right| L_g = \left|g_l\right\rangle \left\langle g^{-1}g_l\right|$.

1.5.4 Quantum double model

Using the vertex A_v^g (1.5.1) and plaquette B_p^g (1.5.3) operators introduced before we can construct a new model, called *quantum double model*, that has some interesting relations with the lattice gauge theory we are interested in [26]. Consider an ordered lattice with V vertices, E links and P plaquettes, a finite group G and a total Hilbert space $\mathcal{H}_T = \otimes_{l\in E}\mathbb{C}[G]$, as for our lattice gauge theory. Consider then the following Hamiltonian:

$$H_{\text{QDM}} = -\sum_{v\in V} A_v - \sum_{p\in P} B_p, \tag{1.5.16}$$

where $B_p \equiv B_p^e$, with e the identity element of the group G, and A_v that is the total vertex operator defined as

$$A_v = \frac{1}{|G|}\sum_{g\in G} A_v^g. \tag{1.5.17}$$

The Hamiltonian H_{QDM} (1.5.16) is the Hamiltonian of the quantum double model. Notice how all addends in it commute, then the two pieces, vertex and plaquette part, can be diagonalized with the same basis.
We just mention that a particular kind of quantum double model, the one based on the 2-cyclic group $G = \mathbb{Z}_2$, is called toric code and has many applications in physics and in particular in fault-tolerant quantum computations [26].

Vertex Hamiltonian and gauge invariance

Let's consider the vertex part $H_v = -\sum_v A_v$. The total vertex operator A_v is a projector, indeed $A_v^2 = A_v$, hence it has eigenvalues 0 and 1. All states $|\psi_0^v\rangle$ that are in the ground eigenspace of the vertex part H_v have eigenvalue 1, then they satisfy

$$A_v |\psi_0^v\rangle = |\psi_0^v\rangle\,, \tag{1.5.18}$$

for all $v \in V$. Notice that this relation is equivalent to the gauge invariance condition (1.3.32) for a lattice gauge theory, recalling also (1.1.6). This means that the vector space of physical states in our lattice gauge theory corresponds to the eigenspace of ground states of the vertex part of the quantum double model.

Plaquette Hamiltonian and magnetic ground state

Consider now the plaquette part $H_p = -\sum_p B_p$. The plaquette operator B_p is a projector, then it has eigenvalues 0 and 1. A ground state $|\psi_0^p\rangle$ of the plaquette part H_p has eigenvalue 1, and satisfies

$$B_p |\psi_0^p\rangle = |\psi_0^p\rangle\,, \tag{1.5.19}$$

for all $p \in P$. There is a relation between the plaquette part H_p of the quantum double model and the magnetic part $H_B = -2\lambda_B \sum_p \operatorname{Re}\operatorname{Tr}\hat{W}_p$ (1.4.11) of the lattice gauge theory, indeed the state that minimizes H_p minimizes also H_B. In order to verify that, consider a single plaquette p and the group element basis state $|g_1, g_2, g_3, g_4\rangle$, where each g_i refers to the i-th link of the plaquette p. The action of the plaquette operator B_p (1.5.3) on this state is

$$B_p |g_1, g_2, g_3, g_4\rangle = \delta(e, g_1 g_2 g_3^{-1} g_4^{-1}) |g_1, g_2, g_3, g_4\rangle , \tag{1.5.20}$$

so we have eigenvalue 1 if $e = g_1 g_2 g_3^{-1} g_4^{-1}$ and 0 otherwise. Thus the ground state of the plaquette Hamiltonian is a superposition of the states $|g_1, g_2, g_3, g_4\rangle$ with $g_1 g_2 g_3^{-1} g_4^{-1} = e$. The magnetic Hamiltonian H_B is the sum of Wilson plaquette operators, and the action of a Wilson plaquette operator $\mathrm{Tr}\, \hat{W}_p$ (3.3.30) on the state $|g_1, g_2, g_3, g_4\rangle$ is

$$\mathrm{Tr}\, \hat{W}_p |g_1, g_2, g_3, g_4\rangle = \chi_F(g_1 g_2 g_3^{-1} g_4^{-1}) |g_1, g_2, g_3, g_4\rangle . \tag{1.5.21}$$

where F is a faithful representation of the gauge group. In order to find the magnetic ground state we have to maximize the character function $\chi_F(g)$. χ_F is the sum of d_F complex roots of unity [49], with d_F the dimension of the representation F, so the maximum of $\chi_F(g)$ is realized when all d_F addends are equal to 1, hence $\chi_F(g) = d_F$. The group element g that satisfies the previous expression for any representation F is the identity element e. So the magnetic ground state of the single plaquette is a state $|g_1, g_2, g_3, g_4\rangle$ where $g_1 g_2 g_3^{-1} g_4^{-1} = e$, just as in the quantum double model.
Summarizing what we have found: the ground state $|\psi_0\rangle$ of the full quantum double model Hamiltonian H_{QDM} corresponds to a state in the lattice gauge theory that is the ground state $|E_0^{\lambda=0}\rangle$ of the magnetic Hamiltonian H_B (in order to minimize the vertex part H_p) and it is gauge invariant (in order to minimize the vertex part H_v).

Topological sectors

If the lattice that we are considering has periodic boundary conditions we can see that the ground state $|\psi_0\rangle$ of the quantum double model (so also of the magnetic Hamiltonian of the lattice gauge theory) is degenerate. Indeed let's consider the two non-contractible loops γ_x and γ_y in Fig. 1.11, and the operator $\hat{\chi}_j(\gamma)$ defined as [34]:

$$\hat{\chi}_j(\gamma) = \sum_{g \in G} \chi_j(g) B_\gamma^g, \tag{1.5.22}$$

where γ is a generic closed path and B_γ^g is the corresponding plaquette operator (1.5.5). When considering the non-local operators $\hat{\chi}_i(\gamma_x)$ and $\hat{\chi}_j(\gamma_y)$ we can verify that they commute with the Hamiltonian H_{QDM} (1.5.16), since $[A_v^g, B_{\gamma_{x,y}}^h] = 0$. This means that these operators don't change the value of the energy and therefore all states $|\psi_0(i,j)\rangle = \hat{\chi}_i(\gamma_x)\hat{\chi}_j(\gamma_y) |\psi_0\rangle$ are ground states as well as $|\psi_0\rangle$. The eigenspace with minimum energy is $|\hat{G}|^2$ dimensional, since there are $|\hat{G}|$ possible values for i and j. To each ground state corresponds a topological sector, i.e. the set of states of the Hilbert space that can be obtained by the corresponding ground state

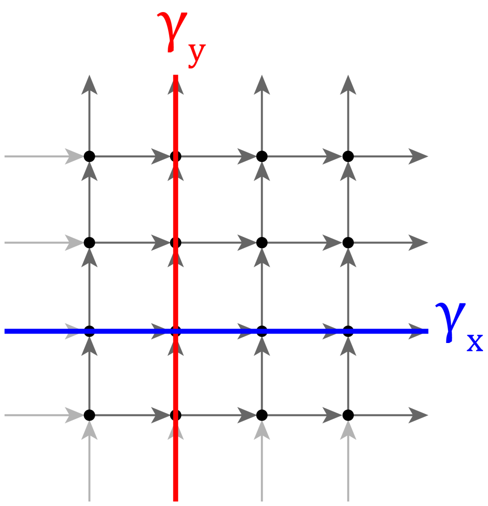

Figure 1.11: A 2-dimensional lattice with periodic boundary conditions and the two non-contractible loops γ_x and γ_y.

by local transformations. One can also construct some operators, called t'Hooft operators, that can be used to identify the topological sector of any state of the Hilbert space, but the design of these operators for an arbitrary non-Abelian gauge group G is not easy. Topological sectors are a very interesting property of quantum double model and they are being extensively studied [16, 26].

Chapter 2

SIMULATION OF A LATTICE GAUGE THEORY

In this chapter we present the general tools to simulate a generic pure lattice gauge theory on a digital quantum computer. The first step is encoding, i.e. mapping the degrees of freedom of the physical model in the degrees of freedom of the quantum simulator in such a way that the map can be inverted and the results of the quantum circuits can be uniquely decoded. The second step is the reproduction of the dynamics of the physical model using a quantum circuit, i.e. we want to create a quantum gate that realizes on the simulator the time evolution operator. This is made possible using Trotter approximation and a set of high level gates whose explicit form depends on the gauge group under study. We discuss also the adiabatic approximation that is very useful to prepare a desired state. Finally we can perform measurements on the quantum simulator to get information about the physical model. A graphical scheme to visualize all quantum simulation procedure is in Fig. 2.5.

2.1 Introduction to quantum simulation

The idea of a quantum simulator was first proposed by R. Feynman in 1982 [20], he suggested that a quantum device would be able to reproduce accurately a quantum system of interest, in particular all its quantum properties that have no classical counterparts and cannot be efficiently simulated on classical simulators or computers. For many years this remained only an idea, since we lacked the technical capabilities to create such devices. Today, thanks to the advance of quantum control systems, we have reached the technology sufficient to realize such quantum simulators, as well as many other quantum technologies, like digital quantum computers. Many platforms have been proposed to implement quantum simulators and quantum computers, such as ultra-cold matter on optical lattices [48], Rydberg atoms [56], superconducting qubits [18], nuclear spins [46] or trapped ions [7]. These devices have been applied to simulate a broad range of physical phenomena in the quantum world, such as superconductivity [23], Ising model [9], particle physics [4] and Hawking radiation [50], showing what the great potential of this technology can be. Digital quantum computers, which are currently rapidly developed and improved with very promising prospective, can be seen as a particular class of quantum simulators. Quantum computers are supposed to be universal, meaning that they should be able to reproduce the dynamics of any quantum system. Whereas a quantum simulator is able to mimic the dynamics of the specific quantum system for which it was designed, in principle a programmable quantum computer can be used to reproduce and study any quantum system using the same hardware [52]. In this thesis we will try to use a digital quantum computer to simulate a non-Abelian lattice gauge theory as the one described in the first chapter.

2.2 Encoding

In this section we see how to encode the degrees of freedom of the physical lattice gauge model in the degrees of freedom of a digital quantum simulator for both states of the Hilbert space and observables. We pay particular attention to those cases in which the physical Hilbert space is infinite dimensional, i.e. the gauge group contains infinite elements, and in order to encode this space in the finite resources of a quantum simulator you need to approximate the gauge group with a finite subgroup.

2.2.1 Encoding of the states

Consider a physical system with total Hilbert space $\mathcal{H}_T$ (1.3.5), this means that every possible configuration of the system is described by a state vector inside this space.
The degrees of freedom of the quantum simulator are described by the Hilbert space $\mathcal{H}_s$. If we use a quantum computer of n qubits as a quantum simulator, the Hilbert space is given by $\mathcal{H}_s = \mathcal{H}_2^{\otimes n}$, where $\mathcal{H}_2$ is the Hilbert space of a two level system, a qubit, the basic element of information in quantum computation. If we want to correctly encode the properties of the physical system in the quantum simulator we need to construct the map $\mathcal{H}_T \rightarrow \mathcal{H}_s$ in such a way that it is isomorphic, or at least 1-1, in order to ensure that every physical state has a corresponding in the quantum simulator and the map can be inverted, allowing us to decode the results of the quantum simulation. While the dimensionality of the Hilbert space of the physical system $\mathcal{H}_T$ is not constrained and can be also infinite, the dimension of the Hilbert space of the quantum simulator $\mathcal{H}_s$ is always finite. For example the Hilbert space of a quantum computer with n qubits has a dimension $\dim \mathcal{H}_s = 2^n$. This means that only finite dimensional Hilbert spaces can be exactly simulated on a quantum computer. For example, in a lattice gauge theory with an infinite size gauge group, we have that the Hilbert space of each link it is infinite dimensional $\dim L^2(G) = \infty$, and so it is impossible to simulate it exactly on a quantum computer. This is the case for many group of interest, like $SU(N)$. There are

many possible strategies to deal with an infinite dimensional system: quantum link model [10], the Fock space truncation [8], dual variables [5] and the finite group approximation [15, 22]; we will deepen in the latter. Once one has encoded the physical degrees of freedom in the degrees of freedom of the simulator we are ready to initialize and prepare an initial state on the simulator.

Notice that we are not restricting to the gauge invariant Hilbert space $\mathcal{H}_{\text{phys}}$ (1.3.33), but we are considering the whole Hilbert space $\mathcal{H}_T$, even if in principle one can also try to do the same for the subspace of gauge invariant states. The total Hilbert space $\mathcal{H}_T$ is much larger that its subset of gauge invariant states $\mathcal{H}_{\text{phys}}$, therefore a common suggestion to limit the qubit-register size is to work with just physical states by gauge fixing, at the cost of increased circuit depth in the time-evolution. Anyway for this approach a practical method for non-Abelian theories remains unknown.

Finite group approximation

Consider a continuous gauge group G that has infinite elements and so it cannot be represented exactly in the finite degrees of freedom of a quantum simulator. The idea is to approximate the group G with one of its finite subgroups. The subgroup has to be chosen properly to best reproduce the geometry and all the relevant properties of the original gauge group. For example to approximate the unitary group $U(1)$ you can use the cyclic group $\mathbb{Z}_n$, indeed in the limit $n \to \infty$ one recovers exactly the original group. The situation is more complicated for non-Abelian groups like the special unitary group $SU(N)$. Let's take as an example $SU(2)$, that is locally isomorphic to the special orthogonal group $SO(3)$, the group of rotations in a three dimensional space, i.e. the group of symmetries of a sphere. To be more precised we should say that $SU(2)$ double covers $SO(3)$. Finite subgroups of $SO(3)$ are the cyclic group $\mathbb{Z}_n$, the dihedral group D_n, the tetrahedral group T, the octahedral group O and the icosahedral group I. The cyclic group $\mathbb{Z}_n$ is probably not a good choice to approximate $SO(3)$, since it is very simple and it is also Abelian, while $SO(3)$ is not. The groups of symmetry of three dimensional polyhedra, like T, O and I are probably the subgroups that reproduce better the geometry of $SO(3)$, but their algebra is not simple and so they are probably not the best choice to start with. A good idea could be the dihedral group D_n, the group of symmetry of 2-dimensional polygons with n sizes. Even if we lose the three-dimensionality of the geometry of $SO(3)$, choosing as subgroup the dihedral group D_n we preserve the non-Abelian character (for $n > 2$) of $SO(3)$ and we work with a sufficiently simple group to begin with.

2.2.2 Encoding of the observables

In addition to states we shall encode in the quantum simulator also the observables of the physical model. Consider an observable O of the system, it can be represented by an Hermitian operator that acts on the Hilbert space $\mathcal{H}_T$. In the simulator a generic observable $O_s^{(1)}$ for a single qubit can be written in terms of the Pauli basis as:

$$O_s^{(1)} = \sum_{\mu=0}^{3} o_\mu \sigma_\mu, \tag{2.2.1}$$

for some coefficients o_μ and where $\sigma_\mu = (\mathbb{I}, \sigma_x, \sigma_y, \sigma_z)$ is the vector of Pauli matrices satisfying $\mathfrak{su}(2)$ algebra. Consider now a generic observable O_s on a n-qubit system. The algebra $\mathfrak{su}(2)^{\otimes n}$ is generated by the operators σ_μ^j, where we act with the Pauli matrix σ_μ on the j-th qubit. A generic n-qubit observable in the simulator can be written in terms of these operators $O_s(\{\sigma_\mu^j\})$. In this case to have a faithful representation of the physical system we have to map each observable O of the physical model in an observable O_s of the qubit-register in such a way that the action of O on the physical Hilbert space $\mathcal{H}_T$ is equivalent to the action of O_s on the n-qubit Hilbert space $\mathcal{H}_s$. Formally we have to build a *-algebra isomorphism $O \to O_s$ between the two operator algebras.

2.3 Time evolution

Once one has mapped the physical model Hilbert space $\mathcal{H}_T$ in the n-qubit Hilbert space $\mathcal{H}_s$, we are able to prepare and initialize in the quantum register an initial state $|\psi_0\rangle$. Notice that we have to make sure that the initial state $|\psi_0\rangle$ is indeed gauge invariant. The preparation of a generic physical state is not trivial and it will discuss later, first in this section we see how to implement time evolution.

In order to make a prepared state evolve in time under some specified external conditions we need first to reproduce the dynamics of the model implementing a time evolution operator. Consider the Hamiltonian that governs the physical model, in the case of a lattice gauge theory this is the Kogut-Susskind Hamiltonian H_{KS} (1.4.43). Using the procedure described in the previous section we can also construct the operator H that acts on the quantum simulator Hilbert space $\mathcal{H}_s$ and governs the dynamics of it, mimicking the dynamics of the physical model. The Kogut-Susskind Hamiltonian is time independent, this means that the corresponding evolution operator $U(t)$ is formally given by:

$$U(t) = e^{-iHt}. \tag{2.3.1}$$

The Hamiltonian H is gauge invariant, indeed it commutes with the generator of gauge transformations $\mathcal{G}$, as we have shown in section 1.4.5. This means that also the evolution operator $U(t)$ commutes with the generator of gauge transformations $\mathcal{G}$, hence if the initial state $|\psi_0\rangle$ is gauge invariant, the evolved state $|\psi(t)\rangle = U(t)\,|\psi_0\rangle$ is still gauge invariant. In order to realize the evolution operator on the simulator we have now to understand how to decompose it in the gates of a quantum circuit.

2.3.1 Trotter formula

We want to decompose the evolution operator $U(t)$ (2.3.1) in the gates of a quantum circuit, but the decomposition reproducing the full evolution operator can be inefficient as the number of elementary operations may be too large, and moreover the decomposition in terms of elementary gates may be difficult to find. To simplify the task let us first notice that the Kogut-Susskind Hamiltonian for a lattice gauge theory (1.4.43) is made of two non-commuting pieces, the electric Hamiltonian H_E and the magnetic Hamiltonian H_B:

$$H = H_E + H_B. \tag{2.3.2}$$

For this kind of Hamiltonian there is a useful relation, called *Trotter formula*. Given an Hamiltonian H that is the sum of two different pieces, like in (2.3.2), Trotter approximation allow us to factor the evolution operator related to H into evolution operators of the single Hamiltonians H_E and H_B up to the order $o(t^2)$ [12]:

$$U(t) = e^{-iHt} = e^{-iH_B t}e^{-iH_E t} + o(t^2). \tag{2.3.3}$$

The previous equation is exact in the case in which the Hamiltonians H_E and H_B commute with each other, so there are no correction of order $o(t^2)$. If instead the Hamiltonians do not commute we can estimate the error δ introduced by Trotter approximation as [12]:

$$\delta = \left\| e^{-iH_B t}e^{-iH_E t} - e^{-iHt} \right\| \leq \frac{t^2}{2}\|[H_B, H_E]\|, \tag{2.3.4}$$

where $\|A\|$ is the operator (or spectral) norm, the largest singular value of the operator A. Provided a sufficiently small time interval t, Trotter formula (2.3.3) provides us a good approximation for the evolution operator $U(t)$, since we can neglect the corrections of higher order in t. If instead the time interval t is not small we can divide it in N_s small steps, such that each one lasts a time interval $\Delta t = t/N_s$ that is small. Therefore the total evolution operator is $U(t) = U(\Delta t)^{N_s}$. For each operator $U(\Delta t)$, now that Δt is small, we can apply the Trotter formula (2.3.3), and in the limit in which $N_s \to \infty$, so $\Delta t \to 0$, we can write exactly:

$$e^{-iHt} = \lim_{N_s\to\infty} \left(e^{-iH_B \Delta t}e^{-iH_E \Delta t}\right)^{N_s}. \tag{2.3.5}$$

If N_s is finite, as in all real applications, at each of the N_s Trotter steps we get an error δ (2.3.3), these errors accumulate and we should sum over all of them to correctly determine the precision of the approximation, getting to a total error:

$$\delta_T = \sum_{j=1}^{N_s} \delta \leq N_s \frac{\Delta t^2}{2}\|[H_B, H_E]\| = \frac{t^2}{2N_s}\|[H_B, H_E]\|. \tag{2.3.6}$$

Trotter approximation (2.3.3) can be applied to our Kogut-Susskind Hamiltonian (1.4.43). In principle the fact that the Trotter formula is just an approximation may lead to a loss of gauge

invariance of the evolved state, but this is not the case since both H_E and H_B are gauge invariant, as we saw in section 1.4.5. If we prepare a gauge invariant state in the quantum register, and act on it with gauge invariant operators like $U_E(\Delta t) = \exp(-iH_E\Delta t)$ and $U_B(\Delta t) = \exp(-iH_B\Delta t)$, we will remain in the gauge invariant subspace.
Using Trotter formula we can decompose the evolution operator $U(t)$ in the product of electric $U_E(\Delta t)$ and magnetic $U_B(\Delta t)$ evolution operators, now we will see ho to implement them on a quantum circuit.

2.3.2 Evolution operator

High level gates

We have seen that using Trotter formula (2.3.3) we can decompose the evolution operator $U(t)$ into a product of evolution operators of the electric Hamiltonian $U_E(\Delta t)$ and magnetic Hamiltonian $U_B(\Delta t)$. Then it is possible to define a set of high level gates into which these evolution operators can be decomposed [30]. These unitary operators are:

1. The *inversion gate* U_{-1}, that acts on the group elements basis state $|g\rangle$ applying the group inversion operation:
$$U_{-1}\,|g\rangle = |g^{-1}\rangle \quad \forall g \in G. \tag{2.3.7}$$

2. The *multiplication gate* $U_\times$, that acts on two group element basis states using the first state as a control while on the second it performs the left group multiplication:
$$U_\times\,|g\rangle\,|h\rangle = |g\rangle\,|gh\rangle \quad \forall g, h \in G. \tag{2.3.8}$$

3. The *trace gate* $U_{\mathrm{tr}}(\theta)$, a parametric gate that acts on the group elements basis state $|g\rangle$ diagonally and introduces a phase that depends on the trace of g in some representation ρ:
$$U_{\mathrm{tr}}(\theta)\,|g\rangle = e^{i\theta\,\mathrm{Re}\,\mathrm{Tr}\,\rho(g)}\,|g\rangle \quad \forall g \in G. \tag{2.3.9}$$

4. The *Fourier transform gate* U_F, a gate that allows us to pass from the group element (position) basis $\{|g\rangle\}$ to the representation (momentum) basis $\{|j_{mn}\rangle\}$. From the duality relation (1.3.20) we can see that:
$$U_F = \sum_{g\in G}\sum_{j\in\hat{G}}\sum_{m,n=1}^{d_j}\sqrt{\frac{d_j}{|G|}}\rho_j(g)_{mn}\,|j_{mn}\rangle\,\langle g|\,. \tag{2.3.10}$$

   We used the duality relation for finite groups, since these are the groups that can be simulated on a quantum computer. The Fourier transform operator can be seen as a

$|G| \times |G|$ matrix where the columns are labeled by group elements g and the rows by the representations j and their components mn; the matrix elements are given by:

$$\langle j_{mn}|U_F|g\rangle = \sqrt{\frac{d_j}{|G|}}\rho_j(g)_{mn}. \tag{2.3.11}$$

The Hermitian conjugate of the Fourier transform gate $U_F^\dagger$ allows us to pass from the representation (momentum) basis $\{|j_{mn}\rangle\}$ to the group element (position) basis $\{|g\rangle\}$, and it is easy to see that

$$U_F^\dagger = \sum_{g\in G}\sum_{j\in\hat{G}}\sum_{m,n=1}^{d_j}\sqrt{\frac{d_j}{|G|}}\rho_j(g)^*_{mn}\,|g\rangle\,\langle j_{mn}|\,. \tag{2.3.12}$$

The matrix elements of this operator are:

$$\langle g|U_F^\dagger|j_{mn}\rangle = \sqrt{\frac{d_j}{|G|}}\rho_j(g)^*_{mn}. \tag{2.3.13}$$

5. The *phase gate* $U_{\text{ph}}(\Delta t)$, that is defined as the electric evolution operator for a single link in the representation basis $\{|j_{mn}\rangle\}$, hence it is diagonal:

$$U_{\text{ph}}(\Delta t) = U_F e^{-iH_E^{(l)}\Delta t}U_F^\dagger, \tag{2.3.14}$$

where $H_E^{(l)}$ is the electric Hamiltonian for the single link l, and it is equal to $H_E^{(l)} = \lambda_E\sum_j f(j)\mathbb{P}_j(l)$ (1.4.42). It is trivial to notice that the projectors $\mathbb{P}_j(l)$ (1.4.26) are diagonal in the representation basis and so is the phase gate:

$$U_{\text{ph}}(\Delta t) = \sum_{j\in\hat{G}}\sum_{m,n=1}^{d_j} e^{-i\lambda_E f(j)\Delta t}\,|j_{mn}\rangle\,\langle j_{mn}|\,. \tag{2.3.15}$$

6. The *Abelian character gates* U_{χ_j} that acts on the group elements basis state $|g\rangle$ diagonally taking out the Abelian character of g:

$$U_{\chi_j}\,|g\rangle = \chi_j(g)\,|g\rangle \quad \forall g\in G, \tag{2.3.16}$$

where j labels an Abelian irreducible representation of the group G. These gates are useful to initialize the excited electric eigenstates.

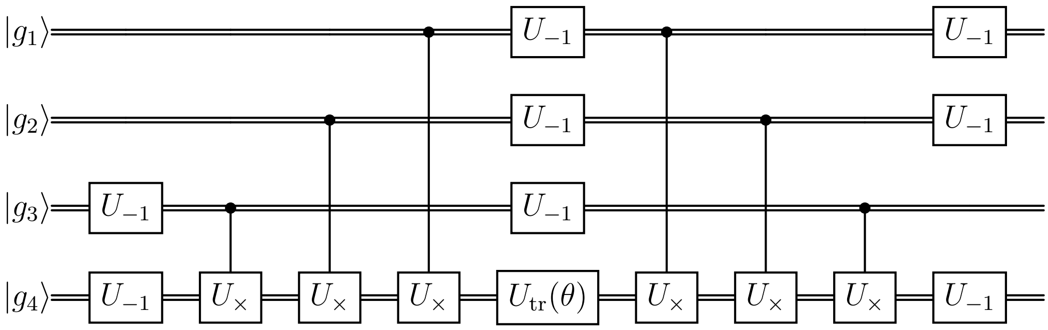

Figure 2.1: Quantum circuit to implement the magnetic evolution operator $U_B^{(p)}(\Delta t)$ for a single plaquette p like the one in Fig. 1.9. The parameter θ appearing in the trace gate U_{tr} has to be fixed to $\theta = 2(1-\lambda)\Delta t$. Each double wire represents the quantum register needed to encode a group element.

Evolution gates

Given the high level operators just described, whose explicit form depends on the gauge group G that we are interested in, we can construct the evolution gates for the electric $U_E(\Delta t)$ and magnetic $U_B(\Delta t)$ Hamiltonian [30]. Let us start from the magnetic one.
The magnetic evolution operator $U_B(\Delta t)$ can be factored in exponential of single plaquettes since the Wilson loops of different plaquettes appearing in H_B (1.4.11) commute, as seen in (1.5.8). Therefore

$$U_B(\Delta t) = e^{-iH_B\Delta t} = \prod_p U_B^{(p)}(\Delta t), \tag{2.3.17}$$

where $U_B^{(p)}(\Delta t)$ is the magnetic evolution operator for the single plaquette p:

$$U_B^{(p)}(\Delta t) = e^{2i(1-\lambda)\,\mathrm{Re\,Tr}\,\hat{W}_p\Delta t}, \tag{2.3.18}$$

where we used the notation $\lambda_B = 1-\lambda$, introduced in (1.4.45). The single plaquette magnetic evolution operator $U_B^{(p)}$ acts on the four-edges Hilbert space of the plaquette p, like the one in Fig. 1.9, that is $\mathcal{H}_p = \mathbb{C}[G]^{\otimes 4}$. The action of $U_B^{(p)}(\Delta t)$ on a group elements basis state $|g_1, g_2, g_3, g_4\rangle \in \mathcal{H}_p$ is simply given by

$$U_B^{(p)}(\Delta t)\,|g_1, g_2, g_3, g_4\rangle = e^{2i(1-\lambda)\,\mathrm{Re\,Tr}\,\rho(g_1g_2g_3^{-1}g_4^{-1})\Delta t}\,|g_1, g_2, g_3, g_4\rangle\,, \tag{2.3.19}$$

where ρ is the chosen representation for G. The single plaquette magnetic evolution operator $U_B^{(p)}(\Delta t)$ can be implemented by the circuit in Fig. 2.1.
A similar discussion can be done for the electric evolution operator $U_E(\Delta t)$. The Laplacians Δ_l (1.4.40), that appear in the electric Hamiltonian H_E (1.4.21), since they act on different

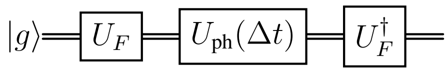

Figure 2.2: Quantum circuit to implement the electric evolution operator $U_E^{(l)}(\Delta t)$ for a single link l.

links then they commute with each other, hence in the electric evolution operator we can factorize the exponentials of single link:

$$U_E(\Delta t) = e^{-iH_E\Delta t} = \prod_{l\in E} U_E^{(l)}(\Delta t), \tag{2.3.20}$$

where $U_E^{(l)}(\Delta t)$ is the electric evolution operator for the single link l:

$$U_E^{(l)}(\Delta t) = e^{-i\lambda\Delta_l\Delta t}, \tag{2.3.21}$$

where we used the notation $\lambda_E = \lambda$ (1.4.45). This operator acts on the Hilbert space of a single link l, that is $\mathcal{H}^{(l)} = \mathbb{C}[G]$. Recalling the expression of the Laplacian Δ_l (1.4.40) and the definition of the projectors $\mathbb{P}_j(l)$, we can see that the operator $U_E^{(l)}(\Delta t)$ is diagonal in the representation basis $\{|j_{mn}\rangle\}$, not in the group element basis. One of the high level gates, the phase gate U_{ph} (2.3.14), represents the single link electric evolution operator in the representation basis, therefore in order to have the expression of the evolution operator in the group element basis we have simply to change basis using the Fourier transform gates:

$$U_E^{(l)}(\Delta t) = U_F^\dagger U_{\text{ph}}(\Delta t) U_F. \tag{2.3.22}$$

The circuit that implements the single link electric evolution operator $U_E^{(l)}(\Delta t)$ is shown in Fig. 2.2.
The total evolution operator $U(t)$ is obtained combining the magnetic evolution operator $U_B(\Delta t)$ and the electric evolution operator $U_E(\Delta t)$, and using Trotter algorithm, as we saw in (2.3.5):

$$U(t) \approx \left(U_B(\Delta t)U_E(\Delta t)\right)^{N_s}, \quad \Delta t = \frac{t}{N_s} \ll 1. \tag{2.3.23}$$

The quantum circuit that implements the evolution operator $U(t)$ for a single plaquette lattice is shown in Fig. 2.3.

2.3.3 State preparation

We have seen how to evolve a state, but first one has to prepare it. We will see that the initialization of some specific ground states on the quantum simulator can be realized without particular problems, for example this is the case for the electric ground state $|E_0^{\lambda=1}\rangle$, i.e. the

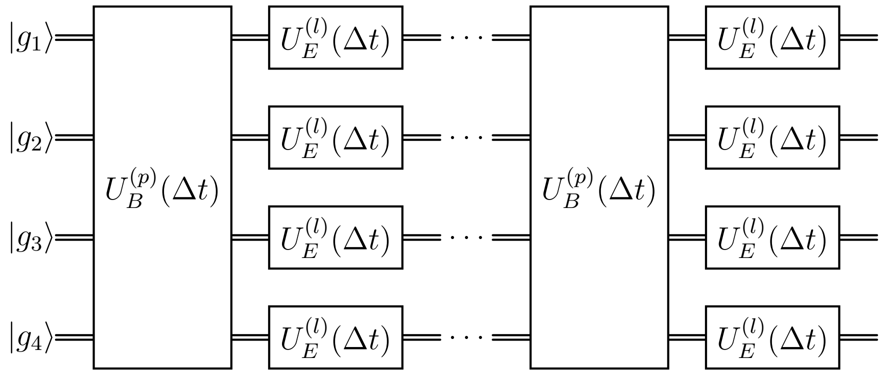

Figure 2.3: Quantum circuit to implement the total evolution operator $U(t)$ (2.3.23) for a single plaquette lattice like the one in Fig. 1.9. $U_B^{(p)}(\Delta t)$ is the single plaquette magnetic evolution gate in Fig. 2.1, and $U_E^{(l)}(\Delta t)$ is the single plaquette magnetic evolution gate in Fig. 2.2. If $\Delta t = t/N_s$, you need N_s layers of $U_B^{(p)}(\Delta t)$ and $U_E^{(l)}(\Delta t)$ gates to implement $U(t)$.

ground state of the Kogut-Susskind Hamiltonian H_{KS} (1.4.43) in the limit in which $\lambda_B = 0$ and $\lambda_E = 1$, or also the magnetic ground state $|E_0^{\lambda=0}\rangle$, i.e. the ground state of H_{KS} in the limit in which $\lambda_E = 0$ and $\lambda_B = 1$. Apart from these two simple cases, preparing exactly the ground state $|E_0^{\lambda}\rangle$ for an Hamiltonian with arbitrary coupling constant $\lambda \in [0, 1]$ it is anything but simple. The preparation of a desired state can be achieved using the *quantum adiabatic algorithm* [19].

The adiabatic theorem states that, given a slowly changing Hamiltonian $H(t)$ and an instantaneous eigenstate of the Hamiltonian at time $t = 0$: $|E_n(t = 0)\rangle$, if time evolution is sufficiently slow the time evolved state will remain very close to the instantaneous eigenstate at time t: $|E_n(t)\rangle$. Basically, if the system begins its time evolution in an eigenstate of $H(0)$ it remains in the corresponding eigenstate of $H(t)$ also at time t. This result is not exact, and in order to be accurate the rate at which the matrix elements of the Hamiltonian H vary has to be small compared to the time scale set by the inverse of the energy gap ΔE^{-1}. If we are evolving the ground state $|E_0(t = 0)\rangle$ from $t = 0$ up to $t = T$, with $|E_1(t)\rangle$ that is the first excited state and $\Delta E(t) = E_1(t) - E_0(t)$ that is the energy gap, we shall impose [47]

$$\max_{t\in[0,T]} \frac{|\langle E_1(t)|\partial H/\partial t|E_0(t)\rangle|}{|\Delta E(t)|^2} \ll 1. \tag{2.3.24}$$

The adiabatic evolution can be realized on the quantum circuit integrating it in the Trotter algorithm described before [44]. Consider the Kogut-Susskind Hamiltonian (1.4.45) but this time the coupling constant λ is not constant, but slightly time-dependent: $\lambda(t)$ and $t \in [0, T]$. The Trotter algorithms modifies such that at the j-th Trotter step the coupling constant has constant values $\lambda_j = \lambda(j\Delta t)$, with $\Delta t = T/N_s$ the time duration of each Trotter step. In

other words at each Trotter step the coupling constant is increased or decreased by a quantity $\Delta\lambda = \lambda_{j+1} - \lambda_j = [\lambda(T) - \lambda(0)]/N_s$.
The total error δ_T emerging from the Trotter approximation can be computed using an equation similar to (2.3.6), but this time you have to take in account that the commutator $[H_E, H_B]$ changes at each Trotter step, since the coupling λ is changing. Using the notation $H_E = \lambda H'_E$ and $H_B = (1-\lambda)H'_B$, with $\lambda \in [0, 1]$, and the fact that $\lambda_j = j\Delta\lambda = j/N_s$ we can verify

$$\begin{aligned}\delta_T = \sum_{j=1}^{N_s} \delta_j &\leq \sum_{j=1}^{N_s} \frac{\Delta t^2}{2}\lambda_j(1-\lambda_j)\|[H'_B, H'_E]\| \\ &= \frac{\Delta t^2}{12N_s}\left(N_s^2 - 1\right)\|[H'_B, H'_E]\| \qquad (2.3.25) \\ &\overset{N_s \gg 1}{\approx} \frac{\Delta t^2}{12} N_s \|[H'_B, H'_E]\| \qquad (2.3.26)\end{aligned}$$

In general fixed a time step Δt the Trotter error δ_T is minimized minimizing the number of Trotter steps N_s, but this is not the end of the story. Therefore one should take into account also the error emerging from the adiabatic approximation, in other words one should provide the condition (2.3.24) to be fulfilled. The time dependence of the Hamiltonian H is restricted to the coupling constant λ, so we can give an estimate of the rate at which the matrix elements of the Hamiltonian H vary using the parameter $r = \Delta\lambda/\Delta t$. The condition (2.3.24) becomes

$$r = \frac{\Delta\lambda}{\Delta t} \ll \Delta E^2, \qquad (2.3.27)$$

where ΔE is the energy gap. If one fixes the time step Δt, the adiabatic parameter r is minimized with a large number N_s of Trotter steps (because we minimize $\Delta\lambda$). Therefore the choice of the number N_s of Trotter step is delicate, it is a trade-off between minimising the Trotter error δ_T ($N_s = 1$) and minimising the adiabatic evolution error ($N_s \gg 1$).
The preparation of a desired ground state can be achieved using the quantum adiabatic algorithm just described, but not only that, other examples include using quantum variational methods [29] and quantum phase estimation [1].

2.4 Measurement

In this section we see how to extract information from the quantum simulator once we have prepared and evolved a given state. First we see how to measure a dynamical correlation function and then we apply this procedure to the special case of the expectation value of an Hermitian operator.

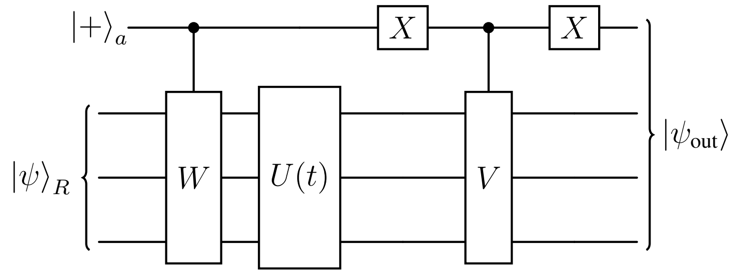

Figure 2.4: Quantum circuit to measure the dynamical correlation function $C_{VW}(t)$ (2.4.1).

2.4.1 Measurement of a dynamical correlation function

Consider the following dynamical correlation function

$$C_{VW}(t) = \langle \psi | U(t)^\dagger V^\dagger U(t) W | \psi \rangle \,, \tag{2.4.1}$$

where $U(t) = \exp(-iHt)$ is the evolution operator, V, W are two unitaries operators and $|\psi\rangle$ is the prepared state that we are interested in. We can measure this quantity using an ancillary qubit a and the quantum circuit shown in Fig. 2.4 [52]. Initializing the ancillary qubit in the state $|+\rangle_a$ and preparing in the quantum register the state $|\psi\rangle_R$, at the end of the circuit one gets the state:

$$|\psi_{\text{out}}\rangle = \frac{1}{\sqrt{2}} \left(|0\rangle_a V U(t) |\psi\rangle_R + |1\rangle_a U(t) W |\psi\rangle_R \right). \tag{2.4.2}$$

If one measures the expectation value of Pauli operator $\sigma_x^{(a)}$ on the ancillary qubit a:

$$\langle \sigma_x^{(a)} \rangle = \mathrm{Tr}\left[|\psi_{\text{out}}\rangle \langle \psi_{\text{out}}| \, (\sigma_x^{(a)} \otimes \mathbb{I}) \right] = \mathrm{Re}[C_{VW}(t)]. \tag{2.4.3}$$

In order to measure the expectation value $\langle \sigma_x^{(a)} \rangle$ on a digital quantum computer one has to apply an Hadamard gate $H^{(a)}$ to the ancillary qubit a and then measure this qubit in the usual computational basis $\sigma_z^{(a)}$.
Otherwise, if one measures the expectation value of Pauli operator $\sigma_y^{(a)}$ on the ancillary qubit a:

$$\langle \sigma_y^{(a)} \rangle = \mathrm{Tr}\left[|\psi_{\text{out}}\rangle \langle \psi_{\text{out}}| \, (\sigma_y^{(a)} \otimes \mathbb{I}) \right] = \mathrm{Im}[C_{VW}(t)]. \tag{2.4.4}$$

In order to measure the expectation value $\langle \sigma_y^{(a)} \rangle$ on a digital quantum computer one has to apply a rotation $R_x(\pi/2)^{(a)}$ to the ancillary qubit a and then measure this qubit in the usual computational basis $\sigma_z^{(a)}$.
Since the eigenevalues of Pauli operators σ_x, σ_y and σ_z are just ± 1, we can write the expecta-

tion values as:

$$\begin{aligned}\mathrm{Re}[C_{VW}(t)] &= \langle\sigma_x^{(a)}\rangle = p_{|\psi_{\text{out}}\rangle}(\sigma_x^{(a)} = +1) - p_{|\psi_{\text{out}}\rangle}(\sigma_x^{(a)} = -1) \\ &= p_{H^{(a)}|\psi_{\text{out}}\rangle}(\sigma_z^{(a)} = +1) - p_{H^{(a)}|\psi_{\text{out}}\rangle}(\sigma_z^{(a)} = -1),\end{aligned} \tag{2.4.5}$$

and

$$\begin{aligned}\mathrm{Im}[C_{VW}(t)] &= \langle\sigma_y^{(a)}\rangle = p_{|\psi_{\text{out}}\rangle}(\sigma_y^{(a)} = +1) - p_{|\psi_{\text{out}}\rangle}(\sigma_y^{(a)} = -1) \\ &= p_{R_x(\pi/2)^{(a)}|\psi_{\text{out}}\rangle}(\sigma_z^{(a)} = +1) - p_{R_x(\pi/2)^{(a)}|\psi_{\text{out}}\rangle}(\sigma_z^{(a)} = -1),\end{aligned} \tag{2.4.6}$$

where $p_{|\psi\rangle}(\sigma_\alpha^{(a)} = \pm 1)$ is the probability of getting the eigenvalue ± 1 measuring the observable $\sigma_\alpha^{(a)}$ on the state $|\psi\rangle$. Recall that the state that has eigenvalue $\sigma_z = +1$ is $|0\rangle$, and the state that has eigenvalue $\sigma_z = -1$ is $|1\rangle$.
From the expressions (2.4.5) and (2.4.6) one can see that to measure the real (or imaginary) part of the dynamical correlation function $C_{VW}(t)$ (2.4.1) for a given state $|\psi\rangle$ is sufficient to apply the quantum circuit in Fig. 2.4, apply the operator $H^{(a)}$ (or $R_x(\pi/2)^{(a)}$) on the ancillary qubit a, measure many times the ancillary qubit and finally take the subtraction between the occurrences of 0 and the occurrences of 1, divided by the total number of measurements.

2.4.2 Measurement of an observable expectation value

If one is interested in measuring the expectation value of an Hermitian operator Q, that corresponds to some relevant observable, we can fall back to the previous procedure. Indeed consider $V = \mathbb{I}$ and $W = U_Q(\theta) = e^{-iQ\theta}$, then using the circuit described before and represented in Fig. 2.4, you can measure the quantity [52]:

$$C_Q(\theta) = \langle\psi|U_Q(\theta)|\psi\rangle\,. \tag{2.4.7}$$

Then we can approximate the expectation value of the observable Q over the state $|\psi\rangle$ as

$$\begin{aligned}\langle Q\rangle &= \langle\psi|Q|\psi\rangle \\ &= i\,\frac{d}{d\theta}\,\langle\psi|e^{-iQ\theta}|\psi\rangle\bigg|_{\theta=0} \\ &\approx i\,\frac{C_Q(\epsilon) - C_Q(0)}{\epsilon},\end{aligned} \tag{2.4.8}$$

where ϵ is a small quantity. Using the spectral decomposition of the operator Q and its eigenstates $|q\rangle$ with relative eigenvalues q, we can write:

$$C_Q(\epsilon) = \sum_q e^{-iq\epsilon} \langle\psi|q\rangle \langle q|\psi\rangle \tag{2.4.9}$$

$$= \sum_q e^{-iq\epsilon} p_{|\psi\rangle}(q) \tag{2.4.10}$$

$$= \sum_q \left[\cos(q\epsilon) p_{|\psi\rangle}(q) - i\sin(q\epsilon) p_{|\psi\rangle}(q)\right] \tag{2.4.11}$$

$$= \sum_q p_{|\psi\rangle}(q) - i \sum_q q\epsilon p_{|\psi\rangle}(q) + o(\epsilon^2) \tag{2.4.12}$$

$$= 1 - i \sum_q q\epsilon p_{|\psi\rangle}(q) + o(\epsilon^2), \tag{2.4.13}$$

where in (2.4.10) we introduce the probability $p_{|\psi\rangle}(q) = |\langle\psi|q\rangle|^2$ of getting the eigenstate q given the state $|\psi\rangle$, in (2.4.12) we expand in powers of ϵ: $\cos(q\epsilon) = 1 + o(\epsilon^2)$ and $\sin(q\epsilon) = q\epsilon + o(\epsilon^2)$, while in (2.4.13) we use the completeness relation $\sum_q p_{|\psi\rangle}(q) = 1$. From the last expression (2.4.13) we see that $C_Q(0) = 1$, and also that $\mathrm{Im}[C_Q(\epsilon)] = -\sum_q q\epsilon p_{|\psi\rangle}(q)$; then the result (2.4.8) becomes

$$\langle Q\rangle \approx i\frac{-i\sum_q q\epsilon p_{|\psi\rangle}(q)}{\epsilon} \tag{2.4.14}$$

$$= -\frac{\mathrm{Im}[C_Q(\epsilon)]}{\epsilon}. \tag{2.4.15}$$

Recall that we have already seen how to measure $\mathrm{Im}[C_Q(\epsilon)]$, using the quantum circuit in Fig. 2.4. We will use the procedure described in this section to measure two kind of observables: the energy, so $Q = H$ and $U_Q(t) = U(t)$, and Wilson loops $Q = \mathrm{Tr}\,\hat{W}[\gamma]$.

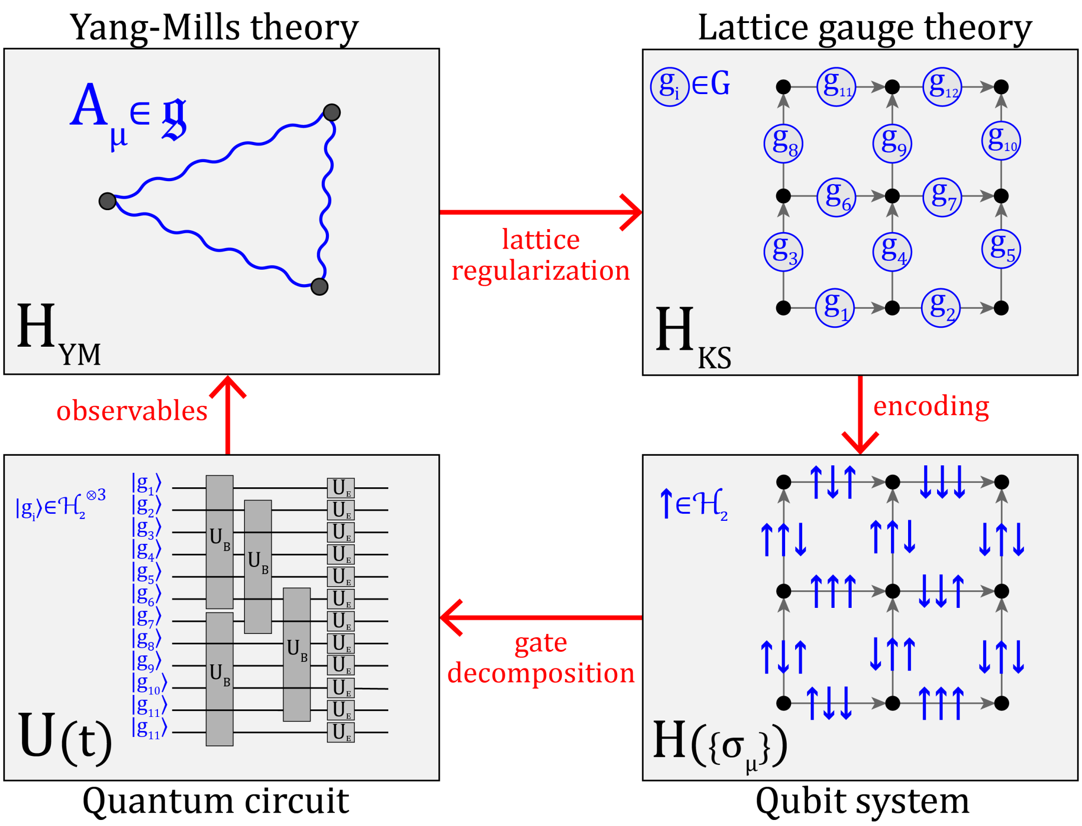

Figure 2.5: Quantum simulation scheme. Consider as physical model the pure Yang-Mills theory in the continuum, the degrees of freedom are in the gauge field A_μ, an element of the group algebra $\mathfrak{g}$, and the dynamics is governed by the Yang-Mills Hamiltonian H_{YM}. Performing the lattice regularization we formulate a lattice gauge theory. Now the degrees of freedom are group elements $g_i \in G$ attached to each edge, the dynamics is governed by the Kogut-Susskind Hamiltonian H_{KS}. Provided a finite group G, through the encoding procedure we can map the degrees of freedom of each edge in n qubits (in the figure $n = 3$), with Hilbert space $\mathcal{H}_2$, the dynamics of this qubit system is governed by an Hamiltonian written in terms of Pauli operators $\{\sigma_\mu\}$. We can now decompose the evolution operator $U(t) = e^{-iHt}$ in a set of gates (like the electric U_E and magnetic U_B evolution gates) and realize the quantum circuit, where the degrees of freedom are the group element states $|g\rangle$, encoded in n qubits. Finally it is possible to extract information about observables of the physical model measuring some qubits of the quantum circuit.

Chapter 3

THEORETICAL RESULTS for DIHEDRAL THEORIES

In this chapter we present some theoretical results for specific lattice gauge theories. We consider two gauge groups, the dihedral group D_4 and D_3, i.e. the group of symmetries of a square and of an equilateral triangle respectively, which are the simplest non-Abelian subgroups of $SO(3)$. We present the relevant properties of these groups and then we apply them to the general context of a lattice gauge theory, as introduced in the first chapter of this thesis. For both D_3 and D_4 we consider two possible systems, a one-plaquette lattice and a two-plaquette lattice. For each one we describe its physical Hilbert space, we compute the matrix elements of the Hamiltonian and derive the full energy spectrum, diagonalizing these matrices. We also look at the Wilson loop observables. The results obtained in this section are those that we want to reproduce using a quantum simulation.

3.1 Dihedral group D_4

In this section we present the dihedral group D_4, the group of symmetries of a square. We give the definition of the group, the list of all its elements and a complete description of its algebra. We study its representation theory, presenting all the 5 inequivalent irreducible representations and finally we show two possible choices for the generating subset Γ.
The relevance of this group lies in the fact that it is the simplest non-Abelian finite subgroup of $SO(3)$, and it can be used to approximate this continuous Lie group. The binary dihedral group $2D_4$ can instead be used to approximate the group $SU(2)$.

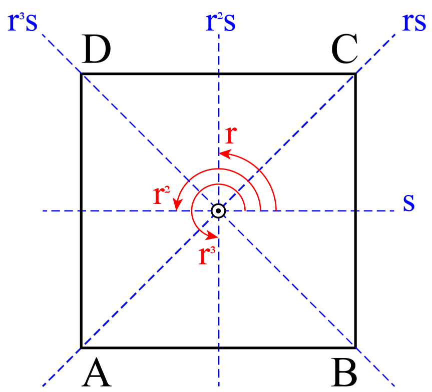

Figure 3.1: Graphical representation of the elements of the group D_4, i.e. the symmetries of a square. Besides the identity element e, we have three rotations r, r^2 and r^3 of an angle $\pi/2$, π and $3\pi/2$ respectively, and four reflections s, rs, r^2s, r^3s.

3.1.1 Definition of the group

The *dihedral group* D_4 is the group of the symmetries of a square. The group generators are the rotation of an angle of $\pi/2$, that we identify as the element r, and the reflection s across one of its axis of symmetry, as you can see in Fig. 3.1. Denoting the neutral element as e, the algebra of the group is fully specified by the following relations: $r^4 = s^2 = e$ and $srs = r^3$. So the presentation of D_4 can be written as

$$D_4 = \langle r, s : r^4 = s^2 = e, srs = r^3 \rangle. \tag{3.1.1}$$

The notation used in (3.1.1) is called presentation of a group and it is one method of specifying a group through its generators. A presentation $\langle S : R \rangle$ of a group G comprises a set S of generators, in our case $\{r, s\}$, so that every element of the group can be written as a product of powers of these generators, and a set R of relations among those generators.
The explicit list of all elements of the group is

$$D_4 = \{e, r, r^2, r^3, s, rs, r^2s, r^3s\}. \tag{3.1.2}$$

It's immediate to see that the size of the group, i.e. the number of its elements, is $|D_4| = 8$. A graphical representation of the action of each group element is shown in Fig. 3.1.
A generic element g of the group can be written as $g = r^a s^b$, where $a = 0, 1, 2, 3$ while $b = 0, 1$. This notation will be particularly useful in the encoding part.
The Cayley table of the group, in which we can see all possible products between group elements, is reported in Table 3.1. The inverse element table, in which we can see the inverse of all group elements, is reported in Table 3.2.

	e	r	r^2	r^3	s	rs	r^2s	r^3s
e	e	r	r^2	r^3	s	rs	r^2s	r^3s
r	r	r^2	r^3	e	rs	r^2s	r^3s	s
r^2	r^2	r^3	e	r	r^2s	r^3s	s	rs
r^3	r^3	e	r	r^2	r^3s	s	rs	r^2s
s	s	r^3s	r^2s	rs	e	r^3	r^2	r
rs	rs	s	r^3s	r^2s	r	e	r^3	r^2
r^2s	r^2s	rs	s	r^3s	r^2	r	e	r^3
r^3s	r^3s	r^2s	rs	s	r^3	r^2	r	e

Table 3.1: Cayley table of the group D_4. The element in the g-row and h-column represents the product gh.

g	e	r	r^2	r^3	s	rs	r^2s	r^3s
g^{-1}	e	r^3	r^2	r	s	rs	r^2s	r^3s

Table 3.2: Inversion table of the group D_4.

3.1.2 Representation theory

The group has 5 conjugacy classes, which are

$$C_0 = \{e\}, C_1 = \{r, r^3\}, C_2 = \{r^2\}, C_3 = \{s, r^2 s\}, C_4 = \{rs, r^3 s\}. \tag{3.1.3}$$

This means that there are 5 inequivalent irreducible representations ρ and we will label them with $j = 0, 1, 2, 3, 4$. In particular, the first four representations $j = 0, 1, 2, 3$ are Abelian and one-dimensional, while the latter $j = 4$ is non-Abelian and two-dimensional. More explicitly we have that for $j = 0$, the trivial representation ρ_0 is

$$\rho_0(g) = +1 \quad \forall g \in D_4, \tag{3.1.4}$$

for $j = 1$ the representation ρ_1 is

$$\rho_1(g) = \begin{cases} +1 & g \in \langle r^2, s \rangle \\ -1 & \text{otherwise} \end{cases}, \tag{3.1.5}$$

for $j = 2$ the sign representation ρ_2 is

$$\rho_2(g) = \begin{cases} +1 & g \in \langle r \rangle \\ -1 & \text{otherwise} \end{cases}, \tag{3.1.6}$$

for $j = 3$ the representation ρ_3 is

$$\rho_3(g) = \begin{cases} +1 & g \in \langle r^2, rs \rangle \\ -1 & \text{otherwise} \end{cases}. \tag{3.1.7}$$

χ_j	e	r, r^3	r^2	s, r^2s	rs, r^3s
χ_0	$+1$	$+1$	$+1$	$+1$	$+1$
χ_1	$+1$	-1	$+1$	$+1$	-1
χ_2	$+1$	$+1$	$+1$	-1	-1
χ_3	$+1$	-1	$+1$	-1	$+1$
χ_4	$+2$	0	-2	0	0

Table 3.3: Character table of the group D_4.

The action of the non-Abelian representation, $j = 4$, on the group elements is described by

$$\rho_4(r^a) = \begin{pmatrix} e^{2\pi i a/4} & 0 \\ 0 & e^{-2\pi i a/4} \end{pmatrix}, \quad \rho_4(r^a s) = \begin{pmatrix} 0 & e^{2\pi i a/4} \\ e^{-2\pi i a/4} & 0 \end{pmatrix}, \quad a = 0, 1, 2, 3. \tag{3.1.8}$$

One can also explicitly compute the character for each group element. Recall that given the representation j and a group element g, the character of g in the j-th representation is $\chi_j(g) = \mathrm{Tr}\,\rho_j(g)$. In Table 3.3 you can see the character of each representation j for each conjugacy class C.

3.1.3 Generating subset

In section 1.4.4 we saw that for the definition of a finite group Laplacian Δ, and thus also the electric Hamiltonian H_E, we first have to select a generating subset $\Gamma \subset D_4$ which is symmetric $\Gamma = \Gamma^{-1}$, it is invariant under conjugation $\Gamma = g\Gamma g^{-1}$ and it does not contain the identity element $e \notin \Gamma$. Such a generating subset should be the union of some conjugacy classes C introduced before. There is more than one possible choice for Γ and each possibility gives rise to a different theory, but in this thesis we will consider just the two following possibilities [36]:

$$\Gamma_1 = C_1 \cup C_3 = \{r, r^3, s, r^2 s\}, \tag{3.1.9}$$

$$\Gamma_2 = C_1 \cup C_3 \cup C_4 = \{r, r^3, s, rs, r^2 s, r^3 s\}. \tag{3.1.10}$$

The subset Γ_1 is very simple, probably it is the most obvious choice for a subset that has to satisfy the conditions listed above. The choice of Γ_2 is especially interesting, because it gives rise to a manifestly Lorentz-invariant theory [36]. Given these two generating subsets we can compute the corresponding eigenvalues $f(j)$ of the electric Hamiltonian, as they were defined in the equation (1.4.41). All possible values of $f(j)$ for any irreducible representation j of D_4 for both Γ_1 and Γ_2 are listed in Table 3.4. The Cayley graphs (D_4, Γ_1) and (D_4, Γ_2), constructed using these two generating subset and that are used to define the graph Laplacian, are shown in Fig. 3.2a and Fig. 3.2b respectively.

Γ	$j=0$	$j=1$	$j=2$	$j=3$	$j=4$
Γ_1	0	4	4	8	4
Γ_2	0	8	8	8	6

Table 3.4: Table of the values of $f(j)$ (1.4.41) for the gauge group D_4 and for different choices of the generating subset Γ.

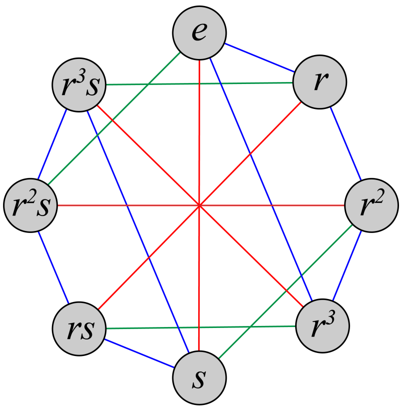

(a) Undirected Cayley graph of (D_4, Γ_1). A link connecting the vertex g_1 to the vertex g_2 means that $g_1 h = g_2$ for some $h \in \Gamma_1$ (3.1.9). If $h = r, r^3$ the edge is blue, if $h = s$ the edge is red and if $h = r^2 s$ the edge is green.

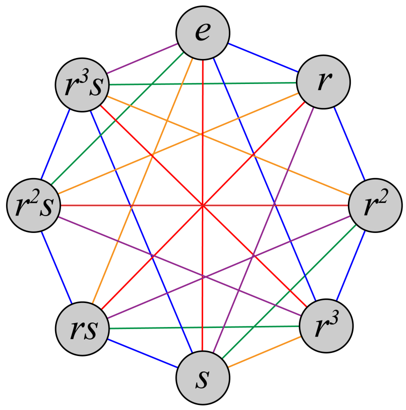

(b) Undirected Cayley graph of (D_4, Γ_2). A link connecting the vertex g_1 to the vertex g_2 means that $g_1 h = g_2$ for some $h \in \Gamma_2$ (3.1.10). If $h = r, r^3$ the edge is blue, if $h = s$ the edge is red, if $h = rs$ the link is orange, if $h = r^2 s$ the edge is green and if $h = r^3 s$ the link is purple.

Figure 3.2: Undirected Cayley graphs of the dihedral group D_4. Each vertex represents an element of the group D_4.

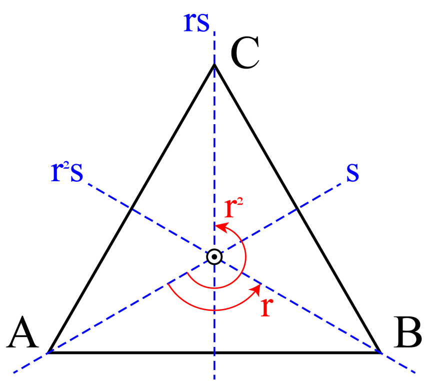

Figure 3.3: Graphical representation of the elements of the group D_3, i.e. the symmetries of an equilateral triangle. Besides the identity element e, we have two rotations r and r^2 of an angle $2\pi/3$ and $4\pi/3$ respectively, and three reflections s, rs, r^2s.

3.2 Dihedral group D_3

In this section we present the dihedral group D_3, the group of symmetries of a equilateral triangle. We give the definition of the group, the list of all its elements and a complete description of its algebra. We study its representation theory, presenting all 3 irreducible representations and finally we show the two possible generating subsets Γ.
The relevance of this group lies in the fact that it is a simple non-Abelian finite subgroup of $SO(3)$, and it can be used to approximate this continuous Lie group. The binary dihedral group $2D_3$ can instead be used to approximate the group $SU(2)$. Another interesting property of D_3 is that it is isomorphic to the symmetric group S_3.

3.2.1 Definition of the group

The *dihedral group* D_3 is the group of symmetries of an equilateral triangle. The group generators are the rotation of an angle of $2\pi/3$, that we identify as the element r, and the reflection s across one of its axis of symmetry, as you can see in Fig. 3.3. This is the smallest possible non-Abelian group. Denoting the neutral element as e, the algebra of the group is fully specified by the following relations: $r^3 = s^2 = e$ and $srs = r^2$. So we can write the group presentation as

$$D_3 = \langle r, s : r^3 = s^2 = e, srs = r^2 \rangle. \tag{3.2.1}$$

The explicit list of all elements of the group is

$$D_3 = \{e, r, r^2, s, rs, r^2s\}. \tag{3.2.2}$$

The size of the group, i.e. the number of its elements, is $|D_3| = 6$. A graphical representation of the action of each group elements is shown in Fig. 3.3.

	e	r	r^2	s	rs	r^2s
e	e	r	r^2	s	rs	r^2s
r	r	r^2	e	rs	r^2s	s
r^2	r^2	e	r	r^2s	s	rs
s	s	r^2s	rs	e	r^2	r
rs	rs	s	r^2s	r	e	r^2
r^2s	r^2s	rs	s	r^2	r	e

Table 3.5: Cayley table of the group D_3. The element in the g-row and h-column represents the product gh.

g	e	r	r^2	s	rs	r^2s
g^{-1}	e	r^2	r	s	rs	r^2s

Table 3.6: Inversion table of the group D_3.

A generic element g of the group can be written as $g = r^a s^b$, where $a = 0, 1, 2$ while $b = 0, 1$. This notation will be particularly useful in the encoding part.
The Cayley table of the group, in which we can see all possible products between group element, is reported in Table 3.5. The inverse element table, in which we can see the inverse of all group elements, is reported in Table 3.6.

3.2.2 Representation theory

The group has 3 conjugacy classes, which are

$$C_0 = \{e\}, C_1 = \{r, r^2\}, C_2 = \{s, rs, r^2s\}. \tag{3.2.3}$$

This means that there are 3 irreducible representations ρ and we will label them with $j = 0, 1, 2$. In particular, the first two representations $j = 0, 1$ are Abelian and one-dimensional, while the latter $j = 2$ is non-Abelian and two-dimensional. More explicitly we have that for $j = 0$, the trivial representation ρ_0 is

$$\rho_0(g) = +1 \quad \forall g \in D_3, \tag{3.2.4}$$

for $j = 1$ the sign-representation ρ_1 is

$$\rho_1(g) = \begin{cases} +1 & g \in \langle r \rangle \\ -1 & \text{otherwise} \end{cases} . \tag{3.2.5}$$

The action of the non-Abelian representation, $j = 2$, on the group elements is described by

$$\rho_2(r^a) = \begin{pmatrix} e^{2\pi i a/3} & 0 \\ 0 & e^{-2\pi i a/3} \end{pmatrix}, \quad \rho_2(r^a s) = \begin{pmatrix} 0 & e^{2\pi i a/3} \\ e^{-2\pi i a/3} & 0 \end{pmatrix}, \quad a = 0, 1, 2. \tag{3.2.6}$$

χ_j	e	r, r^2	s, rs, r^2s
χ_0	$+1$	$+1$	$+1$
χ_1	$+1$	$+1$	-1
χ_2	$+2$	-1	0

Table 3.7: Character table of the group D_3.

Γ	$j=0$	$j=1$	$j=2$
Γ_1	0	6	3
Γ_2	0	6	6

Table 3.8: Table of the values of $f(j)$ (1.4.41) for the gauge group D_3 and for different choices of the generating subset Γ.

One can also explicitly compute the character for each group element. In Table 3.7 you can see the character of each representation j for each conjugacy class C.

3.2.3 Generating subset

In section 1.4.4 we saw that for the definition of a finite group Laplacian Δ, and thus also the electric Hamiltonian H_E, we first have to select a generating subset $\Gamma \subset D_3$ which is symmetric $\Gamma = \Gamma^{-1}$, it is invariant under conjugation $\Gamma = g\Gamma g^{-1}$ and it does not contain the identity element $e \notin \Gamma$. Such a generating subset should be the union of some of the conjugacy classes C introduced before. For the group D_3 there are two possible choices for such a generating subset Γ:

$$\Gamma_1 = C_2 = \{s, rs, r^2s\}, \tag{3.2.7}$$

$$\Gamma_2 = C_1 \cup C_2 = \{r, r^2, s, rs, r^2s\}, \tag{3.2.8}$$

Given these generating subsets we can compute the corresponding eigenvalues $f(j)$ of the electric Hamiltonian, defined in (1.4.41). All possible values of $f(j)$ for any irreducible representation j of D_3 are listed in Table 3.8. The Cayley graphs (D_3, Γ_1) and (D_3, Γ_2) obtained using the generating subsets Γ_1, Γ_2 and used to define the graph Laplacian, are shown in Fig. 3.4a and Fig. 3.4b respectively.

3.2.4 Isomorphism with S_3

An interesting aspect of the group D_3 is that it is isomorphic to the symmetric group S_3, i.e. the set of all permutations that can be performed on 3 symbols: A, B and C. The generators of this group are the adjacent transposition $\sigma_1 = (AB)$ and $\sigma_2 = (BC)$, whose actions are $ABC \to BAC$ and $ABC \to ACB$ respectively. The presentation of the group is:

$$S_3 = \langle \sigma_1, \sigma_2 : \sigma_1^2 = \sigma_2^2 = \sigma_0, (\sigma_1\sigma_2)^3 = \sigma_0 \rangle, \tag{3.2.9}$$

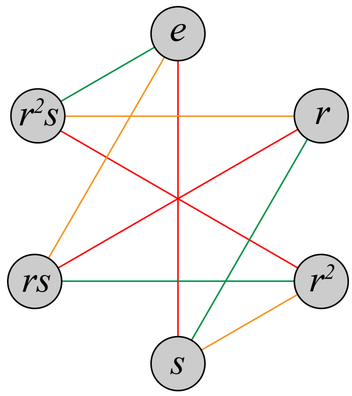

(a) Undirected Cayley graph of (D_3, Γ_1). A link connecting the vertex g_1 to the vertex g_2 means that $g_1h = g_2$ for some $h \in \Gamma_1$ (3.2.7). If $h = s$ the edge is red, if $h = rs$ the link is orange and if $h = r^2s$ the edge is green.

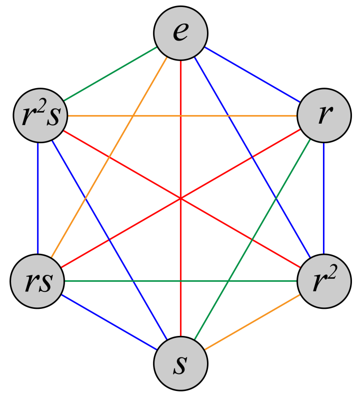

(b) Undirected Cayley graph of (D_3, Γ_2). A link connecting the vertex g_1 to the vertex g_2 means that $g_1h = g_2$ for some $h \in \Gamma_2$ (3.2.8). If $h = r, r^2$ the edge is blue, if $h = s$ the edge is red, if $h = rs$ the link is orange and if $h = r^2s$ the edge is green.

Figure 3.4: Undirected Cayley graphs of the dihedral group D_3. Each vertex represents an element of the group D_3.

where $\sigma_0 = ()$ denotes the identity, whose action is trivial: $ABC \to ABC$. The S_3 group contains $3! = 6$ elements, which are:

$$S_3 = \{\sigma_0, \sigma_1, \sigma_2, \sigma_3, \sigma_4, \sigma_5\}, \tag{3.2.10}$$

where, a part from the identity σ_0, the adjacent transpositions σ_1 and σ_2, we have also the order inversion $\sigma_3 = \sigma_1\sigma_2\sigma_1 = (AC)$ that acts like $ABC \to CBA$, and the cyclic permutations $\sigma_4 = \sigma_2\sigma_1 = (ACB)$ whose action is $ABC \to BCA$, and $\sigma_5 = \sigma_1\sigma_2 = (ABC)$ whose action instead is $ABC \to CAB$.

The non-Abelian groups D_3 and S_3 are isomorphic, indeed consider the function $f : D_3 \to S_3$ such that $f(e) = \sigma_0$, $f(r) = \sigma_5$, $f(r^2) = \sigma_4$, $f(s) = \sigma_1$, $f(rs) = \sigma_3$ and $f(r^2s) = \sigma_2$. In other words the function f is mapping the rotations of D_3 into the 3-cycles of S_3 and the reflections of D_3 into the 2-cycles of S_3. The map f preserves the group product, i.e. the Cayley table in Table 3.5, it is 1-1 and onto, therefore $f : D_3 \to S_3$ is an isomorphism and the dihedral group D_3 is isomorphic to the 3-symmetric group S_3.

The importance of the symmetric groups S_n lies in the fact that these are examples of solvable groups with interesting results for the quantum double model. It has been shown that in this model, for any solvable group G, the preparation of the ground state, the creation of anyon pairs separated by an arbitrary distance, and non-destructive topological charge measurement can be realized by constant-depth adaptive circuits with geometrically local unitary gates and mid-circuit measurements [6].

3.3 One-plaquette system

In this section we derive some theoretical results for a one-plaquette lattice gauge theory with open boundary conditions and using as gauge group the dihedral groups D_4 and D_3 introduced before. We present the total Hilbert space and the gauge invariant Hilbert space for a one-plaquette lattice, for each one we see a possible basis. We use the gauge invariant basis to compute the matrix elements of the Hamiltonian. We numerically diagonalize the Hamiltonian obtaining the energy spectrum and we discuss its eigenstates in the electric and magnetic limit. Finally we consider also the Wilson loop observable.

3.3.1 Hilbert space of a one-plaquette system

Total Hilbert space

We start by considering a generic finite gauge group G, then we will specialize to the D_4 and D_3 cases. Consider a single plaquette system with open boundary conditions, as shown in Fig. 1.9. We associate at each link l of the system a finite-dimensional Hilbert space $\mathcal{H}^{(l)}$ of dimension $|G|$, in this way the total Hilbert space $\mathcal{H}_T$ for a plaquette with four links will be the tensor product of the four single link Hilbert spaces, namely $\mathcal{H}_T = \bigotimes_{l=1}^4 \mathcal{H}^{(l)}$, and it has dimension $|G|^4$. For a single link Hilbert space $\mathcal{H}^{(l)}$ we already know that a possible basis is the set of group element states $\{|g_l\rangle\}$, with $g_l \in G$. For the total Hilbert space $\mathcal{H}_T$ we can take as a basis the set of states $\{|g_1, g_2, g_3, g_4\rangle = \bigotimes_{l=1}^4 |g_l\rangle\}$, with $g_1, g_2, g_3, g_4 \in G$. A generic element $|\psi\rangle$ of the total Hilbert space $\mathcal{H}_T$ can be written as a superposition of these states

$$|\psi\rangle = \sum_{g_1,g_2,g_3,g_4 \in G} \psi(g_1, g_2, g_3, g_4) \, |g_1, g_2, g_3, g_4\rangle \, , \tag{3.3.1}$$

for some coefficients $\psi(g_1, g_2, g_3, g_4)$. Notice that not all states inside $\mathcal{H}_T$ are gauge invariant, and now we will study the constraints to be imposed on $\psi(g_1, g_2, g_3, g_4)$ in order for it to be gauge invariant.

Gauge invariant Hilbert space

Recall that a gauge transformation on a single plaquette is realized by the operator $\mathcal{G}_p = \bigotimes_{v=1}^4 A_v^{g_v}$ (1.5.2) where the product is extended to all four vertices v of the lattice, and $A_v^{g_v}$ is the vertex operator (1.5.1) for the group element g_v and the vertex v. Let's associate a group element to each site of the lattice $g_{v_1}, g_{v_2}, g_{v_3}, g_{v_4} \in G$ as in Fig. 1.7, and then look at how the total wave function $|\psi\rangle$ (3.3.1) changes under the corresponding gauge transformation:

$$\begin{aligned}\mathcal{G}_p |\psi\rangle &= A_{v_1}^{g_{v_1}} A_{v_2}^{g_{v_2}} A_{v_3}^{g_{v_3}} A_{v_4}^{g_{v_4}} |\psi\rangle \\ &= \sum_{g_1,g_2,g_3,g_4 \in G} \psi(g_1, g_2, g_3, g_4) \, |g_{v_1} g_1 g_{v_2}^{-1}, g_{v_2} g_2 g_{v_3}^{-1}, g_{v_4} g_3 g_{v_3}^{-1}, g_{v_1} g_4 g_{v_4}^{-1}\rangle \\ &= \sum_{g_1,g_2,g_3,g_4 \in G} \psi(g_{v_1}^{-1} g_1 g_{v_2}, g_{v_2}^{-1} g_2 g_{v_3}, g_{v_4}^{-1} g_3 g_{v_3}, g_{v_1}^{-1} g_4 g_{v_4}) \, |g_1, g_2, g_3, g_4\rangle \, . \end{aligned} \tag{3.3.2}$$

In this way we have found that in order for the state $|\psi\rangle$ (3.3.1) to be invariant under a gauge transformation $\mathcal{G}_p$ we should have,

$$\psi(g_1, g_2, g_3, g_4) = \psi(g_{v_1}^{-1} g_1 g_{v_2}, g_{v_2}^{-1} g_2 g_{v_3}, g_{v_4}^{-1} g_3 g_{v_3}, g_{v_1}^{-1} g_4 g_{v_4}), \tag{3.3.3}$$

for all $g_1, g_2, g_3, g_4, g_{v_1}, g_{v_2}, g_{v_3}, g_{v_4} \in G$. The only way to realize this condition on a single plaquette is by imposing $\psi(g_1, g_2, g_3, g_4) = \psi(g_1 g_2 g_3^{-1} g_4^{-1})$. For such a single-argument function the gauge condition (3.3.3) reads out as

$$\psi(g) = \psi(hgh^{-1}) \;\; \forall g, h \in G. \tag{3.3.4}$$

A function ψ satisfying the condition (3.3.4) is called a class function, which means that is invariant under the conjugation operation $g \to hgh^{-1}$ with $g, h \in G$, and so it is constant on conjugacy classes. We will see which class functions $\psi(g)$ give us a basis of the gauge invariant Hilbert space $\mathcal{H}_{\text{phys}}$.

One-plaquette gauge invariant basis

Let us first introduce the *electric vacuum* state $|0_E\rangle$, defined as an equal superposition of all the possible grop element states:

$$|0_E\rangle = \frac{1}{\sqrt{|G|^4}} \sum_{g_1,g_2,g_3,g_4 \in G} |g_1, g_2, g_3, g_4\rangle \, . \tag{3.3.5}$$

Notice how this state is trivially gauge invariant, since the constant function $\psi(g) = 1/\sqrt{|G|^4}$ is a class function. One can also directly verify that $A_v^g |0_E\rangle = |0_E\rangle \;\; \forall g \in G, v \in V$. We will see that this state is the ground state of the electric part H_E of the Kogut-Susskind Hamiltonian (1.4.42).
We can now introduce the *plaquette state* $|\tilde{g}\rangle$ through the plaquette operator B_p^g (1.5.3), indeed

$$|\tilde{g}\rangle = \sqrt{|G|} B_p^g |0_E\rangle \, . \tag{3.3.6}$$

Using the explicit expression (1.5.3) for the plaquette operator B_p^g we can see that

$$|\tilde{g}\rangle = \frac{1}{\sqrt{|G|^3}} \sum_{g_1,g_2,g_3,g_4 \in G} \delta(g, g_1 g_2 g_3^{-1} g_4^{-1}) \, |g_1, g_2, g_3, g_4\rangle \, , \tag{3.3.7}$$

where $g_1, g_2, g_3, g_4 \in G$ are the group elements associated to the links of the plaquette p. There is a plaquette state $|\tilde{g}\rangle$ for each group element g, so there are $|G|$ of them. Basically the plaquette state $|\tilde{g}\rangle$ is the superposition of all $|G|^3$ states that have g as the result of the multiplication of the group elements associated to the oriented links. It easy to verify that these states are orthonormal: $\langle\tilde{g}|\tilde{h}\rangle = \delta(g,h)$. The one-plaquette states $\{|\tilde{g}\rangle\}$ are not gauge invariant. Using the commutation rules (1.5.10) between the vertex operator A_v^h (the operator that implements the gauge transformation on the vertex v) and the plaquette operator B_p^g (the operator that initializes the plaquette state $|\tilde{g}\rangle$ on the plaquette p) we can see that

$$A_v^h |\tilde{g}\rangle = \sqrt{|G|} A_v^h B_p^g |0_E\rangle = \sqrt{|G|} B_p^{hgh^{-1}} A_v^h |0_E\rangle = |\widetilde{(hgh^{-1})}\rangle\,, \tag{3.3.8}$$

where we used also the fact that the electric vacuum $|0_E\rangle$ is invariant under the action of A_v^h. The gauge transformation acts like a conjugation of the group element g associated to the whole plaquette and the non-Abelian nature of the group G makes $|\tilde{g}\rangle \neq |\widetilde{(hgh^{-1})}\rangle$. This can also be seen from the fact that the function $\delta(g, g_1 g_2 g_3^{-1} g_4^{-1})$, appearing as coefficient in the definition of the plaquette state $|\tilde{g}\rangle$ (3.3.7), is not a class function and so it does not satisfy the gauge condition (3.3.4). Even if we said that the one-plaquette states in general are not gauge invariant, we can notice that the state $|\tilde{e}\rangle$, where e is the neutral element in the group G, is instead gauge invariant (the conjugation of e gives as a result always e itself). This result is important because we will see that the state $|\tilde{e}\rangle$ is the ground state of the magnetic Hamiltonian H_B (1.4.11).
Even if the plaquette states $|\tilde{g}\rangle$ are not gauge invariant, a linear combination of them can be. Indeed if we take a linear combination of all plaquette states $|\tilde{g}\rangle$ choosing as coefficient a class function, for example the character function χ_j, then we get a gauge invariant state. The states constructed in this way are called *character states* $|\chi_j\rangle$, and are

$$|\chi_j\rangle = \frac{1}{\sqrt{|G|}} \sum_{g\in G} \chi_j(g)\, |\tilde{g}\rangle\,. \tag{3.3.9}$$

There is a character state $|\chi_j\rangle$ for each irreducible representation $j \in \hat{G}$. If one insert the expression (3.3.7) for $|\tilde{g}\rangle$ inside the equation (3.3.9), we obtain an equivalent expression of the character states in terms of the group element basis $\{|g_l\rangle\}$ of each link l:

$$|\chi_j\rangle = \frac{1}{\sqrt{|G|^4}} \sum_{g_1,g_2,g_3,g_4\in G} \chi_j(g_1 g_2 g_3^{-1} g_4^{-1})\, |g_1, g_2, g_3, g_4\rangle\,. \tag{3.3.10}$$

The character function χ_j appearing in (3.3.10) is a class function, it satisfies the gauge condition (3.3.4) and so the character state $|\chi_j\rangle$ is gauge invariant. But that is not all, indeed one can check [49] that the character functions $\chi_j(g)$ form a basis for all class functions $\psi(g)$ which satisfy the condition (3.3.4). This means that the set of character states $\{|\chi_j\rangle\}$, is not only gauge invariant, but also complete: every state of the gauge invariant Hilbert space $\mathcal{H}_{\text{phys}}$ can be written as a superposition of these states, therefore it is a basis. Using the orthogonality theorem for characters (A.3.2) one can also verify that this set is orthonormal:

$$\langle \chi_i | \chi_j \rangle = \frac{1}{|G|} \sum_{g \in G} \chi_i^*(g) \chi_j(g) = \delta_{i,j}. \tag{3.3.11}$$

The character state $|\chi_j\rangle$ can be written also in terms of the representation basis $|j_{mn}\rangle$ at each link. Starting from the expression (3.3.10) for the character state $|\chi_j\rangle$ and using the duality relation (1.3.20) we can find out that

$$\begin{aligned}
|\chi_j\rangle &= \frac{1}{\sqrt{|G|^4}} \sum_{g_1,g_2,g_3,g_4 \in G} \chi_j(g_1 g_2 g_3^{-1} g_4^{-1}) \, |g_1, g_2, g_3, g_4\rangle \\
&= \frac{1}{\sqrt{|G|^4}} \sum_{g_1,\dots,g_4 \in G} \sum_{m_1,\dots,m_4=1}^{d_j} \rho_j(g_1)_{m_1 m_2} \rho_j(g_2)_{m_2 m_3} \rho_j^*(g_3)_{m_4 m_3} \rho_j^*(g_4)_{m_1 m_4} \, |g_1, \dots, g_4\rangle \\
&= \frac{1}{\sqrt{d_j^4}} \sum_{m_1,m_2,m_3,m_4=1}^{d_j} \left| j_{m_1 m2}, j_{m_2 m_3}, j^*_{m_4 m_3}, j^*_{m_1 m_4} \right\rangle ,
\end{aligned} \tag{3.3.12}$$

where we use also some basic results from character theory, like the definition of the character function as $\chi_j(g) = \operatorname{Tr} \rho_j(g)$, the linearity of the representation $\rho_j(gh) = \rho(g)\rho(h)$ and the notion of conjugate representation $\rho_j^*(g) = \rho_j(g^{-1})^T$. From the expression (3.3.12) we can see that in the one-dimensional case, $d_j = 1$, the character state $|\chi_j\rangle$ is simply realized assigning the same representation state $|j_{11}\rangle$ to each link. If the representation j has dimension greater than one, $d_j > 1$, for each link we should take a superposition of all states $|j_{mn}\rangle$ with the same representation representation j. In this sense the character basis $\{|\chi_j\rangle\}$ for the one-plaquette system is analog to the representation basis $\{|j_{mn}\rangle\}$ for the single link, in particular we will see that they both diagonalize the electric Hamiltonian H_E.
It is interesting to notice that one can construct a basis for the one-plaquette system which is the analog of the group element (or position) basis $\{|g\rangle\}$ for the single link and that diagonalize the magnetic Hamiltonian H_B. Given a conjugation class C of size $|C|$, we can define the state

$$|C\rangle = \frac{1}{\sqrt{|C|}} \sum_{g \in C} |\tilde{g}\rangle . \tag{3.3.13}$$

It is easy to see that this state is gauge invariant (a gauge transformation simply reshuffles the elements inside a conjugacy class), and one can also prove [34] that the set of all these states is an orthonormal basis for the gauge invariant Hilbert space $\mathcal{H}_{\text{phys}}$. It exists a duality relation linking this new basis $\{|C\rangle\}$ and the character basis $\{|\chi_j\rangle\}$, which is

$$\langle C | \chi_j \rangle = \sqrt{\frac{|C|}{|G|}} \chi_j(C), \tag{3.3.14}$$

where $\chi_j(C)$ denotes the character of any element inside the conjugacy class C. Appreciate the complete analogy of the relation (3.3.14) with the one (1.3.20) between the position state $|g\rangle$ and the representation state $|j_{mn}\rangle$.
Summarizing what we have seen in this section: the set of the character states $\{|\chi_j\rangle\}$ is an orthonormal basis for the one-plaquette gauge invariant Hilbert space $\mathcal{H}_{\text{phys}}$. The same holds for the set $\{|C\rangle\}$. This result allows us also to establish the dimensionality of the gauge invariant Hilbert space, looking at the number of element in its basis, which is exactly the number of irreducible representations of the group G (or the number of conjugacy classes of the group, that is the same). For the group D_4 there are 5 irreducible representations (or 5 conjugacy classes), so the dimension of the gauge invariant Hilbert space $\mathcal{H}_{\text{phys}}$ is 5, while the total Hilbert space $\mathcal{H}_T$ has dimension $4096 = 8^4$. For the group D_3 there are 3 irreducible representations, so the dimension of the gauge invariant Hilbert space $\mathcal{H}_{\text{phys}}$ is 3, while the total Hilbert space $\mathcal{H}_T$ has dimension $1296 = 6^4$. Now that we have this basis we can use it to compute the matrix elements of the Kogut-Susskind Hamiltonian for a one-plaquette system.

3.3.2 Hamiltonian matrix elements

Now we will proceed in the computation of the matrix elements of the Kogut-Susskind Hamiltonian H_{KS} (1.4.44) using the character basis $\{|\chi_j\rangle\}$. Recall that this Hamiltonian is made of two non commuting parts, the electric Hamiltonian H_E (1.4.42) and the magnetic Hamiltonian H_B (1.4.11), such that $H = H_E + H_B$.

Matrix elements of the electric Hamiltonian

Let's start from the electric part, that is the easiest one since it is diagonal in the character basis $\{|\chi_j\rangle\}$. For the one-plaquette system the electric Hamiltonian H_E (1.4.42) reads out as

$$H_E = \lambda_E \sum_{l=1}^{4} \sum_{j \in \hat{G}} f(j)\mathbb{P}_j(l), \tag{3.3.15}$$

where we recall that we are summing over all 4 links l and irreducible representations j, then $\mathbb{P}_j(l)$ is the projector (1.4.26) onto the subspace of the the representation j of the link l, the function $f(j)$ is defined in the equation (1.4.41) and it depends on the choice of a generating subset Γ. In each link the projectors $\mathbb{P}_j$ are diagonal on the representation basis $\{|j_{mn}\rangle\}$, so using the expression (3.3.12) of the character state $|\chi_j\rangle$ in terms of the representation basis we can easily find that

$$\langle\chi_i| H_E |\chi_j\rangle = \lambda_E \delta_{i,j}[2f(i) + 2f(i^*)]. \tag{3.3.16}$$

For a symmetric generating subset Γ we have that $f(i) = f(i^*)$ and so

$$\langle\chi_i| H_E |\chi_j\rangle = 4\lambda_E f(i)\delta_{i,j}. \tag{3.3.17}$$

Matrix elements of the magnetic Hamiltonian

For the one-plaquette system the magnetic Hamiltonian H_B (1.4.11) reads out as

$$H_B = -2\lambda_B \operatorname{Re}\operatorname{Tr}\hat{W}, \tag{3.3.18}$$

where $\operatorname{Tr}\hat{W}$ is the Wilson loop operator for the unique plaquette present in the system, we defined it in (1.4.10). Let us first notice that the plaquette state $|\tilde{g}\rangle$ is an eigenstate of the Wilson loop operator, in particular we can see that

$$\langle\tilde{g}|\, H_B\, |\tilde{h}\rangle = -2\lambda_B \delta(g,h) \operatorname{Re}\chi_F(g), \tag{3.3.19}$$

where F is a faithful irreducible representation chosen for the magnetic piece. Recalling the expression (3.3.9) of the character state $|\chi_j\rangle$ in terms of the plaquette state $|\tilde{g}\rangle$, we can compute

$$\langle\chi_i|\, H_B\, |\chi_j\rangle = -\frac{2\lambda_B}{|G|}\sum_{g\in G}\chi_j(g)\chi_i^*(g)\operatorname{Re}\chi_F(g). \tag{3.3.20}$$

Matrix elements of the entire Hamiltonian

We can compute the matrix elements of the entire Hamiltonian $H = H_E + H_B$ putting together the two previous results (3.3.17) and (3.3.20), getting

$$\langle\chi_i|\, H\, |\chi_j\rangle = 4\lambda_E f(i)\delta_{i,j} - \frac{2\lambda_B}{|G|}\sum_{g\in G}\chi_j(g)\chi_i^*(g)\operatorname{Re}\chi_F(g). \tag{3.3.21}$$

In order to compute them we have to specify the gauge group G, a generating subset Γ and a representation F for the magnetic part.

3.3.3 Energy spectrum of D_4

Hamiltonian matrix for a D_4 theory

We choose to work with the non-Abelian dihedral group $G = D_4$. All useful information about this group can be found in section 3.1. We use the generating subset Γ_1 (3.1.9) and Γ_2 (3.1.10), and as representation F the unique non-Abelian representation of the group $j = 4$ (3.1.8), that in order to give a more faithful representation of the non-Abelian nature of the group.
For a D_4 theory the matrix elements of the entire Hamiltonian H in the character basis $\{|\chi_j\rangle\}$, using the general relation (3.3.21) are

$$\langle\chi_i|\, H\, |\chi_j\rangle = 4\lambda_E \delta_{i,j} f(i) - \frac{\lambda_B}{4}\sum_{g\in D_4}\chi_j(g)\chi_i^*(g)\operatorname{Re}\chi_4(g). \tag{3.3.22}$$

Explicitly the matrix of the Hamiltonian H in the character basis $\{|\chi_j\rangle\}$ using the generating set Γ_1 is

$$H_1 = \begin{pmatrix} 0 & 0 & 0 & 0 & -2\lambda_B \\ 0 & 32\lambda_E & 0 & 0 & -2\lambda_B \\ 0 & 0 & 32\lambda_E & 0 & -2\lambda_B \\ 0 & 0 & 0 & 32\lambda_E & -2\lambda_B \\ -2\lambda_B & -2\lambda_B & -2\lambda_B & -2\lambda_B & 24\lambda_E \end{pmatrix}, \tag{3.3.23}$$

while using Γ_2 we get

$$H_2 = \begin{pmatrix} 0 & 0 & 0 & 0 & -2\lambda_B \\ 0 & 16\lambda_E & 0 & 0 & -2\lambda_B \\ 0 & 0 & 16\lambda_E & 0 & -2\lambda_B \\ 0 & 0 & 0 & 24\lambda_E & -2\lambda_B \\ -2\lambda_B & -2\lambda_B & -2\lambda_B & -2\lambda_B & 16\lambda_E \end{pmatrix}. \tag{3.3.24}$$

The diagonal elements in the matrices H_1 (3.3.23) and H_2 (3.3.24) come from the electric Hamiltonian H_E, while the elements on the last row and column come from the magnetic Hamiltonian H_B, and the latter are the same in both the matrices since they do not depend on the choice of the generating subset Γ. The diagonalization of these two matrices for arbitrary coupling constants λ_E and λ_B will give us the energy spectrum of the one-plaquette system at that specific coupling regime.

Numerical diagonalization of a D_4 theory

The Hamiltonians H_1 (3.3.23) and H_2 (3.3.24) can be diagonalized numerically. In order to visualize better in a unique graph both the electric ($\lambda_B = 0$) and the magnetic limit ($\lambda_E = 0$) we will use the parametrization of the coupling constants introduced in (1.4.45): $\lambda_E = \lambda$ and $\lambda_B = 1 - \lambda$, with $\lambda \in [0, 1]$.
The numerical diagonalization was performed using the `eig` function of the submodule `linalg` of `numpy` library. The results are plotted in Fig. 3.5a and Fig. 3.5b. As you can see there are 5 states (since the physical Hilbert space in this case is 5-dimensional), but with some degeneracy.

Electrical eigenvalues and eigenstates of a D_4 theory

Let us now focus on the energy eigenvalues and eigenstates of the electric Hamiltonian H_E (3.3.15), so looking at the limit of H (1.4.45) in which $\lambda = 1$. We already know that the electric Hamiltonian is diagonal in the character basis $\{|\chi_j\rangle\}$, so we already know its eigenstates, while the corresponding eigenvalues are simply given by $4f(j)$ (3.3.17). In the Table 3.9 all data about the electric energy spectrum are listed. Notice how the electrical ground state is the character state of the trivial representation $j = 0$. From the expression (3.3.10) for $|\chi_j\rangle$, recalling that $\chi_0(g) = 1$ for all $g \in D_4$ (3.1.4), and comparing it with the definition (3.3.5)

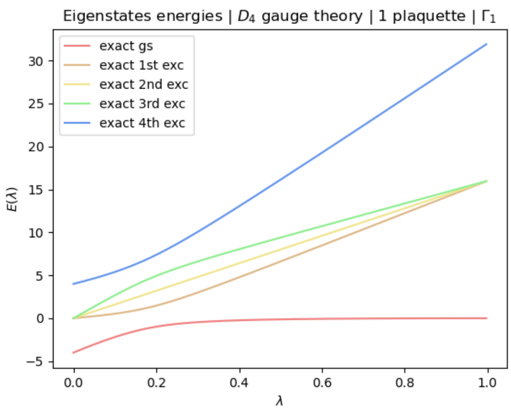

(a) Energy eigenvalues using the generating subset Γ_1 (3.1.9).

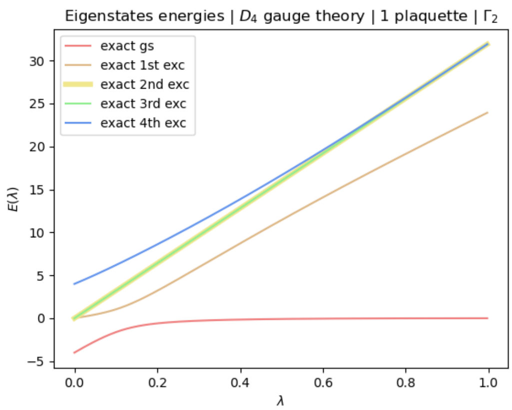

(b) Energy eigenvalues using the generating subset Γ_2 (3.1.10).

Figure 3.5: Energy eigenvalues of the Kogut-Susskind Hamiltonian (1.4.45) as a function of the coupling $\lambda \in [0, 1]$ for a D_4 gauge theory on a one-plaquette system.

$\|\chi_j\rangle$	Γ_1	Γ_2
$\|\chi_0\rangle$	0	0
$\|\chi_1\rangle$	16	32
$\|\chi_2\rangle$	16	32
$\|\chi_3\rangle$	32	32
$\|\chi_4\rangle$	16	24

Table 3.9: Electric eigenstates and corresponding eigenvalues (for both Γ_1 and Γ_2 theory) of the electric Hamiltonian H_E (3.3.15) with the gauge group D_4 in a one-plaquette lattice.

of the electrical vacuum $|0_E\rangle$, one can see that $|\chi_0\rangle = |0_E\rangle$, justifying in this way the name "electrical vacuum" that we assigned to this state before. Notice also that the electric vacuum can be written also as $|0_E\rangle = |0_{11}\rangle^{\otimes 4}$, where we assigned the representation basis state $|0_{11}\rangle$ to each edge.

Magnetic eigenvalues and eigenstates of a D_4 theory

Let us now instead focus on the energy spectrum and the eigenstates of the magnetic Hamiltonian H_B (3.3.18), so looking at the limit of H (1.4.45) in which $\lambda = 0$. Through an analytic calculation one can verify that the magnetic ground state is the plaquette state associated with

eigenstate	eigenvalue
$\|\tilde{e}\rangle$	-4
$(\|\chi_0\rangle - \|\chi_3\rangle)/\sqrt{2}$	0
$(\|\chi_1\rangle - \|\chi_3\rangle)/\sqrt{2}$	0
$(\|\chi_2\rangle - \|\chi_3\rangle)/\sqrt{2}$	0
$\|\widetilde{r^2}\rangle$	$+4$

Table 3.10: Magnetic eigenstates and corresponding eigenvalues of the magnetic Hamiltonian H_B (3.3.18) with the gauge group D_4 in a one-plaquette lattice.

the identity element e of the group:

$$|\tilde{e}\rangle = \frac{1}{\sqrt{8}}(|\chi_0\rangle + |\chi_1\rangle + |\chi_2\rangle + |\chi_3\rangle + 2\,|\chi_4\rangle), \tag{3.3.25}$$

with eigenvalue -4. This result is in line with what expected, since in order to minimize the energy of the magnetic Hamiltonian (3.3.18), you need to maximize the function $\chi_4(g)$, and from character Table 3.3 is easy to see that e is the group element to do so. The full magnetic spectrum is reported in Table 3.10.

3.3.4 Energy spectrum of D_3

Hamiltonian matrix for a D_3 theory

Let's repeat the same procedure for the non-Abelian dihedral group $G = D_3$. All useful information about this group can be found in section 3.2. We use the generating subsets Γ_1 (3.2.7) and Γ_2 (3.2.8) and as faithful representation F the unique non-Abelian representation of the group $j = 2$ (3.2.6).
For D_3 the matrix elements of the entire Hamiltonian H in the character basis $\{|\chi_j\rangle\}$, using the general relation (3.3.21) are

$$\langle\chi_i|\, H\, |\chi_j\rangle = 4\lambda_E \delta_{i,j} f(i) - \frac{\lambda_B}{3} \sum_{g\in D_3} \chi_j(g)\chi_i^*(g)\,\mathrm{Re}\,\chi_2(g). \tag{3.3.26}$$

Explicitly the matrix of the Hamiltonian H in the character basis $\{|\chi_j\rangle\}$ using the generating subset Γ_1 is

$$H_1 = \begin{pmatrix} 0 & 0 & -2\lambda_B \\ 0 & 24\lambda_E & -2\lambda_B \\ -2\lambda_B & -2\lambda_B & 12\lambda_E - 2\lambda_B \end{pmatrix}, \tag{3.3.27}$$

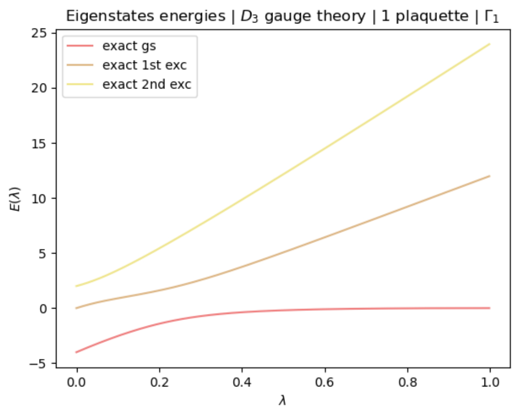

(a) Energy eigenvalues using the generating subset Γ_1 (3.2.7).

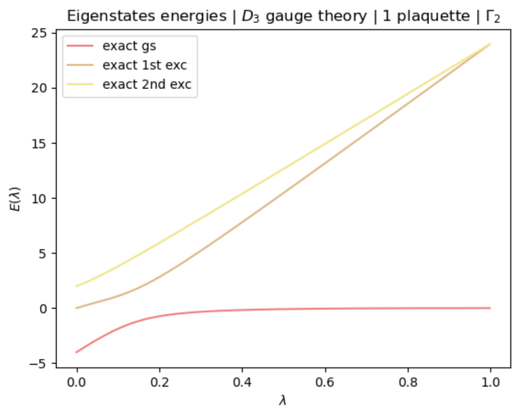

(b) Energy eigenvalues using the generating subset Γ_2 (3.2.8).

Figure 3.6: Energy eigenvalues of the Kogut-Susskind Hamiltonian (1.4.45) as a function of the coupling $\lambda \in [0, 1]$ for a D_3 gauge theory on a one-plaquette system.

while using Γ_2 we get

$$H_2 = \begin{pmatrix} 0 & 0 & -2\lambda_B \\ 0 & 24\lambda_E & -2\lambda_B \\ -2\lambda_B & -2\lambda_B & 24\lambda_E - 2\lambda_B \end{pmatrix}. \tag{3.3.28}$$

The diagonal elements in the matrices H_1 (3.3.27) and H_2 (3.3.28) come from the electric Hamiltonian H_E, while the elements on the last row and column come from the magnetic Hamiltonian H_B. The diagonalization of these matrices for arbitrary coupling constants λ_E and λ_B will give us the energy spectrum of the one-plaquette system at that specific coupling regime.

Numerical diagonalization of a D_3 theory

The Hamiltonians H_1 (3.3.27) and H_2 (3.3.28) can be diagonalize numerically. In order to visualize better in a unique graph both the electric ($\lambda_B = 0$) and the magnetic limit ($\lambda_E = 0$) we will use the parametrization of the coupling constants that we have already adopted for D_4: $\lambda_E = \lambda$, $\lambda_B = 1 - \lambda$ and $\lambda \in [0, 1]$. The results of the numerical diagonalization using this parametrization are plotted in Fig. 3.6a and Fig. 3.6b.

Electrical eigenvalues and eigenstates of a D_3 theory

Let us now focus on the energy eigenvalues and eigenstates of the electric Hamiltonian H_E (3.3.15), so looking at the limit of H (1.4.45) in which $\lambda = 1$. We already know that the electric

$\|\chi_j\rangle$	Γ_1	Γ_2
$\|\chi_0\rangle$	0	0
$\|\chi_1\rangle$	24	24
$\|\chi_2\rangle$	12	24

Table 3.11: Electric eigenstates and corresponding eigenvalues for the generating subsets Γ_1 (3.2.7) and Γ_2 (3.2.8) of the electric Hamiltonian H_E (3.3.15) with the gauge group D_3 in a one-plaquette lattice.

eigenstate	eigenvalue
$\|\tilde{e}\rangle$	-4
$(\|\chi_0\rangle - \|\chi_1\rangle)/\sqrt{2}$	0
$(\|\chi_0\rangle + \|\chi_1\rangle)/\sqrt{2}$	+2

Table 3.12: Magnetic eigenstates and corresponding eigenvalues of the magnetic Hamiltonian H_B (3.3.18) with the gauge group D_3 in a one-plaquette lattice.

Hamiltonian is diagonal in the character basis $\{|\chi_j\rangle\}$, so we already know its eigenstates, while the corresponding eigenvalues are simply given by $4f(j)$ (3.3.17), and recall that $f(j)$ depends on the choice of the generating subset Γ. In the Table 3.11 all data about the electric energy spectrum are listed for both Γ_1 and Γ_2. Notice how the electrical ground state is the character state of the representation $j = 0$. Also for D_3 one can prove in the same way we did for D_4 that $|\chi_0\rangle = |0_E\rangle$. The electric vacuum can be written also as $|0_E\rangle = |0_{11}\rangle^{\otimes 4}$, where we assigned the representation basis state $|0_{11}\rangle$ to each edge.

Magnetic eigenvalues and eigenstates of a D_3 theory

Let us now instead focus on the energy eigenvalues and eigenstates of the magnetic Hamiltonian H_B (3.3.18), so looking at the limit of H (1.4.45) in which $\lambda = 0$. Through an analytic calculation one can verify that the magnetic ground state is the plaquette state associated with the identity element e of the group:

$$|\tilde{e}\rangle = \frac{1}{\sqrt{6}}(|\chi_0\rangle + |\chi_1\rangle + 2\,|\chi_2\rangle), \tag{3.3.29}$$

with eigenvalue -4. This result is in line with what expected, since in order to minimize the energy of the magnetic Hamiltonian (3.3.18), you need to maximize the function $\chi_2(g)$, and from character Table 3.7 is easy to see that e is the group element to do so. The full magnetic spectrum is reported in Table 3.12.

3.3.5 Wilson loop observable

Now we repeat what we have seen for the energy, but this time focusing on the Wilson loop observable $\mathrm{Tr}\,\hat{W}$, just for a D_4 gauge theory. Wilson loops are important observables since they are order parameters for topological phase transitions.

Wilson loop matrix elements

Give a lattice gauge theory with gauge group G in a one-plaquette system it is possible to define just a single Wilson loop operator (1.4.10) on the only plaquette present: $\mathrm{Tr}\,\hat{W} = \mathrm{Tr}\left(\hat{g}_1\hat{g}_2\hat{g}_3^\dagger\hat{g}_4^\dagger\right)$. Notice how the plaqutte state $|\tilde{g}\rangle$ is an eigenstate of the Wilson loop operator, so we can easily compute the matrix elements of this operator in the character basis $\{|\chi_j\rangle\}$ using the expression (3.3.9) for $|\chi_j\rangle$, and we get

$$\langle\chi_i|\,\mathrm{Tr}\,\hat{W}|\chi_j\rangle = \frac{1}{|G|}\sum_{g\in G}\chi_i^*(g)\chi_j(g)\chi_F(g). \tag{3.3.30}$$

In order to compute them we have to specify the gauge group G and a representation F for the magnetic part. Notice that the expression (3.3.30) is proportional to the one of the magnetic Hamiltonian H_B (3.3.20).

Wilson loop for D_4 theory

Consider the group $G = D_4$, let us use as a faithful representation the non-Abelian $j = 4$ representation, such that (3.3.30) becomes

$$\langle\chi_i|\,\mathrm{Tr}\,\hat{W}|\chi_j\rangle = \frac{1}{8}\sum_{g\in D_4}\chi_i^*(g)\chi_j(g)\chi_4(g). \tag{3.3.31}$$

For each $\lambda \in [0,1]$ we compute the expectation value of Wilson loop operator over the ground state of the corresponding Hamiltonian at that specific λ. The results are plotted in Fig. 3.7. In the electric limit $\lambda = 0$, the ground state is the electric vacuum $|0_E\rangle$ (3.3.5), and the expectation value of the Wilson loop operator is zero. In the magnetic limit $\lambda = 1$, the ground state is $|\tilde{e}\rangle$, and the expectation value of Wilson loop operator is $\langle\tilde{e}|\,\mathrm{Tr}\,\hat{W}|\tilde{e}\rangle = \chi_4(e) = 2$, as you can see from character Table 3.3.

3.4 Two-plaquette system

In this section we derive some theoretical results for a two-plaquette lattice gauge theory with open boundary conditions and using as gauge group the dihedral groups D_4 and D_3 introduced before. We present the total Hilbert space and the gauge invariant Hilbert space for a two-plaquette lattice, for each one we see a possible basis. We use the gauge invariant basis to

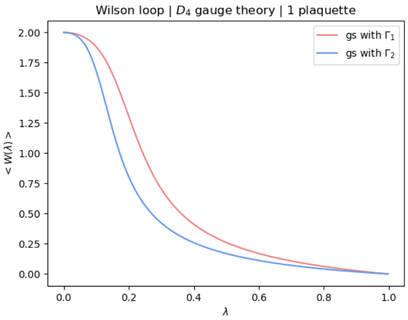

Figure 3.7: Expectation value of the Wilson loop observable $\mathrm{Tr}\,\hat{W}$ with the gauge group D_4, computed on the ground state of the Hamiltonian (1.4.45) for different couplings λ.

compute the matrix elements of the Hamiltonian. We numerically diagonalize the Hamiltonian obtaining the energy spectrum and we discuss its eigenstates in the electric and magnetic limit. Finally we consider also Wilson loop observables.

3.4.1 Hilbert space of a multiple-plaquette system

In this section we are interested in the case of a two-plaquette system with open boundary conditions, but for generality sake we start by considering a lattice with an arbitrary number L of links and V of vertices, with open boundary conditions. The results that we will obtain for this generic model can be easily specialized to the case of a two-plaquette system by imposing $L = 7$ and $V = 6$. We consider also a generic finite gauge group G, then we will specialize in the D_4 and D_3 cases.

Total Hilbert space

We associate at each link l of the system a finite-dimensional Hilbert space $\mathcal{H}^{(l)}$ of dimension $|G|$, in this way the total Hilbert space $\mathcal{H}_T$ for our system of L links will be the tensor product $\mathcal{H}_T = \bigotimes_{l=1}^{L} \mathcal{H}^{(l)}$, and it has dimension $|G|^L$. For a single link Hilbert space $\mathcal{H}^{(l)}$ we already know that a possible basis is the set of group element states $\{|g_l\rangle\}$, for all $g_l \in G$. In the total Hilbert space $\mathcal{H}_T$ we can take as a basis the set of states $\{|g_1, ..., g_L\rangle = \bigotimes_{l=1}^{L} |g_l\rangle\}$, with $g_1, ..., g_L \in G$. A generic element $|\psi\rangle$ of the total Hilbert space $\mathcal{H}_T$ can be written as a superposition of these states

$$|\psi\rangle = \sum_{g_1,...,g_L \in G} \psi(g_1, ..., g_L)\, |g_1, ..., g_L\rangle\,, \tag{3.4.1}$$

for some coefficients $\psi(g_1, ..., g_L)$. Notice that not all states inside $\mathcal{H}_T$ are gauge invariant. In general the identification of the physical gauge invariant Hilbert space $\mathcal{H}_{\text{phys}}$ is not easy, but it exists a simple equation that predicts its dimensionality.

Dimension of the gauge invariant Hilbert space

Working with the formalism of the spin network states one can show that it exists a general equation that predicts the dimensionality of the gauge invariant Hilbert space $\mathcal{H}_{\text{phys}}$ [36]. Given a lattice gauge theory with gauge group G, defined on a lattice with L links and V vertices, the dimension of the corresponding physical Hilbert space is

$$\dim \mathcal{H}_{\text{phys}} = \sum_{C} \left(\frac{|G|}{|C|} \right)^{L-V}, \tag{3.4.2}$$

where the sum is performed over all conjugacy classes C of the group G, and as usual $|G|$ and $|C|$ denote the size of the group G and of the conjugacy class C respectively. The orbit-stabilizer theorem guarantees that the ratio $|G|/|C|$ appearing in (3.4.2) is an integer number [49], and therefore the dimension $\dim \mathcal{H}_{\text{phys}}$ is integer as well. An interesting fact is that among all groups of the same size, the Abelian groups have the gauge invariant Hilbert space of largest possible dimension, $\dim \mathcal{H}_{\text{phys}} = |G|^{L-V+1}$, since their conjugacy classes are singlets. Notice also that the result (3.4.2) predicts the correct dimension for the physical Hilbert space of a one-plaquette lattice $L = V = 4$, that is $\dim \mathcal{H}_{\text{phys}} = |\hat{G}|$, the number of conjugacy classes (or irreducible representations) of G. Indeed in the last section we saw that the character states $\{|\chi_j\rangle\}$, with $j \in \hat{G}$, are a basis for the physical Hilbert space of a one-plaquette system.
Using the equation (3.4.2) we are able to predict the dimensionality of the physical Hilbert space $\mathcal{H}_{\text{phys}}$ of a lattice gauge theory for a generic gauge group G, then in order to construct a basis for such a vector space it will be sufficient to find a number of orthogonal vectors equals to the dimension of the space.

Multiple-plaquette character states

In the previous section we saw that for the one-plaquette system the set of character states $\{|\chi_j\rangle\}$ forms a basis for the physical Hilbert space. We will now extend these states to a multiple-plaquette system and then verify if they form a basis or not.
First of all consider the *electric vacuum state* $|0_E\rangle$:

$$|0_E\rangle = \frac{1}{\sqrt{|G|^L}} \sum_{g_1,...,g_L \in G} |g_1, ..., g_L\rangle, \tag{3.4.3}$$

a simple equal-weight linear superposition of all the possible group element states. This state is gauge invariant, indeed it is possible to directly check that $\mathcal{G}\,|0_E\rangle = |0_E\rangle$, where $\mathcal{G} = \bigotimes_{v=1}^{V} A_v^{g_v}$ is the gauge transformation operator for our system. One can introduce the *multiple-plaquette states* $\{|\tilde{g}_{\gamma_1}, ..., \tilde{g}_{\gamma_M}\rangle\}$ on a open boundary lattice as:

$$|\tilde{g}_{\gamma_1}, ..., \tilde{g}_{\gamma_M}\rangle = \sqrt{|G|^M} B_{\gamma_1}^{g_{\gamma_1}} ... B_{\gamma_M}^{g_{\gamma_M}}\,|0_E\rangle, \tag{3.4.4}$$

where we considered M closed paths γ_m that surround one or more plaquettes, and $B_{\gamma_m}^{g_{\gamma_m}}$ are the corresponding multiple-plaquette operators (1.5.5), with $m = 1, 2, ..., M$. For the purpose of constructing gauge invariant states we will be particularly interested in multiple-plaquette states where all links are included in at least one path γ_m.
The state $|\tilde{g}_{\gamma_1}, ..., \tilde{g}_{\gamma_M}\rangle$ (3.4.4) can be written in terms of the group element basis $\{|g_1, ..., g_L\rangle\}$, substituting the equation for $B_\gamma^{g_\gamma}$ (1.5.5) in (3.4.4), we have

$$|\tilde{g}_{\gamma_1}, ..., \tilde{g}_{\gamma_M}\rangle = \frac{1}{\sqrt{|G|^{L-M}}} \sum_{g_1,...,g_L \in G} \delta\left(g_{\gamma_1}, \prod_{l\in\gamma_1} g[l]\right) \ldots \delta\left(g_{\gamma_M}, \prod_{l\in\gamma_M} g[l]\right) |g_1, ..., g_L\rangle \,, \tag{3.4.5}$$

where we recall that we are considering M closed path γ_m, the products $\prod_{l\in\gamma_m}$ inside the delta are extended to all links l of a precised path γ_m, and by $g[l]$ we mean g_l or g_l^{-1} depending on the orientation of the link with respect to the direction of the path.
As we already saw for the one-plaquette system, the multiple-plaquette states $\{|\tilde{g}_{\gamma_1}, ..., \tilde{g}_{\gamma_M}\rangle\}$ in general are not gauge invariant: the action of a gauge transformations is like a conjugation of the group elements appearing inside the ket. Even if the multiple-plaquette states $\{|\tilde{g}_{\gamma_1}, ..., \tilde{g}_{\gamma_M}\rangle\}$ are not gauge invariant we can use a linear combination of them to construct states which are gauge invariant, as we did for the one-plaquette system. We can introduce the *multiple-plaquette character states* as

$$|\chi_{i_1}(\gamma_1)...\chi_{i_M}(\gamma_M)\rangle = \frac{1}{\sqrt{|G|^M}} \sum_{g_{\gamma_1},...,g_{\gamma_M} \in G} \chi_{i_1}(g_{\gamma_1})...\chi_{i_M}(g_{\gamma_M}) \, |\tilde{g}_{\gamma_1}, ..., \tilde{g}_{\gamma_M}\rangle \,, \tag{3.4.6}$$

where we have M close paths γ_m and at each one we associate a character χ_{i_m}, with $m = 1, 2, ..., M$. As long as all L links are included in at least one path, these states are manifestly gauge invariant, since character function $\chi_i(g)$ is invariant under conjugation (it is a class function) and all group elements (which are conjugated by the gauge transformation) appear inside a character function.

Two-plaquette character states

Let us now focus on a two-plaquette system like the one in Fig. 3.8. There are only three possible choices for a closed path γ: the first plaquette p_1 that contains in order the links 1, 2, 3 and 4, the second plaquette p_2 that contains in order the edges 5, 6, 7 and 2, and a multiple-plaquette loop p_3 that contains in order the links 1, 5, 6, 7, 3 and 4.
Consider the case of multiple-plaquette states where there are $M = 2$ paths and each of them surrounds a single plaquette $\gamma_1 = p_1$ and $\gamma_2 = p_2$. From the equation (3.4.5) one has that their explicit expression is

$$|\tilde{g}_{p_1}, \tilde{g}_{p_2}\rangle = \frac{1}{\sqrt{|G|^5}} \sum_{g_1,...,g_7 \in G} \delta(g_{p_1}, g_1 g_2 g_3^{-1} g_4^{-1}) \delta(g_{p_2}, g_5 g_6 g_7^{-1} g_2^{-1}) \, |g_1, ..., g_7\rangle \,. \tag{3.4.7}$$

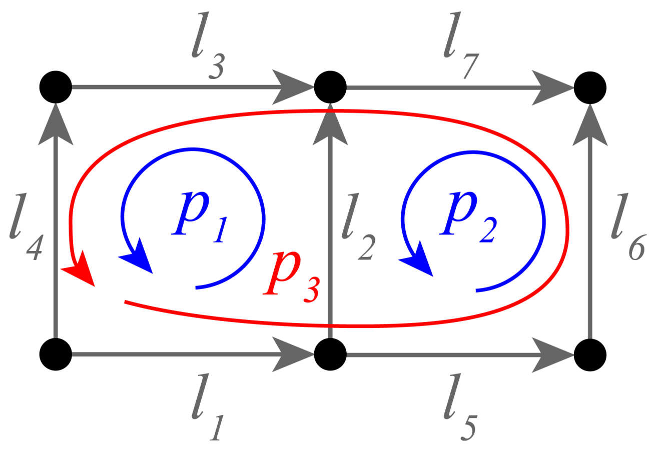

Figure 3.8: Two plaquette system. The lattice contains $V = 6$ vertices and $E = 7$ oriented edges. One can identify three inequivalent loops: first plaquette p_1, second plaquette p_2 and external boundaries p_3.

Basically these states are a linear superposition of all states in which the product of the group elements associated to the edges of the plaquette p_1 give rise to the group element g_{p_1}, and similarly for the plaquette p_2. Another possible multiple-plaquette state involves the single plaquette p_1 and the two-plaquette loop p_3, in this case we can see that:

$$|\tilde{g}_{p_1}, \tilde{g}_{p_3}\rangle = \frac{1}{\sqrt{|G|^5}} \sum_{g_1,\dots,g_7 \in G} \delta(g_{p_1}, g_1 g_2 g_3^{-1} g_4^{-1}) \delta(g_{p_3}, g_1 g_5 g_6 g_7^{-1} g_3^{-1} g_4^{-1}) \, |g_1, \dots, g_7\rangle \,. \quad (3.4.8)$$

The multiple-plaquette character state associated to a state with two single-plaquette loops, p_1 and p_2, can be found inserting the expression (3.4.7) inside (3.4.6), obtaining:

$$\begin{aligned} |\chi_i(p_1)\chi_j(p_2)\rangle &= \frac{1}{\sqrt{|G|^2}} \sum_{g_{p_1}, g_{p_2} \in G} \chi_i(g_{p_1})\chi_j(g_{p_2}) \, |\tilde{g}_{p_1}, \tilde{g}_{p_2}\rangle \\ &= \frac{1}{\sqrt{|G|^7}} \sum_{g_1,\dots,g_7 \in G} \chi_i(g_1 g_2 g_3^{-1} g_4^{-1}) \chi_j(g_5 g_6 g_7^{-1} g_2^{-1}) \, |g_1, \dots, g_7\rangle \,. \end{aligned} \quad (3.4.9)$$

To be more concise we will use the following notation $|\chi_i(p_1)\chi_j(p_2)\rangle \equiv |i, j\rangle$, where the fact that the first index i is the representation of the plaquette p_1 is taken as granted, as well as the fact that the second index j is the representation of the plaquette p_2. The multiple-plaquette character state associated to a state with a single-plaquette loop p_1 and a two-plaquette loop

p_3, can be found inserting the expression (3.4.8) inside (3.4.6), obtaining:

$$\begin{aligned}|\chi_i(p_1)\chi_j(p_3)\rangle &= \frac{1}{\sqrt{|G|^2}} \sum_{g_{p_1},g_{p_3}\in G} \chi_i(g_{p_1})\chi_j(g_{p_3})\,|\tilde{g}_{p_1},\tilde{g}_{p_3}\rangle \\ &= \frac{1}{\sqrt{|G|^7}} \sum_{g_1,\ldots,g_7\in G} \chi_i(g_1g_2g_3^{-1}g_4^{-1})\chi_j(g_1g_5g_6g_7^{-1}g_3^{-1}g_4^{-1})\,|g_1,\ldots,g_7\rangle\,.\end{aligned} \tag{3.4.10}$$

We will use a more compact notation $|\chi_i(p_1)\chi_j(p_3)\rangle \equiv |i,\bar{j}\rangle$, where the fact that the first index i is the representation of the plaquette p_1 is taken as granted, as well as the fact that the second barred index $\bar{j}$ is the representation of the two-plaquette loop p_3. In principle one can construct others multiple-plaquette character states, like $|\chi_i(p_2)\chi_j(p_3)\rangle$ or $|\chi_i(p_1)\chi_j(p_2)\chi_k(p_3)\rangle$, but we don't need them to build a basis for the gauge invariant Hilbert space.
In the one-plaquette system we saw that the character states are orthonormal, a similar result holds also for multiple-plaquette character states, but with some exceptions. Let's consider the scalar product between two character states $|i,j\rangle$ (3.4.6), using the orthogonality theorem for characters (A.3.2) we have

$$\begin{aligned}\langle i_1,i_2|j_1,j_2\rangle &= \frac{1}{|G|^2} \sum_{g_{p_1},g_{p_2}\in G} \chi^*_{i_1}(g_{p_1})\chi^*_{i_2}(g_{p_2})\chi_{j_2}(g_{p_1})\chi_{j_2}(g_{p_2}) \\ &= \delta_{i_1,j_1}\delta_{i_2,j_2}.\end{aligned} \tag{3.4.11}$$

The scalar product (3.4.11) shows that states like $|i,j\rangle$ are orthogonal and so linearly independent. The same can be shown for character states like $|i_1,\bar{i}_2\rangle$ which involves a two-plaquette loop:

$$\langle i_1,\bar{i}_2|j_1,\bar{j}_2\rangle = \delta_{i_1,j_1}\delta_{i_2,j_2}. \tag{3.4.12}$$

The mixed scalar product between a state $|i_1,i_2\rangle$ and a state $|j_1,\bar{j}_2\rangle$ give as a result

$$\begin{aligned}\langle i_1,i_2|j_1,\bar{j}_2\rangle =&\frac{1}{|G|^7} \sum_{g_1,\ldots,g_7\in G} \chi^*_{i_1}(g_1g_2g_3^{-1}g_4^{-1})\chi^*_{i_2}(g_5g_6g_7^{-1}g_2^{-1})\cdot \\ &\cdot \chi_{j_1}(g_1g_2g_3^{-1}g_4^{-1})\chi_{j_2}(g_1g_5g_6g_7^{-1}g_3^{-1}g_4^{-1}) \\ =&\frac{1}{|G|^3} \sum_{g_1,g_{p_1},g_{p_2}\in G} \chi^*_{i_1}(g_{p_1})\chi^*_{i_2}(g_{p_2})\chi_{j_1}(g_{p_1})\chi_{j_2}(g_1g_{p_2}g_1^{-1}g_{p_1}).\end{aligned} \tag{3.4.13}$$

In general the scalar product (3.4.13) is different from zero, and so in general multiple-plaquette character states defined on different paths are not orthogonal.
A multiple character state like $|i,j\rangle$ (3.4.9) can be written also in terms of the representation basis $\{|j_{mn}\rangle\}$ of each link using the duality relation (1.3.20) as we did in the one-plaquette system (3.3.12). In a two-plaquette system there are some problems in the assignment of a specific representation to the shared link $l = 2$, because it belongs to the plaquette p_1 in the

representation i, but it is also part of the plaquette p_2 in the representation j. More explicitly we can see that:

$$
\begin{aligned}
|i,j\rangle =& \frac{1}{\sqrt{|G|^7}} \sum_{g_1,\dots,g_7\in G} \chi_i(g_1 g_2 g_3^{-1} g_4^{-1}) \chi_j(g_5 g_6 g_7^{-1} g_2^{-1}) \,|g_1,\dots,g_7\rangle \\
=& \frac{1}{\sqrt{|G|^7}} \sum_{g_1,\dots,g_7\in G} \sum_{m_1,\dots,m_4=1}^{d_i} \sum_{n_1,\dots,n_4=1}^{d_j} \rho_i(g_1)_{m_1m_2} \rho_i(g_2)_{m_2m_3} \rho_i^*(g3)_{m_4m_3} \rho_i^*(g_4)_{m_1m_4} \cdot \\
& \cdot \rho_j(g_5)_{n_1n_2} \rho_j(g_6)_{n_2n_3} \rho_i^*(g_7)_{n_4n_3} \rho_j^*(g_2)_{n_1n_4} \,|g_1,\dots,g_7\rangle \\
=& \frac{1}{\sqrt{|G| d_i^3 d_j^3}} \sum_{g_2\in G} \sum_{m_1,\dots,m_4=1}^{d_i} \sum_{n_1,\dots,n_4=1}^{d_j} \rho_i(g_2)_{m_2m_3} \rho_j^*(g_2)_{n_1n_4} \cdot \\
& \cdot \left| i_{m_1m_2}, g_2, i^*_{m_4m_3}, i^*_{m_1m_4}, j_{n_1n_2}, j_{n_2n_3}, j^*_{n_4n_3} \right\rangle .
\end{aligned} \tag{3.4.14}
$$

The same problem arises with states like $|i,\bar{j}\rangle$, where the shared edges that cannot have a precise representation, not i not j, are $l = 1, 3, 4$.
In the following we will try to use the gauge invariant states $\{|i,j\rangle, |i,\bar{j}\rangle\}$ to construct a basis for the gauge invariant Hilbert space $\mathcal{H}_{\text{phys}}$, but in order to do so we have to choose a particular group G.

Two-plaquette gauge invariant basis for D_4

Consider as gauge group the dihedral group D_4. The dimensionality of its physical Hilbert space $\mathcal{H}_{\text{phys}}$ is given by the equation (3.4.2) that we discussed before. The group D_4 has three conjugacy classes of size 2 and two conjugacy classes of size 1, then in the case of a two-plaquette system, where there are $L = 7$ links and $V = 6$ vertices, we can easily check that the dimension of the gauge invariant Hilbert space is $\dim \mathcal{H}_{\text{phys}} = 28$. In order to find a basis of this space it will be sufficient to find 28 orthogonal vectors inside this vector space.
The set of multiple-plaquette character states $\{|i,j\rangle, |i,\bar{j}\rangle\}$ forms a set of gauge invariant states, so we might use them to create the basis for the physical Hilbert space $\mathcal{H}_{\text{phys}}$. First we count how many such states we have in a D_4 gauge theory. The indices i and j, that label the representation, can take 5 different values each and so there are $25 = 5^2$ states like $|i,j\rangle$, and others 25 states like $|i,\bar{j}\rangle$: in total 50 gauge invariant states. In principle one could also consider states like $|\chi_i(p_2)\chi_j(p_3)\rangle$ or $|\chi_i(p_1)\chi_j(p_2)\chi_k(p_3)\rangle$, but as we will see they are not necessary, the previous 50 are more than enough to construct a basis. As the dimension of the physical Hilbert space $\mathcal{H}_{\text{phys}}$ for a D_4 gauge theory is 28, we can infer that in the set $\{|i,j\rangle, |i,\bar{j}\rangle\}$ there are at least 22 not linearly independent states that can be removed in order to form an orthonormal basis.
To understand better which of these gauge invariant states are linearly independent, we can look at their scalar products. The scalar product (3.4.11) shows that the set of states $\{|i,j\rangle\}$ is

product	i_1	i_2	j_1	$\bar{j}_2$	product	i_1	i_2	j_1	$\bar{j}_2$
1	0	0	0	0	1	3	2	1	2
1	0	1	1	1	1	3	3	0	3
1	0	2	2	2	1	4	0	4	0
1	0	3	3	3	1	4	1	4	1
1	1	0	1	0	1	4	2	4	2
1	1	1	0	1	1	4	3	4	3
1	1	2	3	2	0.5	0	4	4	4
1	1	3	2	3	0.5	1	4	4	4
1	2	0	2	0	0.5	2	4	4	4
1	2	1	3	1	0.5	3	4	4	4
1	2	2	0	2	0.5	4	4	0	4
1	2	3	1	3	0.5	4	4	1	4
1	3	0	3	0	0.5	4	4	3	4
1	3	1	2	1	0.5	4	4	3	4

Table 3.13: The non vanishing scalar products of the type $\langle i_1, i_2 | j_1, \bar{j}_2 \rangle$ (3.4.13) for the gauge group D_4.

orthonormal, therefore its states are linearly independent. The same can be shown for the character states $\{|i_1, \bar{i}_2\rangle\}$ which involves a two-plaquette loop (3.4.12). The mixed scalar product between a state $|i_1, i_2\rangle$ and a state $|j_1, \bar{j}_2\rangle$, that we computed in (3.4.13), in general is different from zero, in particular the values different from zero for $G = D_4$ are reported in Table 3.13. From this table we can notice that the states $\{|i, \bar{4}\rangle\}$, with $i = 0, 1, 2, 3$ (non-Abelian representation index) are orthogonal to all states $\{|j_1, j_2\rangle\}$ except when $j_1 = j_2 = 4$. Therefore a set of orthogonal states is given by

$$\{|j_1, j_2\rangle \,, |i, \bar{4}\rangle : i \in [0, 3], j_1, j_2 \in [0, 4] \text{ but not } j_1 = j_2 = 4\}. \tag{3.4.15}$$

The set (3.4.15) contains all states made of two one-plaquette character states $|j_1, j_2\rangle = |\chi_{j_1}(p_1)\chi_{j_2}(p_2)\rangle$, except the one in which both the plaquettes are in the non-Abelian representation $j_1 = j_2 = 4$, so there are 24 states of this kind. The set (3.4.15) contains also some multiple-character states $|i, \bar{4}\rangle = |\chi_i(p_1)\chi_4(p_3)\rangle$ in which the plaquette p_1 is in an Abelian representation $i = 0, 1, 2, 3$ while the multiple-plaquette loop p_3 is in the non-Abelian representation, so there are 4 states of this kind. The set (3.4.15) contains 28 states that are gauge invariant and orthogonal states, we already know that the dimension of the gauge invariant Hilbert space is 28, then the set (3.4.15) is a basis of the D_4 lattice gauge theory on a two-plaquette system. It's noteworthy that for a multiple-plaquette system in order to construct a basis we need to take in account states that involves multiple-plaquette loops, like $|i, \bar{4}\rangle$.

Two-plaquette gauge invariant basis for D_3

Consider now as gauge group the dihedral group D_3. The dimensionality of its physical Hilbert space $\mathcal{H}_{\text{phys}}$ is given by the equation (3.4.2) that we discussed before. The group D_3 has one conjugacy class of size 1, one conjugacy class of size 2 and one conjugacy class of size 3, then in the case of a two-plaquette system, where there are $L = 7$ links and $V = 6$ vertices, we can easily check that the dimension of the gauge invariant Hilbert space is $\dim \mathcal{H}_{\text{phys}} = 11$. In order to find a basis of this space it will be sufficient to find 11 orthogonal vectors inside this vector space.
Let's use the set of multiple-plaquette character states $\{|i,j\rangle, |i,\bar{j}\rangle\}$ to construct the basis for the physical Hilbert space, but first count how many states we have inside this set for D_3. The indices i and j, which label the representations, can take 3 different values each and so there are $9 = 3^2$ states like $|i,j\rangle$, and others 9 states like $|i,\bar{j}\rangle$, in total 18 gauge invariant states, that are more than enough to construct a basis. We already know that the dimension of the physical Hilbert space for a D_3 gauge theory is 11, this means that the set $\{|i,j\rangle, |i,\bar{j}\rangle\}$ is over-complete and we have to remove some states in order to have a basis. To understand better which of these gauge invariant states are also linearly independent, we can look at their scalar products. Using the orthogonality theorem for characters we have already seen that the scalar product between two different character states like $|i,j\rangle$ is zero (3.4.11), hence these states are orthogonal and so linearly independent. The same can be shown for the character states $|i_1,\bar{i}_2\rangle$ which involves a two-plaquette loop (3.4.12). The expression of the mixed scalar product between a state $|i_1,i_2\rangle$ and a state $|j_1,\bar{j}_2\rangle$ is (3.4.13), that in general is different from zero. In particular these scalar products for $G = D_3$ are reported in Table 3.14. From this table we can construct a set of orthogonal states:

$$\{|j_1,j_2\rangle, |i,\bar{2}\rangle, |\widetilde{2,2}\rangle : i \in [0,2], j_1, j_2 \in [0,3] \text{ but not } j_1 = j_2 = 2\}, \tag{3.4.16}$$

where the state $|\widetilde{2,2}\rangle$ is obtained from $|2,2\rangle$ removing the components along the directions of $|0,\bar{2}\rangle$ and $|1,\bar{2}\rangle$, to make it orthogonal to all other states in the basis. Therefore the state $|\widetilde{2,2}\rangle$ is defined as

$$|\widetilde{2,2}\rangle = \sqrt{2}\left(|2,2\rangle - \frac{1}{2}|0,\bar{2}\rangle - \frac{1}{2}|1,\bar{2}\rangle\right). \tag{3.4.17}$$

The set (3.4.16) contains 8 states like $|j_1,j_2\rangle$, 2 states like $|i,\bar{2}\rangle$ and finally the state $|\widetilde{2,2}\rangle$, thus the set (3.4.16) contains in total 11 states that are gauge invariant and orthogonal states, we already know that the dimension of the gauge invariant Hilbert space is 11, then the set (3.4.16) is a basis of the D_3 lattice gauge theory on a two-plaquette system.

3.4.2 Hamiltonian matrix elements

Now we see which are the matrix elements of the Kogut-Susskind Hamiltonian H (1.4.44) for a two-plaquette system using the basis made of character states like $\{|i_1,i_2\rangle\}$ (3.4.9) and

product	i_1	i_2	j_1	j_2
1	0	0	0	0
1	0	1	1	1
0.5	0	2	2	2
1	1	0	1	0
1	1	1	0	1
0.5	1	2	2	2
1	2	0	2	0
1	2	1	2	1
0.5	2	2	0	2
0.5	2	2	1	2
0.5	2	2	2	2

Table 3.14: The non vanishing scalar products of the type $\langle i_1, i_2 | j_1, \bar{j_2}\rangle$ (3.4.13) for the gauge group $G = D_3$.

$\{|j_1, \bar{j_2}\rangle\}$ (3.4.10). The full calculations are reported in appendix B for a generic gauge group G, in this subsection we only show the results. Recall that the Kogut-Susskind Hamiltonian is made of two non commuting parts, the electric Hamiltonian H_E and the magnetic Hamiltonian H_B, such that $H = H_E + H_B$.

Matrix elements of the electric Hamiltonian

Let's start from the electric Hamiltonian H_E (1.4.42) for a two-plaquette system, which is diagonal in the multiple-character states. The computations that lead to the results shown here can be found in the appendix B.1. The matrix elements of the character states like $\{|i_1, i_2\rangle\}$ (3.4.9) are

$$\langle i_1, i_2| H_E |j_1, j_2\rangle = \lambda_E \left[3f(i_1) + 3f(i_2) + \bar{f}(i_1, i_2)\right] \delta_{i_1,j_1}\delta_{i_2,j_2}, \tag{3.4.18}$$

where the two-argument function $\bar{f}(i, j)$ is defined as

$$\bar{f}(i, j) = |\Gamma| - \frac{1}{d_i d_j} \sum_{g\in\Gamma} \chi_i^*(g)\chi_j(g). \tag{3.4.19}$$

The matrix elements of the character states like $\{|j_1, \bar{j_2}\rangle\}$ (3.4.10) are

$$\langle i_1, \bar{i_2}| H_E |j_1, \bar{j_2}\rangle = \left[f(i_1) + 3f(i_2) + 3\bar{f}(i_1, i_2)\right] \delta_{i_1,j_1}\delta_{i_2,j_2}. \tag{3.4.20}$$

The mixed matrix elements $\langle i_1, \bar{i_2}| H_E |j_1, j_2\rangle$, or their Hermitian conjugate, are trivially zero.

Matrix elements of the magnetic Hamiltonian

Consider now the magnetic Hamiltonian H_B (1.4.11) for a two-plaquette system. The computations that lead to the results shown here can be found in the appendix B.2. The matrix elements of the character states like $\{|i_1, i_2\rangle\}$ (3.4.9) are

$$\langle i_1, i_2|H_B|j_1, j_2\rangle = -\frac{2\lambda_B}{|G|^2} \sum_{g_{p_1}, g_{p_2} \in G} \chi^*_{i_1}(g_{p_1})\chi^*_{i_2}(g_{p_2})\chi_{j_1}(g_{p_1})\chi_{j_2}(g_{p_2})\cdot \\ \cdot \left[\mathrm{Re}\,\chi_F(g_{p_1}) + \mathrm{Re}\,\chi_F(g_{p_2})\right]. \tag{3.4.21}$$

The matrix elements of the character states like $\{|j_1, \bar{j}_2\rangle\}$ (3.4.10) are

$$\langle i_1, \bar{i}_2|H_B|j_1, \bar{j}_2\rangle = -\frac{2\lambda_B}{|G|^3} \sum_{g_1, g_{p_1}, g_{p_2} \in G} \chi^*_{i_1}(g_{p_1})\chi^*_{i_2}(g_1 g_{p_2} g_1^{-1} g_{p_1})\chi_{j_1}(g_{p_1})\chi_{j_2}(g_1 g_{p_2} g_1^{-1} g_{p_1})\cdot \\ \cdot \left[\mathrm{Re}\,\chi_F(g_{p_1}) + \mathrm{Re}\,\chi_F(g_{p_2})\right]. \tag{3.4.22}$$

The mixed matrix elements are

$$\langle i_1, \bar{i}_2|H_B|j_1, j_2\rangle = -\frac{2\lambda_B}{|G|^3} \sum_{g_1, g_{p_1}, g_{p_2} \in G} \chi^*_{i_1}(g_{p_1})\chi^*_{i_2}(g_1 g_{p_2} g_1^{-1} g_{p_1})\chi_{j_1}(g_{p_1})\chi_{j_2}(g_{p_2})\cdot \\ \cdot \left[\mathrm{Re}\,\chi_F(g_{p_1}) + \mathrm{Re}\,\chi_F(g_{p_2})\right]. \tag{3.4.23}$$

The matrix elements like $\langle i_1, i_2|H_B|j_1, \bar{j}_2\rangle$ are simply the complex conjugate of the expression (3.4.23).
In order to have a more explicit expression of the electric and magnetic Hamiltonian matrix elements we have first to choose a gauge group G, a generating subset Γ and a faithful representation F.

3.4.3 Energy spectrum of D_4

Hamiltonian matrix for a D_4 theory

In the previous discussion we derive the matrix elements of the Kogut-Susskind Hamiltonian H (1.4.44) in a two-plaquette system for generic gauge group G. Now we select the dihedral group D_4, we use the generating subset Γ_1 (3.1.9) and Γ_2 (3.1.10), and as fundamental representation F the unique non-Abelian representation of the group $j = 4$. The matrices will be written in terms of the basis $\{|i_1, i_2\rangle, |j, \bar{4}\rangle\}$ (3.4.15), with $i_1, i_2 = 0, 1, 2, 3, 4$ but not $i_1 = i_2 = 4$ and $j = 0, 1, 2, 3$. In particular the order with which these states appear in the rows and the columns of the matrices is:

$$|0, 0\rangle, |0, 1\rangle, ..., |0, 4\rangle, |1, 0\rangle, |1, 1\rangle, ..., |4, 3\rangle, |0, \bar{4}\rangle, ..., |3, \bar{4}\rangle.$$

The matrix elements of the electric Hamiltonian H_E (B.1.1) are presented in the equations (3.4.18) and (3.4.20), and they depend on the choice of the generating subset Γ, through the functions $f(i)$ and $\bar{f}(i,j)$. Choosing the generating subset Γ_1 (3.1.9) we get

$$H_{1E} = \lambda_E \begin{pmatrix}
0&0&0&0&0&0&0&0&0&0&0&0&0&0&0&0&0&0&0&0&0&0&0&0&0&0&0&0\\
0&16&0&0&0&0&0&0&0&0&0&0&0&0&0&0&0&0&0&0&0&0&0&0&0&0&0&0\\
0&0&16&0&0&0&0&0&0&0&0&0&0&0&0&0&0&0&0&0&0&0&0&0&0&0&0&0\\
0&0&0&32&0&0&0&0&0&0&0&0&0&0&0&0&0&0&0&0&0&0&0&0&0&0&0&0\\
0&0&0&0&16&0&0&0&0&0&0&0&0&0&0&0&0&0&0&0&0&0&0&0&0&0&0&0\\
0&0&0&0&0&16&0&0&0&0&0&0&0&0&0&0&0&0&0&0&0&0&0&0&0&0&0&0\\
0&0&0&0&0&0&24&0&0&0&0&0&0&0&0&0&0&0&0&0&0&0&0&0&0&0&0&0\\
0&0&0&0&0&0&0&32&0&0&0&0&0&0&0&0&0&0&0&0&0&0&0&0&0&0&0&0\\
0&0&0&0&0&0&0&0&40&0&0&0&0&0&0&0&0&0&0&0&0&0&0&0&0&0&0&0\\
0&0&0&0&0&0&0&0&0&28&0&0&0&0&0&0&0&0&0&0&0&0&0&0&0&0&0&0\\
0&0&0&0&0&0&0&0&0&0&16&0&0&0&0&0&0&0&0&0&0&0&0&0&0&0&0&0\\
0&0&0&0&0&0&0&0&0&0&0&32&0&0&0&0&0&0&0&0&0&0&0&0&0&0&0&0\\
0&0&0&0&0&0&0&0&0&0&0&0&24&0&0&0&0&0&0&0&0&0&0&0&0&0&0&0\\
0&0&0&0&0&0&0&0&0&0&0&0&0&40&0&0&0&0&0&0&0&0&0&0&0&0&0&0\\
0&0&0&0&0&0&0&0&0&0&0&0&0&0&28&0&0&0&0&0&0&0&0&0&0&0&0&0\\
0&0&0&0&0&0&0&0&0&0&0&0&0&0&0&32&0&0&0&0&0&0&0&0&0&0&0&0\\
0&0&0&0&0&0&0&0&0&0&0&0&0&0&0&0&40&0&0&0&0&0&0&0&0&0&0&0\\
0&0&0&0&0&0&0&0&0&0&0&0&0&0&0&0&0&40&0&0&0&0&0&0&0&0&0&0\\
0&0&0&0&0&0&0&0&0&0&0&0&0&0&0&0&0&0&48&0&0&0&0&0&0&0&0&0\\
0&0&0&0&0&0&0&0&0&0&0&0&0&0&0&0&0&0&0&40&0&0&0&0&0&0&0&0\\
0&0&0&0&0&0&0&0&0&0&0&0&0&0&0&0&0&0&0&0&16&0&0&0&0&0&0&0\\
0&0&0&0&0&0&0&0&0&0&0&0&0&0&0&0&0&0&0&0&0&28&0&0&0&0&0&0\\
0&0&0&0&0&0&0&0&0&0&0&0&0&0&0&0&0&0&0&0&0&0&28&0&0&0&0&0\\
0&0&0&0&0&0&0&0&0&0&0&0&0&0&0&0&0&0&0&0&0&0&0&40&0&0&0&0\\
0&0&0&0&0&0&0&0&0&0&0&0&0&0&0&0&0&0&0&0&0&0&0&0&24&0&0&0\\
0&0&0&0&0&0&0&0&0&0&0&0&0&0&0&0&0&0&0&0&0&0&0&0&0&28&0&0\\
0&0&0&0&0&0&0&0&0&0&0&0&0&0&0&0&0&0&0&0&0&0&0&0&0&0&28&0\\
0&0&0&0&0&0&0&0&0&0&0&0&0&0&0&0&0&0&0&0&0&0&0&0&0&0&0&32
\end{pmatrix},$$

while choosing Γ_2 (3.1.10) we get

$$H_{2E} = \lambda_E \begin{pmatrix}
0&0&0&0&0&0&0&0&0&0&0&0&0&0&0&0&0&0&0&0&0&0&0&0&0&0&0&0\\
0&32&0&0&0&0&0&0&0&0&0&0&0&0&0&0&0&0&0&0&0&0&0&0&0&0&0&0\\
0&0&32&0&0&0&0&0&0&0&0&0&0&0&0&0&0&0&0&0&0&0&0&0&0&0&0&0\\
0&0&0&32&0&0&0&0&0&0&0&0&0&0&0&0&0&0&0&0&0&0&0&0&0&0&0&0\\
0&0&0&0&24&0&0&0&0&0&0&0&0&0&0&0&0&0&0&0&0&0&0&0&0&0&0&0\\
0&0&0&0&0&32&0&0&0&0&0&0&0&0&0&0&0&0&0&0&0&0&0&0&0&0&0&0\\
0&0&0&0&0&0&48&0&0&0&0&0&0&0&0&0&0&0&0&0&0&0&0&0&0&0&0&0\\
0&0&0&0&0&0&0&56&0&0&0&0&0&0&0&0&0&0&0&0&0&0&0&0&0&0&0&0\\
0&0&0&0&0&0&0&0&56&0&0&0&0&0&0&0&0&0&0&0&0&0&0&0&0&0&0&0\\
0&0&0&0&0&0&0&0&0&48&0&0&0&0&0&0&0&0&0&0&0&0&0&0&0&0&0&0\\
0&0&0&0&0&0&0&0&0&0&32&0&0&0&0&0&0&0&0&0&0&0&0&0&0&0&0&0\\
0&0&0&0&0&0&0&0&0&0&0&56&0&0&0&0&0&0&0&0&0&0&0&0&0&0&0&0\\
0&0&0&0&0&0&0&0&0&0&0&0&48&0&0&0&0&0&0&0&0&0&0&0&0&0&0&0\\
0&0&0&0&0&0&0&0&0&0&0&0&0&56&0&0&0&0&0&0&0&0&0&0&0&0&0&0\\
0&0&0&0&0&0&0&0&0&0&0&0&0&0&48&0&0&0&0&0&0&0&0&0&0&0&0&0\\
0&0&0&0&0&0&0&0&0&0&0&0&0&0&0&32&0&0&0&0&0&0&0&0&0&0&0&0\\
0&0&0&0&0&0&0&0&0&0&0&0&0&0&0&0&56&0&0&0&0&0&0&0&0&0&0&0\\
0&0&0&0&0&0&0&0&0&0&0&0&0&0&0&0&0&56&0&0&0&0&0&0&0&0&0&0\\
0&0&0&0&0&0&0&0&0&0&0&0&0&0&0&0&0&0&48&0&0&0&0&0&0&0&0&0\\
0&0&0&0&0&0&0&0&0&0&0&0&0&0&0&0&0&0&0&48&0&0&0&0&0&0&0&0\\
0&0&0&0&0&0&0&0&0&0&0&0&0&0&0&0&0&0&0&0&24&0&0&0&0&0&0&0\\
0&0&0&0&0&0&0&0&0&0&0&0&0&0&0&0&0&0&0&0&0&48&0&0&0&0&0&0\\
0&0&0&0&0&0&0&0&0&0&0&0&0&0&0&0&0&0&0&0&0&0&48&0&0&0&0&0\\
0&0&0&0&0&0&0&0&0&0&0&0&0&0&0&0&0&0&0&0&0&0&0&48&0&0&0&0\\
0&0&0&0&0&0&0&0&0&0&0&0&0&0&0&0&0&0&0&0&0&0&0&0&36&0&0&0\\
0&0&0&0&0&0&0&0&0&0&0&0&0&0&0&0&0&0&0&0&0&0&0&0&0&44&0&0\\
0&0&0&0&0&0&0&0&0&0&0&0&0&0&0&0&0&0&0&0&0&0&0&0&0&0&44&0\\
0&0&0&0&0&0&0&0&0&0&0&0&0&0&0&0&0&0&0&0&0&0&0&0&0&0&0&44
\end{pmatrix}.$$

The matrix elements of the magnetic Hamiltonian H_B are presented in the equations (3.4.21), (3.4.22) and (3.4.23), the corresponding matrix is

$$H_B = -\lambda_B \begin{pmatrix}
0&0&0&0&2&0&0&0&0&0&0&0&0&0&0&0&0&0&0&0&2&0&0&0&0&0&0&0\\
0&0&0&0&2&0&0&0&0&0&0&0&0&0&0&0&0&0&0&0&0&2&0&0&0&0&0&0\\
0&0&0&0&2&0&0&0&0&0&0&0&0&0&0&0&0&0&0&0&0&0&2&0&0&0&0&0\\
0&0&0&0&2&0&0&0&0&0&0&0&0&0&0&0&0&0&0&0&0&0&0&2&0&0&0&0\\
2&2&2&2&0&0&0&0&0&0&0&0&0&0&0&0&0&0&0&0&0&0&0&0&1&1&1&1\\
0&0&0&0&0&0&0&0&0&2&0&0&0&0&0&0&0&0&0&0&2&0&0&0&0&0&0&0\\
0&0&0&0&0&0&0&0&0&2&0&0&0&0&0&0&0&0&0&0&0&2&0&0&0&0&0&0\\
0&0&0&0&0&0&0&0&0&2&0&0&0&0&0&0&0&0&0&0&0&0&2&0&0&0&0&0\\
0&0&0&0&0&0&0&0&0&2&0&0&0&0&0&0&0&0&0&0&0&0&0&2&0&0&0&0\\
0&0&0&0&0&2&2&2&2&0&0&0&0&0&0&0&0&0&0&0&0&0&0&0&1&1&1&1\\
0&0&0&0&0&0&0&0&0&0&0&0&0&0&2&0&0&0&0&0&2&0&0&0&0&0&0&0\\
0&0&0&0&0&0&0&0&0&0&0&0&0&0&2&0&0&0&0&0&0&2&0&0&0&0&0&0\\
0&0&0&0&0&0&0&0&0&0&0&0&0&0&2&0&0&0&0&0&0&0&2&0&0&0&0&0\\
0&0&0&0&0&0&0&0&0&0&0&0&0&0&2&0&0&0&0&0&0&0&0&2&0&0&0&0\\
0&0&0&0&0&0&0&0&0&0&2&2&2&2&0&0&0&0&0&0&0&0&0&0&1&1&1&1\\
0&0&0&0&0&0&0&0&0&0&0&0&0&0&0&0&0&0&0&2&2&0&0&0&0&0&0&0\\
0&0&0&0&0&0&0&0&0&0&0&0&0&0&0&0&0&0&0&2&0&2&0&0&0&0&0&0\\
0&0&0&0&0&0&0&0&0&0&0&0&0&0&0&0&0&0&0&2&0&0&2&0&0&0&0&0\\
0&0&0&0&0&0&0&0&0&0&0&0&0&0&0&0&0&0&0&2&0&0&0&2&0&0&0&0\\
0&0&0&0&0&0&0&0&0&0&0&0&0&0&0&2&2&2&2&0&0&0&0&0&1&1&1&1\\
2&0&0&0&0&2&0&0&0&0&2&0&0&0&0&2&0&0&0&0&0&0&0&0&1&1&1&1\\
0&2&0&0&0&0&2&0&0&0&0&2&0&0&0&0&2&0&0&0&0&0&0&0&1&1&1&1\\
0&0&2&0&0&0&0&2&0&0&0&0&2&0&0&0&0&2&0&0&0&0&0&0&1&1&1&1\\
0&0&0&2&0&0&0&0&2&0&0&0&0&2&0&0&0&0&2&0&0&0&0&0&1&1&1&1\\
0&0&0&0&1&0&0&0&0&1&0&0&0&0&1&0&0&0&0&1&1&1&1&1&0&0&0&0\\
0&0&0&0&1&0&0&0&0&1&0&0&0&0&1&0&0&0&0&1&1&1&1&1&0&0&0&0\\
0&0&0&0&1&0&0&0&0&1&0&0&0&0&1&0&0&0&0&1&1&1&1&1&0&0&0&0\\
0&0&0&0&1&0&0&0&0&1&0&0&0&0&1&0&0&0&0&1&1&1&1&1&0&0&0&0
\end{pmatrix}.$$

Numerical diagonalization of a D_4 theory

In order to visualize better in a unique graph both the electric ($\lambda_B = 0$) and the magnetic limit ($\lambda_E = 0$) for the complete Hamiltonian H we use the parametrization of the coupling constants introduced in (1.4.45): $\lambda_E = \lambda$ and $\lambda_B = 1 - \lambda$, with $\lambda \in [0, 1]$.
The numerical diagonalization was performed using the `eig` function of the submodule `linalg` of `numpy` library. The results of the numerical diagonalization using this parametrization are plotted in Fig. 3.9a and Fig. 3.9b. Notice the high degeneracy of the excited states, instead the ground state is non-degenerate.

Electrical eigenvalues and eigenstates of a D_4 theory

Let us now focus on the eigenvalues and eigenstates of the electric Hamiltonian H_E (B.1.1), so looking at the limit of H in which $\lambda = 1$ ($\lambda_B = 0$). We already know that that the electric Hamiltonian is diagonal in the character basis $\{|i_1, i_2\rangle, |j, \bar{4}\rangle\}$ (3.4.15), therefore we already know its eigenstates, while the corresponding eigenvalues are simply given by $\bar{f}(i_1, i_2) + 3f(i_1) + 3f(i_2)$ (3.4.18) and $f(j) + 3f(4) + 3\bar{f}(j, 4)$ (3.4.20). The smallest eigenvalue is 0 in correspondence to the eigenstate $|0, 0\rangle$. Comparing the expression (3.4.9) for the state $|0, 0\rangle$

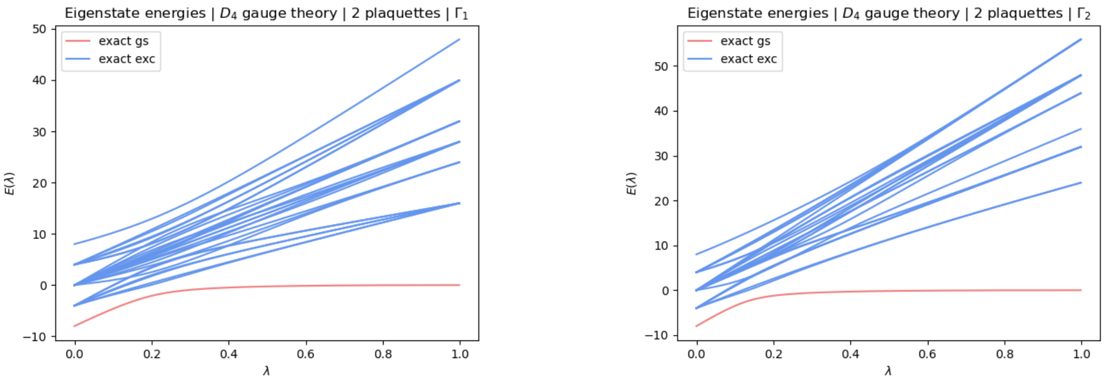

(a) Energy eigenvalues using the generating subset Γ_1 (3.1.9).

(b) Energy eigenvalues using the generating subset Γ_2 (3.1.10).

Figure 3.9: Energy eigenvalues of the Kogut-Susskind Hamiltonian H (1.4.45) as a function of the coupling $\lambda \in [0, 1]$ for a D_4 gauge theory on a two-plaquette system. All the 28 energy eigenvalues are plotted, in red the ground state (gs), in blue the excitations (exc).

and the definition (3.4.3) of the electrical vacuum $|0_E\rangle$, recalling also that $\chi_0(g) = 1$ for all $g \in D_4$, then it is easy to convince yourself that the electrical vacuum is nothing more than the electrical ground state, $|0, 0\rangle = |0_E\rangle$. Notice also that the electrical vacuum can be written as $|0_E\rangle = |0_{11}\rangle^{\otimes 7}$, where we assigned the trivial representation $j = 0$ state at each link.

Magnetic eigenvalues and eigenstates of a D_4 theory

Let us now instead focus on the eigenvalues and eigenstates of the magnetic Hamiltonian H_B (B.2.1), so looking at the limit of H in which $\lambda = 0$ ($\lambda_E = 0$). The magnetic Hamiltonian is not diagonal in the character basis (3.4.15) that we use to compute the matrix elements, so finding the ground state and the other eigenstates is slightly more complicated than in the previous case. We already know from (B.2.2) that the magnetic Hamiltonian H_B is diagonal in the multiple-plaquette states $|\tilde{g}_{p_1}, \tilde{g}_{p_2}\rangle$, so it is reasonable to look for the ground state between these states or a linear combination of them. When H_B acts on the multiple-plaquette state $|\tilde{g}_{p_1}, \tilde{g}_{p_2}\rangle$ it produces an eigenvalue $-2\lambda_B[\mathrm{Re}\,\chi_F(g_{p_1}) + \mathrm{Re}\,\chi_F(g_{p_2})]$ (B.2.2). If we are interested in the ground state we should try to maximize the value of the character function $\chi_F(g)$ for both the two terms, p_1 and p_2. Given a generic representation j of dimension d_j, the character function χ_j is the sum of d_j complex roots of unity [49], so the maximum of $\mathrm{Re}\,\chi_F(g)$ is realized when all addends are equal to 1 and therefore at maximum $\mathrm{Re}\,\chi_F(g) = d_F$. Notice that whatever fundamental representation F is chosen, the previous condition will be always satisfied by $g = e$, the neutral element of the group, indeed $\mathrm{Re}\,\chi_F(e) = d_F$. This means that the magnetic ground state for the two-plaquette system is $|\tilde{e}_{p_1}, \tilde{e}_{p_2}\rangle$ and the corresponding eigenvalue is

$-4d_F$. In our case the fundamental representation F is $j = 4$ and $d_4 = 2$, then the magnetic lowest eigenvalue is -8, as confirmed by the numerical analysis in Fig. 3.9a and in Fig. 3.9b. Notice also how the state $|\tilde{e}_{p_1}, \tilde{e}_{p_2}\rangle$ is gauge invariant, the conjugation introduced by a gauge transformation does not affect the neutral element e, indeed $geg^{-1} = e$ for all $g \in G$.
The magnetic ground state $|\tilde{e}_{p_1}, \tilde{e}_{p_2}\rangle$ of this lattice gauge theory is also the ground state of a related model, the quantum double model and it is sometimes called "loop gas", as it is a superposition of all possible combinations of loops [34].
For what concerns the second lowest energy level it has energy -4 and correspond to the situation in which $\mathrm{Re}\,\chi_F(g_{p_1}) = 2$ (and so $g_{p_1} = e$) and $\mathrm{Re}\,\chi_F(g_{p_2}) = 0$ (and so $g_{p_2} = r, r^3, s, rs, r^2s, r^3s$) or vice versa. Imposing the gauge invariance condition one can construct the following six degenerate magnetic eigenstates:

$$\begin{gathered}\frac{|\tilde{e}_{p_1}, \tilde{r}_{p_2}\rangle + |\tilde{e}_{p_1}, \widetilde{r^3}_{p_2}\rangle}{\sqrt{2}}, \frac{|\tilde{e}_{p_1}, \widetilde{rs}_{p_2}\rangle + |\tilde{e}_{p_1}, \widetilde{r^3s}_{p_2}\rangle}{\sqrt{2}}, \frac{|\tilde{e}_{p_1}, \tilde{s}_{p_2}\rangle + |\tilde{e}_{p_1}, \widetilde{r^2s}_{p_2}\rangle}{\sqrt{2}}, \\ \frac{|\tilde{r}_{p_1}, \tilde{e}_{p_2}\rangle + |\widetilde{r^3}_{p_1}, \tilde{e}_{p_2}\rangle}{\sqrt{2}}, \frac{|\widetilde{rs}_{p_1}, \tilde{e}_{p_2}\rangle + |\widetilde{r^3s}_{p_1}, \tilde{e}_{p_2}\rangle}{\sqrt{2}}, \frac{|\tilde{s}_{p_1}, \tilde{e}_{p_2}\rangle + |\widetilde{r^2s}_{p_1}, \tilde{e}_{p_2}\rangle}{\sqrt{2}}.\end{gathered} \tag{3.4.24}$$

In an analogous way we can construct 14 degenerate magnetic eigenstates with energy 0, 6 degenerate states with energy $+4$ and one state, $|\widetilde{r^2}_{p_1}, \widetilde{r^2}_{p_2}\rangle$, with energy $+8$. All these states are gauge invariant.

3.4.4 Energy spectrum of D_3

Hamiltonian matrix for a D_3 theory

Let's repeat the same analysis also for the dihedral group D_3. We use the generating subsets Γ_1 (3.2.7) and Γ_2 (3.2.8), and as fundamental representation F the unique non-Abelian representation of the group $j = 2$. The matrices will be written in terms of the basis $\{|i_1, i_2\rangle, |j, \bar{2}\rangle, |\widetilde{2,2}\rangle\}$ (3.4.15), with $i_1, i_2 = 0, 1, 2$ but not $i_1 = i_2 = 2$ and $j = 0, 1$. In particular the order with which these states appear in the rows and the columns of the matrices is:

$$|0,0\rangle, |0,1\rangle, |0,2\rangle, |1,0\rangle, |1,1\rangle, |1,2\rangle, |2,0\rangle, |2,1\rangle, |0,\bar{2}\rangle, |1,\bar{2}\rangle, |\widetilde{2,2}\rangle.$$

The matrix elements of the electric Hamiltonian H_E (B.1.1) are presented in the equations (3.4.18) and (3.4.20), and they depend on the choice of the generating subset Γ, through the functions $f(i)$ and $\bar{f}(i,j)$. Choosing the generating subset Γ_1 (3.2.7) we get

$$H_{1E} = \lambda_E \begin{pmatrix} 0 & 0 & 0 & 0 & 0 & 0 & 0 & 0 & 0 & 0 & 0 \\ 0 & 24 & 0 & 0 & 0 & 0 & 0 & 0 & 0 & 0 & 0 \\ 0 & 0 & 12 & 0 & 0 & 0 & 0 & 0 & 0 & 0 & 0 \\ 0 & 0 & 0 & 24 & 0 & 0 & 0 & 0 & 0 & 0 & 0 \\ 0 & 0 & 0 & 0 & 36 & 0 & 0 & 0 & 0 & 0 & 0 \\ 0 & 0 & 0 & 0 & 0 & 30 & 0 & 0 & 0 & 0 & 0 \\ 0 & 0 & 0 & 0 & 0 & 0 & 12 & 0 & 0 & 0 & 0 \\ 0 & 0 & 0 & 0 & 0 & 0 & 0 & 30 & 0 & 0 & 0 \\ 0 & 0 & 0 & 0 & 0 & 0 & 0 & 0 & 18 & 0 & 3\sqrt{2}/2 \\ 0 & 0 & 0 & 0 & 0 & 0 & 0 & 0 & 0 & 24 & -3\sqrt{2}/2 \\ 0 & 0 & 0 & 0 & 0 & 0 & 0 & 0 & 3\sqrt{2}/2 & -3\sqrt{2}/2 & 21 \end{pmatrix},$$

while choosing Γ_2 (3.1.10) we get

$$H_{2E} = \lambda_E \begin{pmatrix} 0 & 0 & 0 & 0 & 0 & 0 & 0 & 0 & 0 & 0 & 0 \\ 0 & 24 & 0 & 0 & 0 & 0 & 0 & 0 & 0 & 0 & 0 \\ 0 & 0 & 24 & 0 & 0 & 0 & 0 & 0 & 0 & 0 & 0 \\ 0 & 0 & 0 & 24 & 0 & 0 & 0 & 0 & 0 & 0 & 0 \\ 0 & 0 & 0 & 0 & 36 & 0 & 0 & 0 & 0 & 0 & 0 \\ 0 & 0 & 0 & 0 & 0 & 42 & 0 & 0 & 0 & 0 & 0 \\ 0 & 0 & 0 & 0 & 0 & 0 & 24 & 0 & 0 & 0 & 0 \\ 0 & 0 & 0 & 0 & 0 & 0 & 0 & 42 & 0 & 0 & 0 \\ 0 & 0 & 0 & 0 & 0 & 0 & 0 & 0 & 36 & 0 & 9\sqrt{2}/4 \\ 0 & 0 & 0 & 0 & 0 & 0 & 0 & 0 & 0 & 42 & -3\sqrt{2}/4 \\ 0 & 0 & 0 & 0 & 0 & 0 & 0 & 0 & 9\sqrt{2}/4 & -3\sqrt{2}/4 & 81/2 \end{pmatrix}.$$

The matrix elements of the magnetic Hamiltonian H_B are presented in the equations (3.4.21), (3.4.22) and (3.4.23), the corresponding matrix is

$$H_B = -\lambda_B \begin{pmatrix} 0 & 0 & 2 & 0 & 0 & 0 & 2 & 0 & 0 & 0 & 0 \\ 0 & 0 & 2 & 0 & 0 & 0 & 0 & 2 & 0 & 0 & 0 \\ 2 & 2 & 2 & 0 & 0 & 0 & 0 & 0 & 1 & 1 & \sqrt{2} \\ 0 & 0 & 0 & 0 & 0 & 2 & 2 & 0 & 0 & 0 & 0 \\ 0 & 0 & 0 & 0 & 0 & 2 & 0 & 2 & 0 & 0 & 0 \\ 0 & 0 & 0 & 2 & 2 & 2 & 0 & 0 & 1 & 1 & \sqrt{2} \\ 2 & 0 & 0 & 2 & 0 & 0 & 2 & 0 & 1 & 1 & \sqrt{2} \\ 0 & 2 & 0 & 0 & 0 & 0 & 0 & 2 & 1 & 1 & \sqrt{2} \\ 0 & 0 & 1 & 0 & 0 & 1 & 1 & 1 & 0 & 0 & 2\sqrt{2} \\ 0 & 0 & 1 & 0 & 0 & 1 & 1 & 1 & 0 & 0 & 2\sqrt{2} \\ 0 & 0 & \sqrt{2} & 0 & 0 & \sqrt{2} & \sqrt{2} & \sqrt{2} & 2\sqrt{2} & 2\sqrt{2} & 0 \end{pmatrix}.$$

Numerical diagonalization of a D_3 theory

In order to visualize better in a unique graph both the electric ($\lambda_B = 0$) and the magnetic limit ($\lambda_E = 0$) for the complete Hamiltonian H we use the parametrization of the coupling constants introduced in (1.4.45): $\lambda_E = \lambda$ and $\lambda_B = 1 - \lambda$, with $\lambda \in [0,1]$.
The results of the numerical diagonalization using this parametrization are plotted in Fig. 3.10a and Fig. 3.10b. Notice the high degeneracy of the excited states, instead the ground state is non-degenerate.

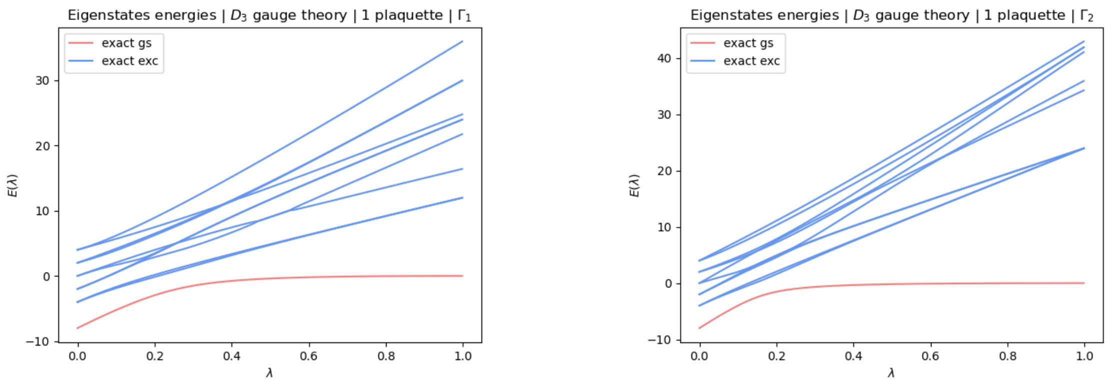

(a) Energy eigenvalues using the generating subset Γ_1 (3.2.7)..

(b) Energy eigenvalues using the generating subset Γ_2 (3.2.8).

Figure 3.10: Energy eigenvalues of the Kogut-Susskind Hamiltonian H (1.4.45) as a function of the coupling $\lambda \in [0, 1]$ for a D_3 gauge theory on a two-plaquette system. All the 11 energy eigenvalues are plotted, in red the ground state (gs), in blue the excitations (exc)

Electrical eigenvalues and eigenstates of a D_3 theory

Let us now focus on the eigenvalues and eigenstates of the electric Hamiltonian H_E (B.1.1), so looking at the limit of H in which $\lambda = 1$ ($\lambda_B = 0$). We already know that that the electric Hamiltonian is diagonal in the multiple-character states $\{|i_1, i_2\rangle\}$ ($i_1, i_2 = 0, 1, 2$ but not $i_1 = i_2 = 2$), but not in the states $\{|j, \bar{2}\rangle, |\widetilde{2, 2}\rangle\}$ ($j = 0, 1$) of the basis (3.4.16). That because the matrix elements $\langle j, \bar{2}|H_E|\widetilde{2, 2}\rangle$ are different from zero. Eight eigenstates are the multiple-character states $\{|i_1, i_2\rangle\}$ and the corresponding eigenvalues are simply given by $\bar{f}(i_1, i_2) + 3f(i_1) + 3f(i_2)$ (3.4.18). The remaining three eigenstates are a linear combination of the states $\{|j, \bar{2}\rangle, |\widetilde{2, 2}\rangle\}$ with non trivial eigenvalues.
The smallest eigenvalue is 0 in correspondence to the eigenstate $|0, 0\rangle$. Comparing the expression (3.4.9) for the state $|0, 0\rangle$ and the definition (3.4.3) of the electrical vacuum $|0_E\rangle$, recalling also that $\chi_0(g) = 1$ for all $g \in D_3$, then it is easy to see that the electrical vacuum is nothing more than the electrical ground state, $|0, 0\rangle = |0_E\rangle$.

Magnetic eigenvalues and eigenstates of a D_3 theory

Let us now instead focus on the eigenvalues and eigenstates of the magnetic Hamiltonian H_B (B.2.1), so looking at the limit of H in which $\lambda = 0$ ($\lambda_E = 0$). The magnetic Hamiltonian is not diagonal in the character basis (3.4.16) that we use to compute the matrix elements, but following the same procedure used for the gauge group D_4 we can see that the magnetic ground state for the two-plaquette system is $|\tilde{e}_{p_1}, \tilde{e}_{p_2}\rangle$ and the corresponding eigenvalue is -8,

since we have to maximize the function $\chi_2(g)$, and that is realized by $g = e$ and $\chi_2(e) = 2$. This result is confirmed by the numerical analysis in Fig. 3.10a and in Fig. 3.10b.
For what concerns the second lowest energy level it has energy -4 and the two corresponding degenerate magnetic eigenstates are

$$\frac{|\tilde{e}_{p_1}, \tilde{s}_{p_2}\rangle + |\tilde{e}_{p_1}, \widetilde{rs}_{p_2}\rangle + |\tilde{e}_{p_1}, \widetilde{r^2 s}_{p_2}\rangle}{\sqrt{3}}, \frac{|\tilde{s}_{p_1}, \tilde{e}_{p_2}\rangle + |\widetilde{rs}_{p_1}, \tilde{e}_{p_2}\rangle + |\widetilde{r^2 s}_{p_1}, \tilde{e}_{p_2}\rangle}{\sqrt{3}}, \tag{3.4.25}$$

In an analogous way we can construct two degenerate magnetic eigenstates with energy -2, two degenerate states with energy 0, two degenerate magnetic eigenstates with energy $+2$ and two degenerate magnetic eigenstates with energy $+2$ with energy $+4$. All these states are gauge invariant.

3.4.5 Wilson loop observables

Now we repeat what we have seen for the energy, but this time focusing on the Wilson loop observables $\mathrm{Tr}\,\hat{W}_{p_1}$ and $\mathrm{Tr}\,\hat{W}_{p_3}$, just for a D_4 gauge theory.

Wilson loop matrix elements

Give a lattice gauge theory with gauge group G in a two-plaquette system, as the one in Fig. 3.8, it is possible to define three single Wilson loop operators (1.4.10): $\mathrm{Tr}\,\hat{W}_{p_1} = \mathrm{Tr}\big(\hat{g}_1\hat{g}_2\hat{g}_3^{-1}\hat{g}_4^{-1}\big)$, $\mathrm{Tr}\,\hat{W}_{p_2} = \mathrm{Tr}\big(\hat{g}_5\hat{g}_6\hat{g}_7^{-1}\hat{g}_2^{-1}\big)$ and $\mathrm{Tr}\,\hat{W}_{p_3} = \mathrm{Tr}\big(\hat{g}_1\hat{g}_5\hat{g}_6\hat{g}_7^{-1}\hat{g}_3^{-1}\hat{g}_4^{-1}\big)$. The operators $\mathrm{Tr}\,\hat{W}_{p_1}$ and $\mathrm{Tr}\,\hat{W}_{p_2}$ are completely equivalent for symmetric reasons, since they are both single plaquette loops. The matrix elements of Wilson loop operators of the states $|i,j\rangle$ can be computed using (3.4.9):

$$\langle i_1, i_2|\,\mathrm{Tr}\,\hat{W}_{p_1}|j_1, j_2\rangle = \frac{1}{|G|^2}\sum_{g_{p_1}, g_{p_2}\in G}\chi^*_{i_1}(g_{p_1})\chi^*_{i_2}(g_{p_2})\chi_{j_1}(g_{p_1})\chi_{j_2}(g_{p_2})\chi_F(g_{p_1}), \tag{3.4.26}$$

$$\begin{aligned}\langle i_1, i_2|\,\mathrm{Tr}\,\hat{W}_{p_3}|j_1, j_2\rangle =&\frac{1}{|G|^3}\sum_{g_1, g_{p_1}, g_{p_2}\in G}\chi^*_{i_1}(g_{p_1})\chi^*_{i_2}(g_{p_2})\chi_{j_1}(g_{p_1})\chi_{j_2}(g_{p_2})\cdot\\ &\cdot\chi_F(g_1 g_{p_2} g_1^{-1} g_{p_1}),\end{aligned} \tag{3.4.27}$$

The same can be done for the state $|i,\bar{j}\rangle$, using the expression (3.4.10):

$$\langle i_1, \bar{i}_2|\,\mathrm{Tr}\,\hat{W}_{p_1}|j_1, \bar{j}_2\rangle = \frac{1}{|G|^2}\sum_{g_{p_1}, g_{p_3}\in G}\chi^*_{i_1}(g_{p_1})\chi^*_{i_2}(g_{p_3})\chi_{j_1}(g_{p_1})\chi_{j_2}(g_{p_3})\chi_F(g_{p_1}), \tag{3.4.28}$$

$$\langle i_1, \bar{i}_2|\,\mathrm{Tr}\,\hat{W}_{p_3}|j_1, \bar{j}_2\rangle = \frac{1}{|G|^2}\sum_{g_{p_1}, g_{p_3}\in G}\chi^*_{i_1}(g_{p_1})\chi^*_{i_2}(g_{p_3})\chi_{j_1}(g_{p_1})\chi_{j_2}(g_{p_3})\chi_F(g_{p_3}), \tag{3.4.29}$$

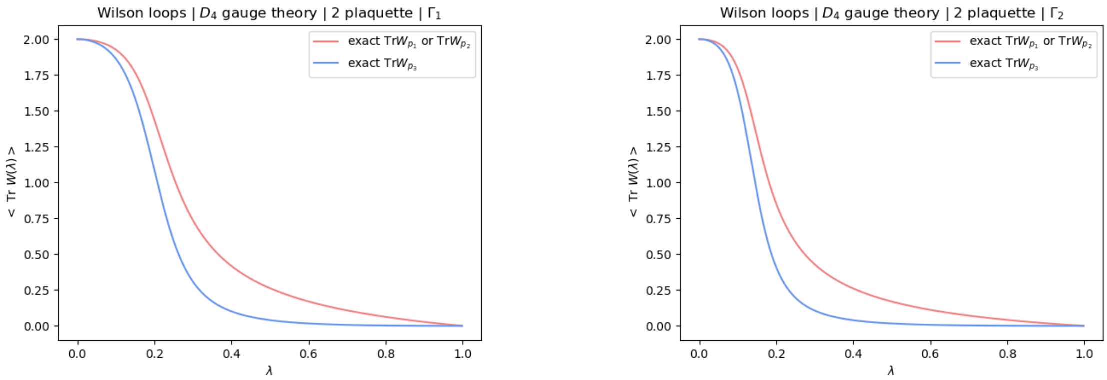

(a) Wilson loop observables $\mathrm{Tr}\,\hat{W}_{p_1}$ and $\mathrm{Tr}\,\hat{W}_{p_3}$ with generating subset Γ_1.

(b) Wilson loop observables $\mathrm{Tr}\,\hat{W}_{p_1}$ and $\mathrm{Tr}\,\hat{W}_{p_3}$ with generating subset Γ_2.

Figure 3.11: Expectation value of the Wilson loop observables $\mathrm{Tr}\,\hat{W}_{p_1}$ and $\mathrm{Tr}\,\hat{W}_{p_3}$ with the gauge group D_4 and a two plaquette system, computed on the ground state of the Hamiltonian (1.4.45) for different couplings $\lambda \in [0,1]$.

and

$$\langle i_1, \bar{i}_2 | \,\mathrm{Tr}\,\hat{W}_{p_1} | j_1, j_2 \rangle = \frac{1}{|G|^3} \sum_{g_1, g_{p_1}, g_{p_2} \in G} \chi^*_{i_1}(g_{p_1}) \chi^*_{i_2}(g_1 g_{p_2} g_1^{-1} g_{p_1}) \chi_{j_1}(g_{p_1}) \cdot \\ \cdot \chi_{j_2}(g_{p_2}) \chi_F(g_{p_1}), \tag{3.4.30}$$

$$\langle i_1, \bar{i}_2 | \,\mathrm{Tr}\,\hat{W}_{p_3} | j_1, j_2 \rangle = \frac{1}{|G|^3} \sum_{g_1, g_{p_1}, g_{p_2} \in G} \chi^*_{i_1}(g_{p_1}) \chi^*_{i_2}(g_1 g_{p_2} g_1^{-1} g_{p_1}) \chi_{j_1}(g_{p_1}) \cdot \\ \cdot \chi_{j_2}(g_{p_2}) \chi_F(g_1 g_{p_2} g_1^{-1} g_{p_1}). \tag{3.4.31}$$

In order to compute them we have to specify the gauge group G and a representation F for the magnetic part.

Wilson loop observable for D_4 theory

Consider the group $G = D_4$, let us use as a faithful representation the non-Abelian $j = 4$ representation. For each $\lambda \in [0,1]$ we compute the expectation value of Wilson loop operators over the ground state of the Hamiltonian at that specific λ. The results are plotted in Fig. 3.11.

Chapter 4

QUANTUM SIMULATION RESULTS for DIHEDRAL THEORIES

In this chapter we discuss how to simulate on a digital quantum computer a D_4 and D_3 lattice gauge theory on a one-plaquette and two-plaquette system. We try to apply the generic procedure of quantum simulation discussed in chapter 2 to the specific cases of our gauge theories, describing the encoding and how to implement the high level quantum gates required to realize the evolution operator. Once the quantum algorithm is prepared we simulate it using the software `Qiskit`, trying to reproduce all interesting results that we reviewed in chapter 3 on a D_4 and D_3 lattice gauge theory on a one-plaquette and two-plaquette system.

4.1 Quantum algorithm for D_4

In this section we discuss how to encode the 8 degrees of freedom of each edge of a D_4 lattice gauge theory in the degrees of freedom of the quantum simulator. We also see how to implement the set of gates requested to reproduce the time evolution and how to prepare any particular eigenstate of the Hamiltonian.

4.1.1 Encoding

There are 8 possible group elements $g \in D_4$, so in order to represents all of them we need 3 qubits ($2^3 = 8$). We encode the group elements in the quantum register as shown in Table 4.1. Let us stress some properties of this encoding choice. Given a generic group element of the group $g = r^a s^b \in D_4$, where $a = 0, 1, 2, 3$ and $b = 0, 1$, we can encode it in the state $|ba_1a_2\rangle$, where b is exactly the exponent of s, while $a_1, a_2 = 0, 1$ are the two binary numbers needed to write a in binary code: $a = a_1 2^1 + a_2 2^0$.

g	e	r	r^2	r^3	s	rs	r^2s	r^3s
state	$\|000\rangle$	$\|001\rangle$	$\|010\rangle$	$\|011\rangle$	$\|100\rangle$	$\|101\rangle$	$\|110\rangle$	$\|111\rangle$

Table 4.1: Encoding table of the group D_4. A generic group element $g = r^a s^b$, where $a = 0, 1, 2, 3$ and $b = 0, 1$, can be encoded in the state $|ba_1a_2\rangle$, where b is exactly the exponent of s, while $a_1, a_2 = 0, 1$ are the two binary numbers needed to write a in binary code.

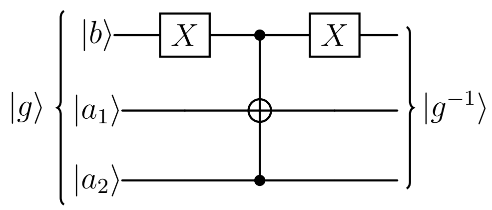

Figure 4.1: Quantum circuit that implements the inversion gate $U_{-1}|g\rangle = |g^{-1}\rangle$ (2.3.7) for the group D_4.

A group element $g \in D_4$, encoded in 3 qubits, is associated at each eadge, then given a lattice with E edges, we need $3E$ qubits in order to represent the entire lattice in a quantum circuit.

4.1.2 Evolution operator

In this section we show how we constructed the high level quantum gates needed to simulate a D_4 lattice gauge theory. The gates implemented in this section were introduced in section 2.3.2. Once these high level gates are implemented we can realized the magnetic evolution operator for a single plaquette $U_B^{(p)}(\Delta t)$ using the quantum circuit in Fig. 2.1, while the electric evolution operator for a single link $U_E^{(l)}(\Delta t)$ is realized by the quantum circuit in Fig. 2.2. The total evolution gate $U(t)$ for a single plaquette is shown in Fig. 2.3. A discussion on gates for a generic D_{2^n} gauge theory can be found in [2]. All circuits were implemented using the software `Qiskit` [45].

Inversion gate

The inversion gate U_{-1} is defined in the relation (2.3.7). Looking at the inversion Table 3.2 we can see that the inversion operation simply exchanges the states $|r\rangle = |001\rangle$ and $|r^3\rangle = |011\rangle$. We can realize this operation using a Toffoli gate. The gate is represented in Fig. 4.1.

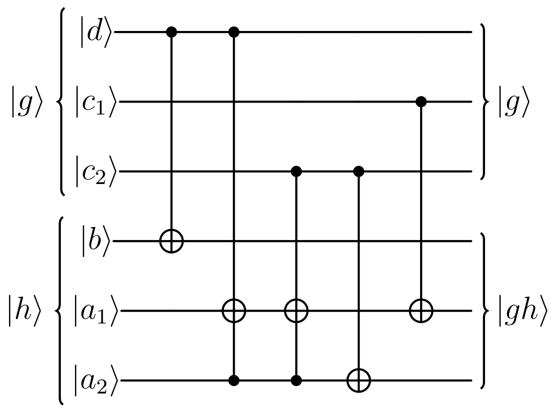

Figure 4.2: Quantum circuit that implements the multiplication gate $U_\times |g\rangle |h\rangle = |g\rangle |gh\rangle$ (2.3.8) for the group D_4. Given two input states $|g = r^c s^d\rangle$ and $|h = r^a s^b\rangle$, the first CNOT gate implements $b \oplus_2 d$, the first Toffoli gate implements $(-1)^d a$, while the last three gates perform the sum $c \oplus_4 (-1)^d a$.

Multiplication gate

The multiplication gate $U_\times$ is defined in the relation (2.3.8). For the realization of the circuit we use the following property: given two elements of the group $g = r^c s^d$ and $h = r^a s^b$, with $a, c = 0, 1, 2, 3$ and $b, d = 0, 1$, their product is given by

$$g \cdot h = r^c s^d \cdot r^a s^b = r^{c \bigoplus_4 (-1)^d a} s^{b \bigoplus_2 d}, \tag{4.1.1}$$

where $\bigoplus_4$ and $\bigoplus_2$ are a sum modulo 4 and modulo 2 respectively. The property (4.1.1) can be directly verifies on the Cayley Table 3.1. The gate is represented in Fig. 4.2. The first CNOT gate implements the operation $b \oplus_2 d$, the first Toffoli gate implements $(-1)^d a$, so it transforms the sum modulo 4 in a difference modulo 4 if and only if $d = 1$. Then the last three gates perform the sum $c \oplus_4 (-1)^d a$.

Trace gate

The trace gate $U_{\text{tr}}(\theta)$ is a parametric gate defined in the relation (2.3.9). Considering the non-Abelian representation ρ_4, one can see that

$$\text{Tr}(g) = \text{Tr}\big(r^a s^b\big) = 2\delta_{b,0} \cos\Big(\frac{\pi a}{2}\Big). \tag{4.1.2}$$

The trace gate $U_{\text{tr}}(\theta)$ can be implemented by the quantum circuit in Fig. 4.3.

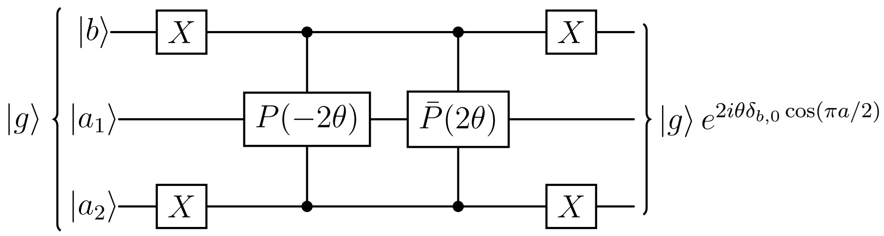

Figure 4.3: Quantum circuit that implements the trace gate $U_{\mathrm{tr}}(\theta)\,|g\rangle = |g\rangle\, e^{i\theta\,\mathrm{Re}\,\mathrm{Tr}[\rho_4(g)]}$ (2.3.9) for the group D_4. The gate $P(\theta)$ is the phase gate, described by the operator $P(\theta) = \mathrm{diag}(1, e^{i\theta})$, while the gate $\bar{P}(\theta) = XP(\theta)X$ is described by the operator $\bar{P}(\theta) = \mathrm{diag}(e^{i\theta}, 1)$.

Fourier transform gate

The Fourier transform gate U_F allows us to move from the group element basis $\{|g\rangle\}$ to the representation basis $\{|j_{mn}\rangle\}$ and it is defined in (2.3.10). This gate is defined as

$$U_F = \sum_{g\in D_4}\sum_{j=0}^{4}\sum_{m,n=1}^{d_j}\sqrt{\frac{d_j}{8}}\rho_j(g)_{mn}\,|j_{mn}\rangle\,\langle g|\,, \tag{4.1.3}$$

where $(\rho_j)_{mn}$ is the mn component of the j-th representation, and $|\rho_j, mn\rangle$ is the corresponding element in the representation basis. The matrix elements of U_F are given by

$$\langle j_{mn}|U_F|g\rangle = \sqrt{\frac{d_j}{8}}\rho_j(g)_{mn}. \tag{4.1.4}$$

Given the expression (4.1.4) for the matrix elements of U_F we can easily construct the corresponding 8×8 matrix:

$$U_F = \frac{1}{\sqrt{8}}\begin{pmatrix}
1 & 1 & 1 & 1 & 1 & 1 & 1 & 1\\
1 & -1 & 1 & -1 & 1 & -1 & 1 & -1\\
1 & 1 & 1 & 1 & -1 & -1 & -1 & -1\\
1 & -1 & 1 & -1 & -1 & 1 & -1 & 1\\
\sqrt{2} & i\sqrt{2} & -\sqrt{2} & -i\sqrt{2} & 0 & 0 & 0 & 0\\
0 & 0 & 0 & 0 & \sqrt{2} & i\sqrt{2} & -\sqrt{2} & -i\sqrt{2}\\
0 & 0 & 0 & 0 & \sqrt{2} & -i\sqrt{2} & -\sqrt{2} & i\sqrt{2}\\
\sqrt{2} & -i\sqrt{2} & -\sqrt{2} & i\sqrt{2} & 0 & 0 & 0 & 0
\end{pmatrix}, \tag{4.1.5}$$

and using the `Qiskit` class `Operator` we can transform this matrix in the corresponding 3-qubits quantum circuit. The same it can be done for the Hermitian conjugate of the Fourier transform gate $U_F^\dagger$ (2.3.12).

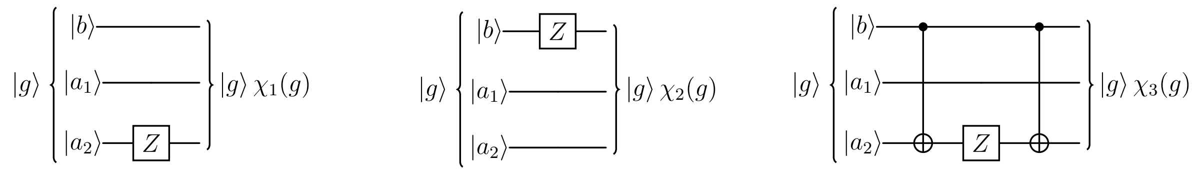

(a) The character gate U_{χ_1}. (b) The character gate U_{χ_2}. (c) The character gate U_{χ_3}.

Figure 4.4: Abelian character gates U_{χ_j} for the representations $j = 1, 2, 3$ in the D_4 gauge theory.

Phase gate

The phase gate $U_{\text{ph}}(\Delta t)$ is defined as the diagonal form of the electric evolution operator $U_E^{(l)}$ for the single link l as shown in the expression (2.3.14). The 8×8 matrix associated to this 3-qubit operator is

$$U_{\text{ph}}(\Delta t) = \begin{pmatrix} 1 & 0 & 0 & 0 & 0 & 0 & 0 & 0 \\ 0 & e^{-i\lambda_E f(1)\Delta t} & 0 & 0 & 0 & 0 & 0 & 0 \\ 0 & 0 & e^{-i\lambda_E f(2)\Delta t} & 0 & 0 & 0 & 0 & 0 \\ 0 & 0 & 0 & e^{-i\lambda_E f(3)\Delta t} & 0 & 0 & 0 & 0 \\ 0 & 0 & 0 & 0 & e^{-i\lambda_E f(4)\Delta t} & 0 & 0 & 0 \\ 0 & 0 & 0 & 0 & 0 & e^{-i\lambda_E f(4)\Delta t} & 0 & 0 \\ 0 & 0 & 0 & 0 & 0 & 0 & e^{-i\lambda_E f(4)\Delta t} & 0 \\ 0 & 0 & 0 & 0 & 0 & 0 & 0 & e^{-i\lambda_E f(4)\Delta t} \end{pmatrix}. \quad (4.1.6)$$

The 3-qubit quantum circuit that implement this matrix can be obtained using the `Qiskit` class `Operator`. Since the phase gate U_{ph} depends on the electric Hamiltonian, it depends also on the choice of the generating subset Γ, through the function $f(j)$ (1.4.41).

Abelian character gates

The Abelian character gates U_{χ_j}, with $j = 0, 1, 2, 3$, are defined in the relation (2.3.16). Looking at the character Table 3.3 we see that U_{χ_0} is trivially the identity, U_{χ_1} is realized by the quantum circuit in Fig. 4.4a, U_{χ_2} by the one in Fig. 4.4b and U_{χ_3} by the one in Fig. 4.4c.

4.1.3 State preparation

Now let's see how to prepare two particular states, the electric ground state $|E_0^{\lambda=1}\rangle$ and the magnetic ground state $|E_0^{\lambda=0}\rangle$, that are the ground states of the Kogut-Susskind Hamiltonian (1.4.45) in the limit where $\lambda = 1$ ($\lambda_B = 0$) and $\lambda = 0$ ($\lambda_E = 0$) respectively. Using the same approach one can construct also the excited eigenstates both in the electric and magnetic limit. If instead one is interested in an energy eigenstate at a generic $\lambda \neq 0, 1$, one has first to prepare the corresponding electric or the magnetic eigenstate, and then apply the adiabatic evolution described in section 2.3.3, slightly changing λ at each Trotter step up to the desired value.

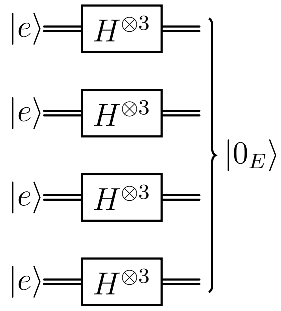

Figure 4.5: Quantum circuit to prepare the electric ground state $|E_0^{\lambda=1}\rangle = |0_E\rangle$ (3.3.5) for the D_4 group and in the case of a one-plaquette system. Each double line represents the three qubits needed to encode an edge.

Electric ground state preparation

The electric ground state $|E_0^{\lambda=1}\rangle$ is the electric vacuum $|0_E\rangle$ that we defined in (3.3.5) and in (3.4.3) for the one-plaquette and two-plaquette system respectively. In both cases $|0_E\rangle$ is an equal weight linear superposition of all possible group element states and so it ca be prepared applying an Hadamard gate H at each qubit in the $|0\rangle$ state. Recalling that each link is represented by three qubits, the quantum circuit to prepare the electric ground state $|E_0^{\lambda=1}\rangle$ in a one-plaquette system is shown in Fig. 4.5. The extension of this circuit to a multiple-plaquette system is trivial.

Other electric eigenstates

As we saw in sections (3.3.3) and (3.4.3) electric eigenstates for the one and two plaquette system are the character states $\{|\chi_i\rangle\}$ (3.3.9) and $\{|i_1, i_2\rangle, |j, \bar{4}\rangle\}$ (3.4.9, 3.4.10) respectively. Let us focus on the single plaquette case, the generalization to a multiple plaquette system is straightforward. Using the expression (3.3.10) for $|\chi_j\rangle$, with $j = 0, 1, 2, 3$ an Abelian one-dimensional representation, since $\chi_j(g) = \rho_j(g)$ and $\chi_j(g^{-1}) = \chi_j(g)$ we can write:

$$|\chi_j\rangle = \frac{1}{\sqrt{8^4}} \sum_{g_1,g_2,g_3,g_4 \in D_4} \chi_j(g_1)\chi_j(g_2)\chi_j(g_3)\chi_j(g_4) |g_1, g_2, g_3, g_4\rangle . \tag{4.1.7}$$

Then the state $|\chi_j\rangle$ can be obtained starting with the electric vacuum $|0_E\rangle$ and applying the Abelian character gate U_{χ_j} (2.3.16) in Fig. 4.4 to each link of the lattice.
If $j = 4$, the non-Abelian representation, the procedure is more delicate. From the expressions

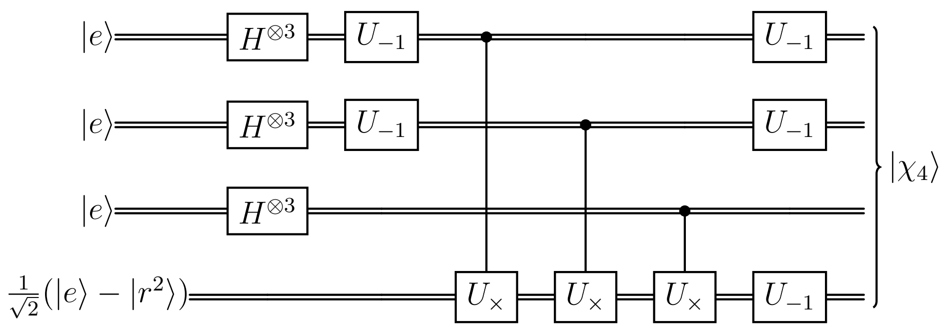

Figure 4.6: Quantum circuit to prepare the electric eigenstate $|\chi_4\rangle = (|\tilde{e}\rangle - |\tilde{r^2}\rangle)/\sqrt{2}$ (4.1.9) for the D_4 group and in the case of a one-plaquette system. Each double line represents the three qubits needed to encode an edge.

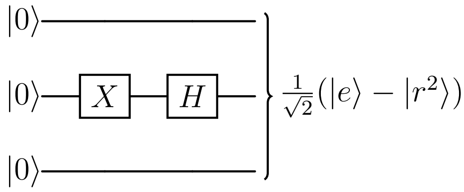

Figure 4.7: Quantum circuit to prepare the electric eigenstate $|\chi_4\rangle = (|\tilde{e}\rangle - |\tilde{r^2}\rangle)/\sqrt{2}$ (4.1.9) for the D_4 group and in the case of a one-plaquette system. Each double line represents the three qubits needed to encode an edge.

(3.3.9) and (3.3.7) we have that

$$\begin{aligned} |\chi_4\rangle &= \frac{1}{\sqrt{8}} \sum_{g\in D_4} \chi_j(g)\, |\tilde{g}\rangle \\ &= \frac{1}{\sqrt{2}}(|\tilde{e}\rangle - |\tilde{r^2}\rangle) \\ &= \frac{1}{\sqrt{8^3}} \sum_{g_1,g_2,g_3\in D_4} \frac{1}{\sqrt{2}}(|g_1,g_2,g_3,g_1g_2g_3^{-1}\rangle - |g_1,g_2,g_3,r^2g_1g_2g_3^{-1}\rangle). \end{aligned} \tag{4.1.8}$$

This state can be realized using the quantum circuit in Fig. 4.6, where the state $(|e\rangle - |r^2\rangle)/\sqrt{2}$ in last three qubits is realized by the circuit in Fig. 4.7.

Magnetic ground state preparation

The magnetic ground state $|E_0^{\lambda=0}\rangle$ is the plaquette state $|\tilde{e}\rangle$ and multiple-plaquette state $|\tilde{e}_{p_1}, \tilde{e}_{p_2}\rangle$ for the one-plaquette and two-plaquette system respectively. We focus just on the preparation

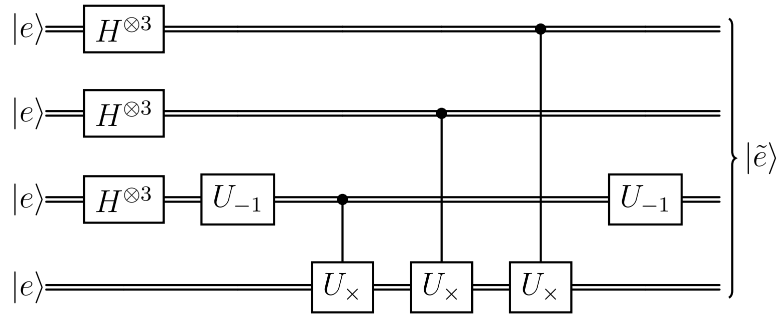

Figure 4.8: Quantum circuit to prepare the magnetic ground state $|E_0^{\lambda=0}\rangle = |\tilde{e}\rangle$ (4.1.9) for the D_4 group and in the case of a one-plaquette system. Each double line represents the three qubits needed to encode an edge.

of the state $|\tilde{e}\rangle$, then the generalization to a multiple plaquette system is straightforward. From the expression (3.3.7) we have that

$$|\tilde{e}\rangle = \frac{1}{\sqrt{8^3}} \sum_{g_1,g_2,g_3 \in D_4} |g_1, g_2, g_3, g_1 g_2 g_3^{-1}\rangle \,, \tag{4.1.9}$$

where we performed the sum over g_4 removing the delta $\delta(e, g_1 g_2 g_3^{-1} g_4^{-1})$. From the previous expression you can see that to prepare the magnetic ground state $|\tilde{e}\rangle$ we can create an equal weight linear superposition off all group element states for the first three edges g_1, g_2, g_3, while on the fourth we can act with the multiplication gate $U_\times$ and the inversion gate U_{-1} to reconstruct the state $|g_1 g_2 g_3^{-1}\rangle$. The circuit that realizes that is represented in Fig. 4.8.

Other magnetic eigenstates

As we saw in sections (3.3.3) and (3.4.3) magnetic eigenstates for the one and two plaquette system are linear combinations plaquette states $\{|\tilde{g}\rangle\}$ (3.3.7) and $\{|\tilde{g}_{p_1}, \tilde{g}_{p_2}\rangle\}$ (3.4.5) respectively. Let us focus on the single plaquette case, the generalization to a multiple plaquette system is straightforward. The idea is to use the quantum circuit in Fig. 4.6, where in the last three qubits, that refer to the fourth link of the plaquette, we initialize a superposition of group element states $\sum_g |g\rangle$, then at the end of the circuit we get the superposition of plaquette states $\sum_g |\tilde{g}\rangle$. The explicit form of the quantum gates needed to prepare the fourth link for each magnetic eigenstate is not difficult to to be found.

4.2 Quantum algorithm for D_3

In this section we discuss how to encode the 8 degrees of freedom of each edge of a D_3 lattice gauge theory in the degrees of freedom of the quantum simulator. We also see how to

g	e	r	r^2	s	rs	r^2s
state	$\|000\rangle$	$\|001\rangle$	$\|010\rangle$	$\|100\rangle$	$\|101\rangle$	$\|110\rangle$

Table 4.2: Encoding table of the group D_3. A generic group element $g = r^a s^b$, where $a = 0, 1, 2$ and $b = 0, 1$, can be encoded in the state $|ba_1a_2\rangle$, where b is exactly the exponent of s, while $a_1, a_2 = 0, 1$ are the two binary numbers needed to write a in binary code. Since $a < 3$ we cannot have $a_1 = a_2 = 1$.

implement the set of gates requested to reproduce the time evolution and how to prepare any particular eigenstate of the Hamiltonian.

4.2.1 Encoding

There are 6 possible group elements $g \in D_3$, so in order to represents all of them we need 3 qubits ($2^3 = 8$). Notice that in the quantum simulator we have an Hilbert space that is bigger than the Hilbert space of the physical model and we will have to deal with this redundancy. We encode the group elements in the quantum register as shown in Table 4.2.
Let us stress some properties of this encoding choice. Given a generic group element of the group $g = r^a s^b \in D_3$, where $a = 0, 1, 2$ and $b = 0, 1$, we can encode it in the state $|ba_1a_2\rangle$, where b is exactly the exponent of s, while $a_1, a_2 = 0, 1$ are the two binary numbers needed to write a in binary code. Since a is limited to assume the values $0, 1, 2$, we have that the states $|011\rangle$ and $|111\rangle$ (so when $a = 3$ and $a_1 = a_2 = 1$) of the quantum simulator have no counterparts in the physical model. During the simulation we will try never to initialize the states $|011\rangle$ and $|111\rangle$ and during the time evolution not to obtain these states, designing quantum gates that act diagonally on them. With respect to D_4 this is a complication.
A group element $g \in D_3$, encoded in 3 qubits, is associated at each link, then given a lattice with E edges, we need $3E$ qubits to represents it on a quantum circuit.

4.2.2 Evolution operator

In this section we show how we constructed the high level quantum gates needed to simulate a D_3 lattice gauge theory. The gates implemented in this section were introduced in section 2.3.2. Once these high level gates are implemented we can realized the magnetic evolution operator for a single plaquette $U_B^{(p)}(\Delta t)$ using the quantum circuit in Fig. 2.1, while the electric evolution operator for a single link $U_E^{(l)}(\Delta t)$ is realized by the quantum circuit in Fig. 2.2. The total evolution gate $U(t)$ for a single plaquette is shown in Fig. 2.3. All circuits were implemented using the software `Qiskit` [45].

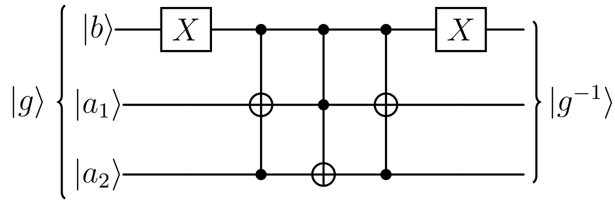

Figure 4.9: Quantum circuit that implements the inversion gate $U_{-1}|g\rangle = |g^{-1}\rangle$ (2.3.7) for the group D_3.

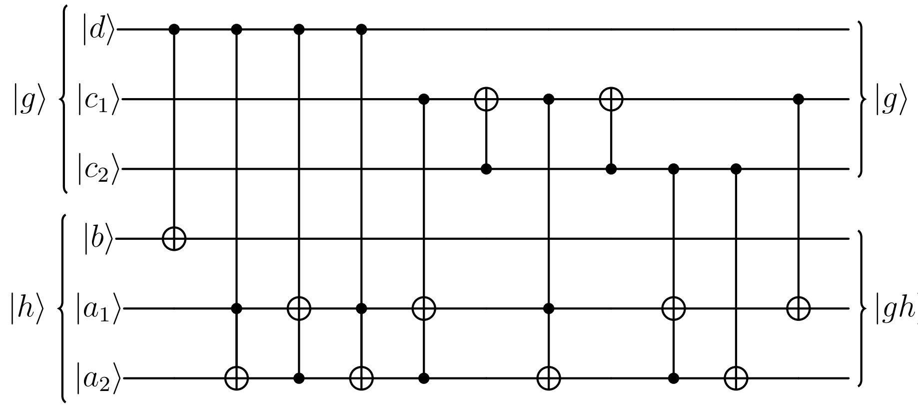

Figure 4.10: Quantum circuit that implements the multiplication gate $U_\times |g\rangle |h\rangle = |g\rangle |gh\rangle$ (2.3.8) for the group D_3. Given two input states $|g = r^c s^d\rangle$ and $|h = r^a s^b\rangle$, the first CNOT gate implements $b \oplus_2 d$, then there are three Toffoli gates that implement $\oplus_3 a \to \oplus_3 (-1)^d a$, there are 4 gates that implement $\oplus_3 \to \oplus_4$, while the last three gates perform the sum $c \oplus_4 (-1)^d a$.

Inversion gate

The inversion gate U_{-1} is defined in the relation (2.3.7). Looking at the inversion Table 3.6 we can see that the inversion operation simply exchanges the states $|r\rangle = |001\rangle$ and $|r^2\rangle = |010\rangle$. We can realize this operation using three Toffoli gates. The quantum circuit is represented in Fig. 4.9.

Multiplication gate

The multiplication gate $U_\times$ is defined in the relation (2.3.8). For the realization of the circuit we use the following property, given two elements of the group $g = r^c s^d$ and $h = r^a s^b$, with

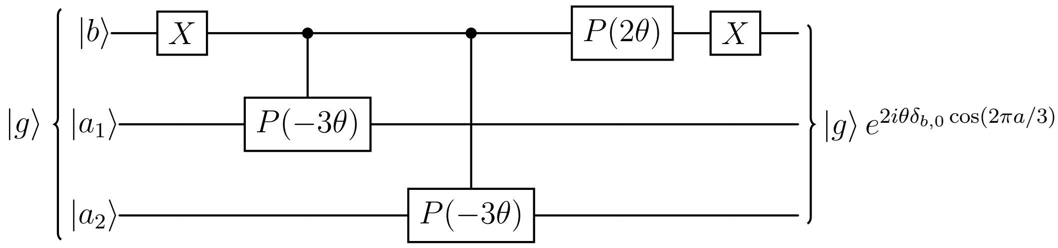

Figure 4.11: Quantum circuit that implements the trace gate $U_{\mathrm{tr}}(\theta)\,|g\rangle = |g\rangle\, e^{i\theta\,\mathrm{Re}\,\mathrm{Tr}[\rho_2(g)]}$ (2.3.9) for the group D_3. The gate $P(\theta)$ is the phase gate, described by the operator $P(\theta) = \mathrm{diag}(1, e^{i\theta})$.

$a, c = 0, 1, 2$ and $b, d = 0, 1$, their product is given by

$$gh = r^c s^d \cdot r^a s^b = r^{c \bigoplus_3 (-1)^d a} s^{b \bigoplus_2 d}, \tag{4.2.1}$$

where $\bigoplus_3$ and $\bigoplus_2$ are a sum modulo 3 and modulo 2 respectively. The property (4.1.1) can be directly verifies on the Cayley Table 3.5. Implementing the sum modulo 3 using binary numbers is not trivial, but it can be done using some more gates with respect to the D_4 case [14]. The gate is represented in Fig. 4.10. The first CNOT gate implements the operation $b \oplus_2 d$, then there are three Toffoli gates that implement $\oplus_3 a \to \oplus_3 (-1)^d a$, so they transforms the sum modulo 3 in a difference modulo 3 if and only if $d = 1$. Then there are four gates that transform the sum modulo 4 in a sum modulo 3, and finally the last three gates perform the sum $c \oplus_4 (-1)^d a$.

Trace gate

The trace gate $U_{\mathrm{tr}}(\theta)$ is a parametric gate defined in the relation (2.3.9). Considering the non-Abelian representation ρ_2, one can see that

$$\mathrm{Tr}(g) = \mathrm{Tr}\big(r^a s^b\big) = 2\delta_{b,0} \cos\left(\frac{2\pi a}{3}\right). \tag{4.2.2}$$

The figure of the gate is Fig. 4.11.

Fourier transform gate

The Fourier transform gate U_F allows us to move from the group element basis $\{|g\rangle\}$ to the representation basis $\{|j_{mn}\rangle\}$ and it is defined in (2.3.10). This gate is defined as

$$U_F = \sum_{g \in D_3} \sum_{j=0}^{2} \sum_{m,n=1}^{d_j} \sqrt{\frac{d_j}{6}} \rho_j(g)_{mn} \, |j_{mn}\rangle \langle g| \,, \tag{4.2.3}$$

where $(\rho_j)_{mn}$ is the mn component of the j-th representation, and $|\rho_j, mn\rangle$ is the corresponding element in the representation basis. The matrix elements of U_F are given by

$$\langle j_{mn}|U_F|g\rangle = \sqrt{\frac{d_j}{6}}\rho_j(g)_{mn}. \tag{4.2.4}$$

Given the expression (4.2.4) for the matrix elements of U_F we can easily construct the corresponding 8×8 matrix:

$$U_F = \frac{1}{\sqrt{6}}\begin{pmatrix} 1 & 1 & 1 & 0 & 1 & 1 & 1 & 0 \\ 1 & 1 & 1 & 0 & -1 & -1 & -1 & 0 \\ \sqrt{2} & -\frac{\sqrt{2}}{2}+i\frac{\sqrt{6}}{2} & -\frac{\sqrt{2}}{2}-i\frac{\sqrt{6}}{2} & 0 & 0 & 0 & 0 & 0 \\ 0 & 0 & 0 & 1 & 0 & 0 & 0 & 0 \\ 0 & 0 & 0 & 0 & \sqrt{2} & -\frac{\sqrt{2}}{2}+i\frac{\sqrt{6}}{2} & -\frac{\sqrt{2}}{2}-i\frac{\sqrt{6}}{2} & 0 \\ 0 & 0 & 0 & 0 & \sqrt{2} & -\frac{\sqrt{2}}{2}-i\frac{\sqrt{6}}{2} & -\frac{\sqrt{2}}{2}+i\frac{\sqrt{6}}{2} & 0 \\ \sqrt{2} & -\frac{\sqrt{2}}{2}-i\frac{\sqrt{6}}{2} & -\frac{\sqrt{2}}{2}+i\frac{\sqrt{6}}{2} & 0 & 0 & 0 & 0 & 0 \\ 0 & 0 & 0 & 0 & 0 & 0 & 0 & 1 \end{pmatrix}, \tag{4.2.5}$$

and using the Qiskit class Operator we can transform this matrix in the corresponding 3-qubits quantum circuit. Recall that the states $|011\rangle$ and $|111\rangle$ have no physical counterparts, and the matrix U_F is designed in such a way that it acts diagonally on these states.
The same procedure can be applied to construct the Hermitian conjugate of the Fourier transform gate $U_F^\dagger$ (2.3.12).

Phase gate

The phase gate $U_{\text{ph}}(\Delta t)$ is defined as the diagonal form of the electric evolution operator $U_E^{(l)}$ for the single link l as shown in the expression (2.3.14). The 8×8 matrix associated to this 3-qubit operator is

$$U_{\text{ph}}(\Delta t) = \begin{pmatrix} 1 & 0 & 0 & 0 & 0 & 0 & 0 & 0 \\ 0 & e^{-i\lambda_E f(1)\Delta t} & 0 & 0 & 0 & 0 & 0 & 0 \\ 0 & 0 & e^{-i\lambda_E f(2)\Delta t} & 0 & 0 & 0 & 0 & 0 \\ 0 & 0 & 0 & 1 & 0 & 0 & 0 & 0 \\ 0 & 0 & 0 & 0 & e^{-i\lambda_E f(2)\Delta t} & 0 & 0 & 0 \\ 0 & 0 & 0 & 0 & 0 & e^{-i\lambda_E f(2)\Delta t} & 0 & 0 \\ 0 & 0 & 0 & 0 & 0 & 0 & e^{-i\lambda_E f(2)\Delta t} & 0 \\ 0 & 0 & 0 & 0 & 0 & 0 & 0 & 1 \end{pmatrix}. \tag{4.2.6}$$

The 3-qubit quantum circuit that implement this matrix can be obtained using the Qiskit class Operator. Since the phase gate U_{ph} depends on the electric Hamiltonian, it depends also on the choice of the generating subset Γ, through the function $f(j)$ (1.4.41). Notice that U_{ph} acts diagonally on the states $|011\rangle$ and $|111\rangle$.

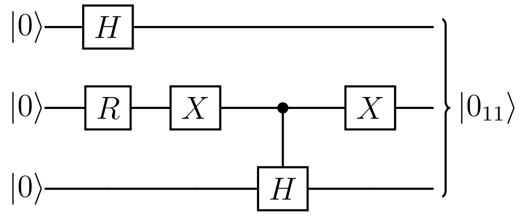

Figure 4.12: Quantum circuit $\mathbb{H}$ that prepares the electric ground state $|0_E\rangle = |0_{11}\rangle$ for the D_3 group on a single link. The gate R is the rotation (4.2.7).

4.2.3 State preparation

Now let's see how to prepare two particular states, the electric ground state $|E_0^{\lambda=1}\rangle$ and the magnetic ground state $|E_0^{\lambda=0}\rangle$, which are the ground state of the Kogut-Susskind Hamiltonian (1.4.45) in the limit where $\lambda = 1$ ($\lambda_B = 0$) and $\lambda = 0$ ($\lambda_E = 0$) respectively. Using the same approach one can construct also the excited eigenstates both in the electric and magnetic limit. If instead one is interested in an energy eigenstate at a generic $\lambda \neq 0, 1$, one has first to prepare the corresponding electric or the magnetic eigenstate, and then apply the adiabatic evolution described in section 2.3.3, slightly changing λ at each Trotter step up to the desired value.

Electric ground state preparation

The electric ground state $|E_0^{\lambda=1}\rangle$ is the electric vacuum $|0_E\rangle$ that we defined in (3.3.5) and in (3.4.3) for the one-plaquette and two-plaquette system respectively. In both cases $|0_E\rangle$ is a equal weight linear superposition of all possible group element states. While in the D_4 theory the electric vacuum can be prepared applying an Hadamard gate H at each qubit in the $|0\rangle$ state, this is no more true for a D_3 theory, since the states $|011\rangle$ and $|111\rangle$ have no physical counterparts and we don't want them to appear in the quantum register.
Consider the three-qubit quantum register that represents a single link, the quantum circuit represented in Fig. 4.12, let's call it $\mathbb{H}$, prepares the electric ground state of a single link in a D_3 theory. In the circuit appears the single qubit gate R, that is the rotation described by the matrix

$$R = \begin{pmatrix} \frac{\sqrt{2}}{\sqrt{3}} & -\frac{1}{\sqrt{3}} \\ \frac{1}{\sqrt{3}} & \frac{\sqrt{2}}{\sqrt{3}} \end{pmatrix}. \tag{4.2.7}$$

Recalling that each link is represented by three qubits, the quantum circuit to prepare the electric ground state $|E_0^{\lambda=1}\rangle$ in a one-plaquette system is shown in Fig. 4.5, where you have to replace the Hadamard gates $H^{\otimes 3}$ with the gates $\mathbb{H}$. The extension of this circuit to a multiple plaquette system is trivial.

Other electric eigenstates

As we saw in sections (3.3.4) and (3.4.4) electric eigenstates for the one and two plaquette system are the character states $\{|\chi_i\rangle\}$ (3.3.9) and $\{|i_1, i_2\rangle, |j, \bar{2}\rangle\}$ (3.4.9, 3.4.10) respectively. The preparation of these states is completely analog to what we have seen for D_4 in section 4.1.3.

Magnetic ground state preparation

The magnetic ground state $|E_0^{\lambda=0}\rangle$ is the plaquette state $|\tilde{e}\rangle$ and multiple-plaquette state $|\tilde{e}_{p_1}, \tilde{e}_{p_2}\rangle$ for the one-plaquette and two-plaquette system respectively. We focus just on the preparation of the state $|\tilde{e}\rangle$, then the generalization to a multiple plaquette system is straightforward. The circuit that realizes that is the same of D_4, the one represented in Fig. 4.8, you have only to replace the Hadamard gates $H^{\otimes 3}$ with the gates $\mathbb{H}$.

Other magnetic eigenstates

As we saw in sections (3.3.4) and (3.4.4) electric eigenstates for the one and two plaquette system are linear combinations plaquette states $\{|\tilde{g}\rangle\}$ (3.3.7) and $\{|\tilde{g}_{p_1}, \tilde{g}_{p_2}\rangle\}$ (3.4.5) respectively. The preparation of these states is completely analog to what we have seen for D_4 in section 4.1.3.

4.3 Results of the quantum simulation

In this section we illustrate the results of quantum simulations, in order to verify if they are able to reproduce the theoretical results discussed in chapter 3. In particular we consider a one-plaquette system and we look at its full energy spectrum for both D_4 and D_3 gauge theories and the Wilson loop observable over the ground state for the group D_4. Then we consider a two-plaquette system and we look at the ground state energy for both D_4 and D_3 gauge theories and Wilson loop observables over the ground state for the group D_4.

4.3.1 One-plaquette system

D_4 lattice gauge theory

In order to simulate a one-plaquette D_4 lattice gauge theory we need 13 qubits: 12 qubits are required to encode the physical degrees of freedom of the 4 edges, while an ancillary qubit is needed to perform the measurements, as we saw in section 2.4.
The circuit that we use to measure the energy eigenvalues is shown in Fig. 4.13. The structure of the circuit is the same that we see in Fig. 2.4, where we have an ancillary qubit a, and a quantum register of 12 qubits (each double line represents the three qubits associated to a link

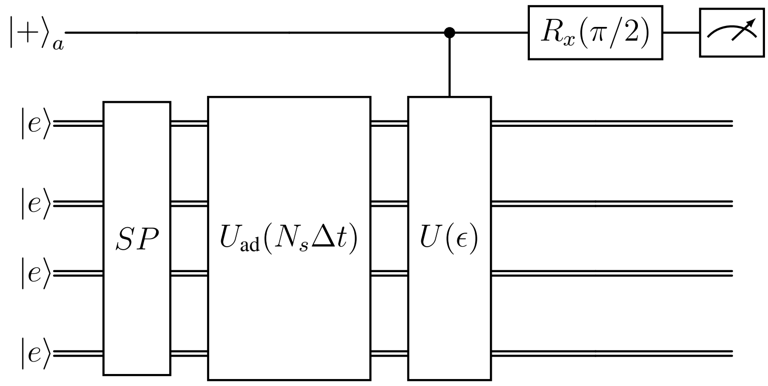

Figure 4.13: Quantum circuit to measure the expectation value of the energy in the one-plaquette system. Each double line represents the 3 qubits of an edge. The structure of the circuit is the same that we see in Fig. 2.4, with $V = \mathbb{I}$ and $W = U(\epsilon)$, the evolution operator shown in Fig. 2.3. The gate SP prepares the electric (or magnetic) ground state, hence it corresponds to the gate shown in Fig. 4.5 (or Fig. 4.8). The gate $U_{\text{ad}}(N_s\Delta t)$ performs an adiabatic evolution in N_s Trotter steps with a time step of Δt, slightly modifying the coupling constant λ.

of the lattice). We are interested in measuring the expectation value of the energy $\langle E_0^\lambda|H|E_0^\lambda\rangle$ over the ground state of the Hamiltonian H for some fixed coupling λ. Referring to the gates in Fig. 2.4 we put $V = \mathbb{I}$ and $W = U_Q(\epsilon) = U(\epsilon)$, the evolution operator of the Hamiltonian for a time interval ϵ that is shown in Fig. 2.3. Then we measure the ancillary qubit in the y-basis applying the $R_x(\pi/2)$ gate (2.4.14). The ground state $|E_0^\lambda\rangle$ whose energy we are interested in is prepared in the quantum register using the quantum gates SP and $U_{\text{ad}}(N_s\Delta t)$. The gate SP prepares the electric (or magnetic) ground state using the quantum circuit in Fig. 4.5 (or in Fig. 4.8), hence it prepares the state $|E_0^{\lambda=1}\rangle$ (or $|E_0^{\lambda=0}\rangle$). The gate $U_{\text{ad}}(N_s\Delta t)$ performs the adiabatic evolution described in section 2.3.3 in N_s Trotter steps, slightly changing the coupling constant λ from 1 (or 0) up to the desired final value, getting the state $|E_0^\lambda\rangle$. This is the ground state of which we measure the energy.
The same procedure can be applied also to measure the energy of other eigenstates $|E_n^\lambda\rangle$, not only the ground state $n \neq 0$. You can still use the circuit in Fig. 4.13, with the only difference that this time the gate SP prepares an electric (or magnetic) eigenstate $|E_n^{\lambda=1}\rangle$ (or $|E_n^{\lambda=0}\rangle$) using the quantum circuits described in section 3.3.3 (or 3.3.3).
The parameters that have to be fixed are the time interval ϵ, the time step Δt and the number of Trotter steps N_s. We fix the time step $\Delta t = 0.01 \ll 1$, a sufficient small quantity to make precise the Trotter approximation. The time interval ϵ should be as small as possible, as we see in (2.4.8), then we fix $\epsilon = \Delta t$. The choice of the number of Trotter steps N_s is critical

and delicate. From the expression (2.3.25) we can see that the Trotter error is minimized by choosing $N_s = 1$, but in this way we are not taking in account the adiabatic approximation (2.3.27), and this is a problem since this is the main source of errors. Suppose we want to evolve the magnetic ground state $|E_0^{\lambda=0}\rangle$, where the coupling constant is $\lambda(0) = 0$, up to the ground state $|E_0^{\bar{\lambda}}\rangle$ of the Hamiltonian where $\bar{\lambda} = \lambda(N_s \Delta t)$. At each Trotter step of the adiabatic evolution we increase the coupling of $\Delta\lambda = \bar{\lambda}/N_s$. In order for the adiabatic approximation to be precise we have to satisfy the relation (2.3.27), so one should have

$$N_s \gg \frac{\bar{\lambda}}{\Delta t \Delta E^2}, \tag{4.3.1}$$

where ΔE^2 is the minimum energy gap between the ground state and the first excitation. In a D_4 lattice gauge theory with a single plaquette, from the numerical analysis in Fig. 3.5, we can see that $\Delta E = 2.38$ using the generating subset Γ_1, and $\Delta E = 2.65$ using the generating subset Γ_2. Therefore a good choice for the number of steps could be $N_s = 2000\bar{\lambda}$, that means a coupling step $\Delta\lambda = 0.0005$, hence 2000 steps to move from $\lambda = 0$ to $\lambda = 1$. From some empirical tests we verify that we get good results starting from a much small number of steps, like $N_s \approx 500\bar{\lambda}$, hence $\Delta\lambda \approx 0.002$, provided a final coupling constant not too large $\bar{\lambda} \lesssim 0.5$ (for larger λ one could start from the electric ground state, where $\lambda = 1$, and decrease the coupling constant instead of starting from the magnetic ground state, where $\lambda = 0$). In practical applications one wants to minimize the depth of the circuit, so the number of Trotter steps N_s, this can be achieved also increasing the time step Δt at the price of less precision in the Trotter approximation.

The results of the quantum circuits are plotted in Fig. 4.14. In these plots you can see continuous lines, which represent the exact results that we obtained by a numerical diagonialization of the Hamiltonian, while dots represent the results of the quantum circuit simulation, different colors identify different eigenstates and the error bars are the Trotter errors (2.3.25). The results of the quantum circuit reproduce quite well the the expected behaviour of the spectrum, except when two states are degenerate both in the magnetic and in the electric limit. If two states are degenerate, then the energy gap is zero $\Delta E = 0$ and the adiabatic approximation no longer applies. Almost all these eigenstates are prepared starting by the corresponding electrical eigenstate $|\chi_j\rangle$ ($\lambda = 1$) and then evolving it adiabatically, and this can be seen from the fact that the Trotter error bars increase decreasing λ. The only exception is the blue state with Γ_2, where we start with the magnetic eigenstate $|\widetilde{r^2}\rangle$ and then we increase λ adiabatically, indeed the error bars for this state increase with λ. The reason behind this difference is to avoid the degeneracy of this state in the electric limit.

In Fig. 4.15 you can see results of the quantum circuit simulation regarding the expectation value of the Wilson loop operator over the ground state. Even in this case there is a good agreement between the simulation and the theoretical predictions.

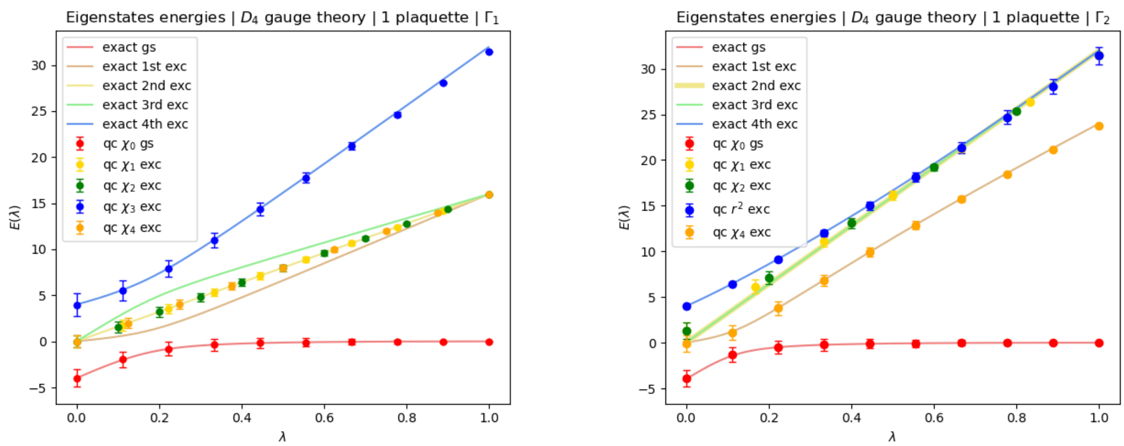

(a) Energy eigenvalues using the generating subset Γ_1.

(b) Energy eigenvalues using the generating subset Γ_2.

Figure 4.14: Energy eigenvalues as a function of the coupling constant λ for a D_4 gauge theory on a single-plaquette system. Continuous lines are the results from the exact diagonalization of the Hamiltonian, dots refer to the results obtained by the quantum circuit (qc) and the relative error bars come from the Trotter error. The red elements refer to the ground state (gs), the others to the excited states (exc). For these simulations we use a number of steps equal to $N_s = 1000\lambda$ and a time step $\Delta t = 0.01$.

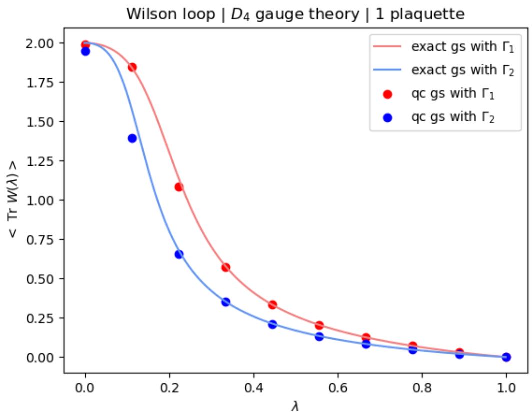

Figure 4.15: Wilson loop observable $\mathrm{Tr}\,\hat{W}$ as a function of the coupling constant λ for a D_4 gauge theory on a single-plaquette system. Continuous lines are the results from the numerical evaluation of the expected value of $\mathrm{Tr}\,\hat{W}$ on the ground state of the Hamiltonian, dots refer to the results obtained by the quantum circuit (qc). Red elements refer to Γ_1, blue elements to Γ_2.

D_3 lattice gauge theory

In order to simulate a one-plaquette D_3 lattice gauge theory we need 13 qubits: 12 qubits are required to encode the physical degrees of freedom of the 4 edges, while an ancillary qubit is needed to perform the measurements, as we saw in section 2.4.
The circuit that we used to measure the energy eigenvalues is the same of D_4 and it is shown in Fig. 4.13. The only differences, with respect to the D_4 case, are first in the form of high level gates used to construct the evolution operator $U(t)$ in Fig. 2.3, and also the structure of the state preparation gate SP. If one wants to prepare the electric (or magnetic) ground state should use the quantum circuit in Fig. 4.5 (or in Fig. 4.8) replacing the Hadamard gates $H^{\otimes 3}$ with the gate $\mathbb{H}$ in Fig. 4.12.
As for D_4 we fix the time step to $\Delta t = 0.01$, the time interval $\epsilon = \Delta t$. In order for the adiabatic approximation to be precise we have to satisfy the relation (4.3.1). In a D_3 lattice gauge theory with a single plaquette, from the numerical analysis in Fig. 3.6, we can see that $\Delta E = 3.01$ using the generating subset Γ_1, and $\Delta E = 2.92$ using the generating subset Γ_2. Therefore a good choice for the number of steps could be $N_s = 1000\bar{\lambda}$, that means a coupling step $\Delta\lambda = 0.001$, hence 1000 steps to move from $\lambda = 0$ to $\lambda = 1$. From some empirical tests we verify that for D_3 we get good results starting from a much small number of steps, like $N_s \approx 200\bar{\lambda}$.
The results of the quantum circuits are plotted in Fig. 4.16. In these plots you can see continuous lines, which represent the exact results that we obtained by a numerical diagonialization of

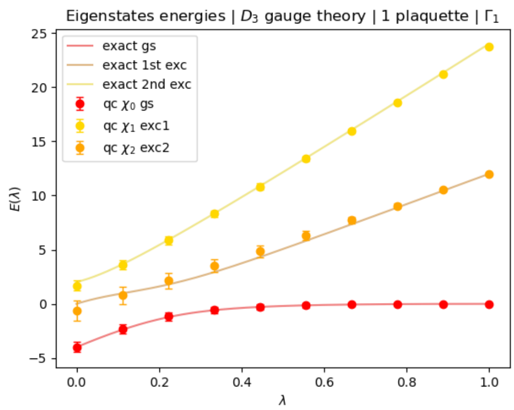

(a) Energy eigenvalues using the generating subset Γ_1.

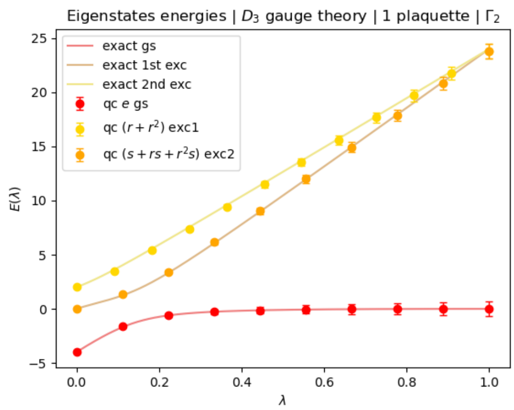

(b) Energy eigenvalues using the generating subset Γ_2.

Figure 4.16: Energy eigenvalues as a function of the coupling constant λ for a D_3 gauge theory on a single-plaquette system. Continuous lines are the results from the exact diagonalization of the Hamiltonian, dots refer to the results obtained by the quantum circuit (qc) and the relative error bars come from the Trotter error. The red elements refer to the ground state, the others to excited states (exc). For these simulations we use a number of steps equal to $N_s \approx 800\lambda$.

the Hamiltonian, while dots represent the results of the quantum circuit simulation, and error bars are Trotter errors (2.3.25). The results of the quantum circuit reproduce quite well the expected behaviour of the spectrum. Different colors identify different eigenstates. In the Γ_2, Fig. 4.16a case we begin the adiabatic evolution of all states from the magnetic limit ($\lambda = 0$), since all magnetic eigenstates are non-degenerate, while in the Γ_2, Fig. 4.16b case we begin the adiabatic evolution of all states from the magnetic limit ($\lambda = 0$), for the same reason.

4.3.2 Two-plaqutte system

D_4 lattice gauge theory

In order to simulate a two-plaquette D_4 lattice gauge theory we need 22 qubits: 21 qubits are required to encode the physical degrees of freedom of the 7 edges, while an ancillary qubit is needed to perform the measurements, as we saw in section 2.4.
The circuit that we use to measure the energy eigenvalues is completely analog to the one shown in Fig. 4.13, the only difference is that now, with two plaquettes, the qubit register contains 7 double lines (21 qubits). The ground state $|E_0^\lambda\rangle$ whose energy we are interested in is prepared in the quantum register using the quantum gates SP and $U_{\text{ad}}(N_s\delta t)$. The gate SP

prepares an electric (or magnetic) ground state using the two-plaquette analog of the quantum circuit in Fig. 4.5 (or in Fig. 4.8), hence it prepares the state $|E_0^{\lambda=1}\rangle$ (or $|E_0^{\lambda=0}\rangle$). The gate $U_{\text{ad}}(N_s\Delta t)$ performs the adiabatic evolution described in section 2.3.3 in N_s Trotter steps, slightly changing the coupling constant λ from 1 (or 0) up to the desired final value, getting the state $|E_0^{\lambda}\rangle$. This is the ground state of which we measure the energy.
The parameters that have to be fixed are the time interval ϵ, the time step Δt and the number of Trotter steps N_s. We fix the time step $\Delta t = 0.01 \ll 1$ a sufficient small quantity to make precise the Trotter approximation. Then we fix the time interval ϵ to $\epsilon = \Delta t$. In a D_4 lattice gauge theory with two plaquette, from the numerical analysis in Fig. 3.9, we can see that $\Delta E = 2.13$ using the generating subset Γ_1, and $\Delta E = 2.38$ using the generating subset Γ_2. Therefore a good choice for the number of steps could be $N_s = 25000\bar{\lambda}$, that means a coupling step $\Delta\lambda = 0.0004$, hence 2500 steps to move from $\lambda = 0$ to $\lambda = 1$. The simulation of 22 is very demanding, in terms of computational resources, so we use much less Trotter steps, still obtaining good results.
The results of the quantum circuits are plotted in Fig. 4.17. In these plots you can see continuous lines, which represent the exact results that we obtained by a numerical diagonialization of the Hamiltonian, while dots represent the results of the quantum circuit simulation, and the error bars are the Trotter errors (2.3.25). The results of the quantum circuit reproduce quite well the expected behaviour of the spectrum. In both plots the ground state for an arbitrary λ is realized starting by the corresponding electrical ground state $|0,0\rangle$ ($\lambda = 1$) and then evolving it adiabatically.
In Fig. 4.18 you can see results of the quantum circuit simulation regarding the expectation value of the Wilson loop operator over the ground state. Even in these cases there is a good agreement between the simulation and the theoretical predictions.

D_3 lattice gauge theory

In order to simulate a two-plaquette D_3 lattice gauge theory we need 22 qubits: 21 qubits are required to encode the physical degrees of freedom of the 7 edges, while an ancillary qubit is needed to perform the measurements, as we saw in section 2.4.
The circuit that we used to measure the energy eigenvalues is completely analog to the one used to simulate a two-plaquette D_4 theory. The only differences with respect to the D_4 cases are first in the form of the high level gates use to construct the evolution operator $U(t)$ in Fig. 2.3, and also the structure of the state preparation gate SP . If one wants to prepare the electric (or magnetic) ground state should use the two-plaquette version quantum circuit in Fig. 4.5 (or in Fig. 4.8) replacing the Hadamard gates H with the gates $\mathbb{H}$ in Fig. 4.12.
As for D_4 we the time step $\Delta t = 0.01$ and the time interval $\epsilon = \Delta t$. In a D_3 lattice gauge theory with two plaquette, from the numerical analysis in Fig. 3.10, we can see that $\Delta E = 2.77$ using the generating subset Γ_1, and $\Delta E = 2.66$ using the generating subset Γ_2. Therefore a good choice for the number of steps could be $N_s = 20000\bar{\lambda}$, that means a coupling step $\Delta\lambda = 0.0005$, hence 2000 steps to move from $\lambda = 0$ to $\lambda = 1$. The simulation of 22 is very

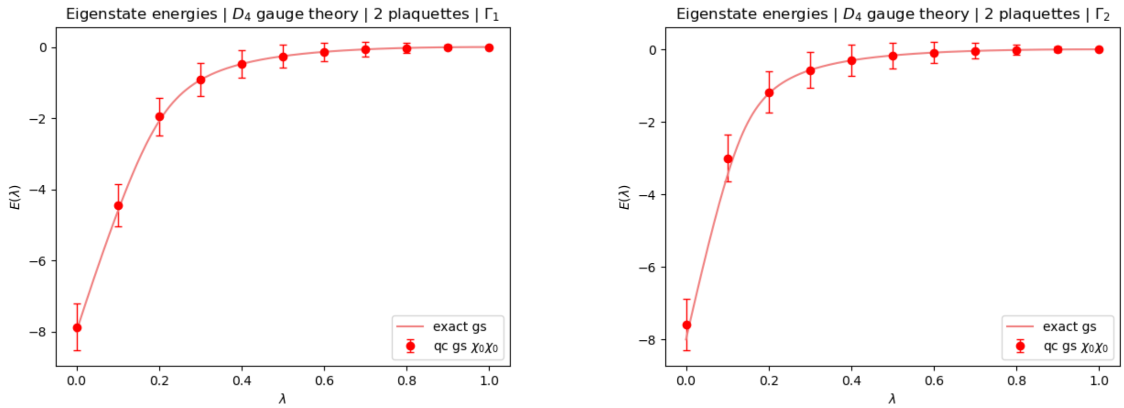

(a) Energy of the ground state using the generating subset Γ_1.

(b) Energy of the ground state using the generating subset Γ_2.

Figure 4.17: Energy of the ground state (gs) as a function of the coupling constant λ for a D_4 gauge theory on a two-plaquette system. Continuous lines are the results from the exact diagonalization of the Hamiltonian, dots refer to the results obtained by the quantum circuit (qc) and the relative error bars come from the Trotter error. For these simulations we use a number of steps equal to $N_s \approx 1000\lambda$ and a time step $\Delta t = 0.01$.

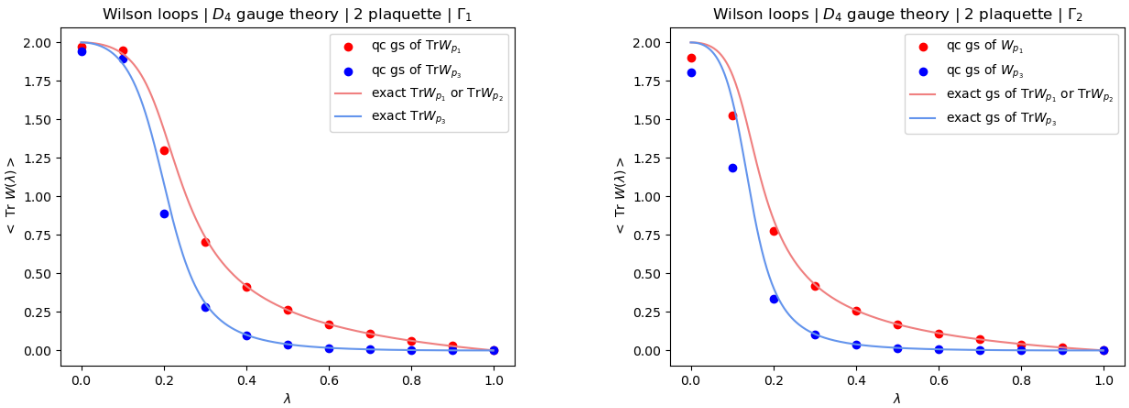

(a) Wilson loops over the ground state using Γ_1.

(b) Wilson loops over the ground states using Γ_2.

Figure 4.18: Wilson loops over the ground state (gs) as a function of the coupling constant λ for a D_4 gauge theory on a two-plaquette system. Continuos line are the exact results, the dots refer to the results obtained by the quantum circuit (qc). For these simulations we used a number of steps equal to $N_s \approx 1000\lambda$ and a time step $\Delta t = 0.01$.

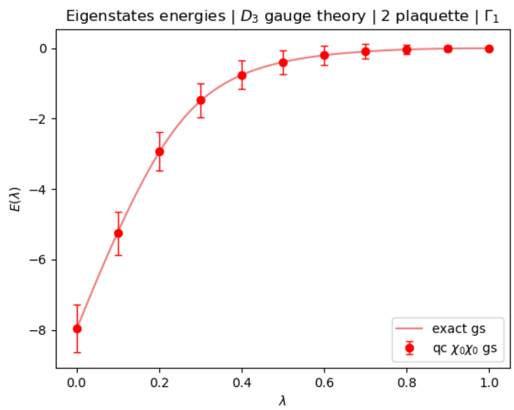

(a) Energy of the ground state using the generating subset Γ_1.

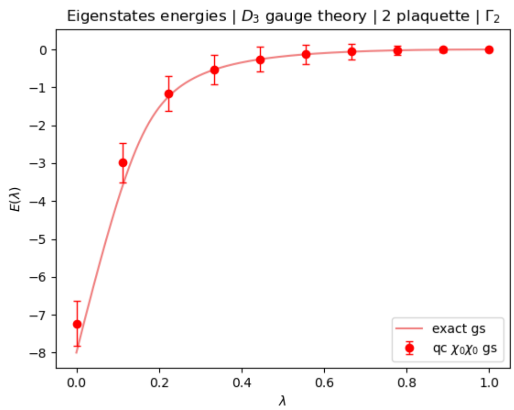

(b) Energy of the ground state using the generating subset Γ_2.

Figure 4.19: Energy of the ground state (gs) as a function of the coupling constant λ for a D_3 gauge theory on a two-plaquette system. Continuous lines are the results from the exact diagonalization of the Hamiltonian, dots refer to the results obtained by the quantum circuit (qc) and the relative error bars come from the Trotter error. For these simulations we use a number of steps equal to $N_s \approx 1000\lambda$ and a time step $\Delta t = 0.01$.

demanding, in terms of computational resources, so we used much less Trotter steps, obtaining good results.
The results of the quantum circuits are plotted in Fig. 4.19. In these plots you can see the continuous lines, that represent the exact results that we obtained by a numerical diagonialization of the Hamiltonian, while the dots represents the results of the quantum circuit simulation, and the error bars are the Trotter errors (2.3.25). The results of the quantum circuit reproduce quite well the the expected behaviour of the spectrum. In both plots the ground state for an arbitrary λ is realized starting by the corresponding electrical ground state $|0, 0\rangle$ ($\lambda = 1$) and then evolving it adiabatically.

4.3.3 Resources required

The algorithm that we propose in this section can be easily extended to arbitrary large lattice, the only thing that prevented us from simulating a larger number of plaquettes are the computational limitation for a classical computer to simulate a quantum circuit with a large number of qubits. Let us now examine how many quantum resources are required to simulate a lattice gauge theory on a quantum computer, and how they scale with the size of the lattice.
Consider an $N \times N$ two-dimensional lattice, the number of links (and so of qubits) scales as $2N(N-1) \approx 2N^2$, and the number of plaquette scales as $(N-1)^2 \approx N^2$. If we want to

implement a single step of the Trotter algorithm we need an electric evolution operator U_E for each link and a magnetic evolution operator U_B for each plaquette, hence the number of operators U_E scales as $2N^2$ and the number of operators U_B scales as N^2. In principle the depth of the circuit does not scale at all with the size of the lattice, since at each Trotter step on each link acts just a single electric operator U_E and a maximum of two magnetic operator U_B (a link can be shared by just two plaquettes), and this is regardless of the size N of the circuit. In practice we expect that the gap ΔE decreases increasing the lattice size N, therefore from (4.3.1) you see that to keep the same precision in the adiabatic evolution you should increase the number of Trotter step N_s, hence the number of U_B and U_E that acts on each qubit, hence the depth of the circuit.
The quantum gate implemented in `Qiskit` can be optimised using the transpiler in order to optimize the circuit for execution on present day noisy quantum systems. This means trying to reduce the number of circuit operations (expecially the non-local gates) and the depth of the circuit. For D_4, upon optimization, the gate U_B has a depth of 480 (368) and contains 856 (627) gates (the second option has more non-local gates), the gate U_E has a depth of 116 and contains 119 gates. For a very basic simulation you need $N_s = 100$ Trotter steps, so the depth of the whole circuit will be of the order of 2×10^5, not affordable for nowadays noisy quantum computers.

CONCLUSION

In this thesis we study the Hamiltonian formulation of a non-Abelian lattice gauge theory using the dihedral gauge groups D_4 and D_3. We construct all quantum gates needed to simulate this theory and we use these gates to realize the quantum circuit that implements the time evolution operator, using the standard Trotter procedure. Using this circuit, once an initial state is initialized, it is possible to make it evolve in time, allowing us to measure at any time the observables we are interested in, like energy or Wilson loops. Using the quantum adiabatic algorithm it is possible to prepare the ground state of the Hamiltonian for any coupling, starting from the ground state in the electric (or magnetic) limit, that can be easily initialized in the quantum register. All simulations of this work are realized using the `Qiskit` toolkit. Using these techniques we are able to successfully initialize many relevant states of the one and two plaquette system (like the electric and magnetic ground state, but also some excited states). We are also able to reconstruct the full energy spectrum and the values of Wilson loop operators for one and two plaquette systems in any coupling constant regime. The results obtained from the quantum circuit are validated by comparing them with the spectra that we get from a numerical exact diagonalization of the gauge-invariant Hamiltonian, the agreement between these two techniques is very good. From this result we can deduce that the quantum circuit is able to successfully describe systems with a higher number of plaquettes, when the exact diagonalization of the gauge invariant Hamiltonian becomes much more complicated, while the extension of the quantum algorithm is straightforward. We also discuss the feasibility of carrying out this simulation on a near-term noisy quantum computer, and conclude that it is beyond the capability of nowadays quantum computers, but it can be achieved in the future thanks to the current development of quantum technologies.

Outlooks

Many of the most studied group of symmetries in physics, like $SU(3)$ or $SU(2)$ are non-Abelian and they contain an infinite number of elements, but it is reasonable to think that these groups can be well approximated by some of their finite non-Abelian subgroups, like the dihedral groups D_n, as we did in this thesis, but following the same logic and procedure it is also possible to do the same for more complicated finite gauge groups that approximate better and better the continuous group that we are interested in. A possible choice is the binary tetrahedral group $2T$. Moreover it could be interesting to specify the simulations for some applications of gauge theories (from condensed matter to Standard Model) or apply the same technique used in this work to related physical systems, like the quantum double model, thus paving the way for a wide range of applications. With the development of quantum technologies this approach for the study of physical systems will become even more efficient and feasible, providing new tools for studying and understanding physical phenomena.

Appendix A

Finite group theory

In this appendix we collect some results on finite groups, their representation theory, their algebra and their character theory. We use as main references [49] and [57], here one can find the proofs of the theorems of this section. We consider a finite group G, denoting with $|G|$ its size, i.e. the number of elements that it contains.

A.1 Representation theory

Definition 1. *A representation of a group G is a pair (V, ρ) where V is a complex vector space and $\rho : G \to \mathrm{End}(V)$ is a group homomorphism.*

In this thesis we often refer to ρ as the representation itself, but no confusion should arise.

Definition 2. *Two representations (V_1, ρ_1) and (V_2, ρ_2) are equivalent if there is a one-to-one and onto linear map $T : V_1 \to V_2$ such that $\rho_2(g)T = T\rho_1(g)$ for all $g \in G$.*

A representation is called unitary if $\rho(g)^{-1} = \rho(g^{-1}) = \rho(g)^\dagger$ for all $g \in G$.

Definition 3. *If (V, ρ) is a representation of G, U is a subspace of V, and $\rho(g)u \in U$ for all $g \in G$ and $u \in U$ we see that $(U, \rho|_U)$ is also a representation of G. In this case we call $(U, \rho|_U)$ a subrepresentation of (V, ρ) and U a invariant subspace of V.*

Definition 4. *If a representation (V, ρ) contains a proper nonzero subrepresentation, we say that it is reducible. Otherwise, we say that it is irreducible.*

In other words a representation is called irreducible if it does not contain any non-trivial invariant subspaces.

Theorem 1. *Let G be a finite group and $\hat{G}$ the set of equivalence classes of irreducible representations of G. Then $\hat{G}$ is finite, and the representative of each class can be chosen to be* *unitary.*

We label the irreducible representation of a group with the index j, and denote with $|\hat{G}|$ the number of inequivalent irreducible representations inside $\hat{G}$.

A.2 Group algebra

Definition 5. *The group algebra $\mathbb{C}[G]$ is the set of all functions $f : G \to \mathbb{C}$.*

In this group we can define three important binary operations, given $f_1, f_2 \in \mathbb{C}[G]$ we have:

1. The Hermitian product
$$\langle f_1, f_2 \rangle = \sum_{g\in G} f_1^*(g) f_2(g). \tag{A.2.1}$$

2. The function product
$$(f_1 f_2)(g) = f_1(g) f_2(g). \tag{A.2.2}$$

3. The convolution
$$f_1 \star f_2(g) = \frac{1}{|G|} \sum_{h\in G} f_1(gh^{-1}) f_2(h). \tag{A.2.3}$$

An orthonormal basis of the group algebra $\mathbb{C}[G]$ is given by the set e_h, with $h \in G$, defined such that $e_h(g) = \delta(h, g)$ is a Kronecker delta. Any other function $f \in \mathbb{C}[G]$ can be written as

$$f = \sum_{g\in G} f(g) e_g. \tag{A.2.4}$$

Interpreting the group algebra as a Hilbert space and introducing the Dirac formalism we can associate e_g to the group element state $|g\rangle$.

Definition 6. *A class function on a group G is a function which is constant on conjugate classes, i.e. $f(g) = f(hgh^{-1})$ for all $g, h \in G$.*

A.3 Character theory

Definition 7. *We define the character of a representation (V, ρ) to be the map $\chi_\rho : G \to \mathbb{C}$, where $\chi_\rho(g) = \mathrm{Tr}\,\rho(g)$ for any $g \in G$.*

Proposition 1. *If χ_ρ is a character of a representation of a finite group G of finite dimension d_ρ, then for any $g, h \in G$:*

1. $\chi_\rho(1) = d_\rho$,

2. $\chi_\rho(g^{-1}) = \chi^*(g)$,
3. $\chi(gh) = \chi(hg)$.

Theorem 2. ***(Burnside's theorem)*** *Let G be a finite group. Then:*

1. *If d_j is the dimension of the j-th inequivalent irreducible representation of G, and there are $|\hat{G}|$ such, then*
$$\sum_{j\in\hat{G}} d_j^2 = |G|. \tag{A.3.1}$$

2. *The number $|\hat{G}|$ of inequivalent irreducible representations of G is equal to the number of conjugacy classes of G.*

If we collect the values for all irreducible characters on all conjugacy classes of G we obtain the character table, which is a square table useful to collect information about the representations. Some examples are the Table 3.3 for D_4 and Table 3.7 for D_3.
There are as many irreducible characters χ_j as there are inequivalent irreducible representations ρ_j. An important result for the characters of irreducible representations is

Theorem 3. *The characters of irreducible representations $\{\chi_j\}$ of a group G form a basis for the space of class functions on G.*

Theorem 4. ***(Orthogonality theorem for characters)*** *The irreducible characters $\{\chi_j\}$, with $j \in \hat{G}$, of a finite group G are orthonormal, in the sense that*

$$\frac{1}{|G|}\sum_{g\in G} \chi_i^*(g)\chi_j(g) = \delta_{i,j}. \tag{A.3.2}$$

The characters also satisfy a different kind of orthogonality relation, where one sums over characters rather than over group elements:

Theorem 5. *The irreducible characters $\{\chi_i\}$ of a finite group G satisfy*

$$\sum_{i\in\hat{G}} \chi_i^*(g)\chi_i(h) = \begin{cases} \dfrac{|G|}{|C|} & \text{if } g,h \in C \\ 0 & \text{otherwise} \end{cases}, \tag{A.3.3}$$

where i labels the irreducible characters and $|C|$ is the size of the conjugacy class C

Proposition 2. *The convolution of two characters is again a character:*

$$\chi_i \star \chi_j = \frac{|G|}{d_j}\delta_{i,j}\chi_j. \tag{A.3.4}$$

Appendix B

Hamiltonian matrix elements for two-plaquette

In this appendix we show the computation of the matrix elements of the Kogut-Susskind Hamiltonian H (1.4.44) for a two-plaquette system using the basis made of character states like $\{|i_1, i_2\rangle\}$ (3.4.9) and $\{|j_1, \bar{j_2}\rangle\}$ (3.4.10). We perform the calculations for a generic gauge group G, with generating subset Γ and a faithful representation F. Recall that the Kogut-Susskind Hamiltonian is made of two non commuting parts, the electric Hamiltonian H_E and the magnetic Hamiltonian H_B, such that $H = H_E + H_B$.

B.1 Matrix elements of the electric Hamiltonian

Let's start from the electric part, which is diagonal in the multiple-character states (and we will see why). For the two-plaquette system the electric Hamiltonian H_E (1.4.42) reads out as

$$H_E = \sum_{l=1}^{7} H_E^{(l)} = \lambda_E \sum_{l=1}^{7} \sum_{j \in \hat{G}} f(j)\mathbb{P}_j(l), \tag{B.1.1}$$

where

$$H_E^{(l)} = \lambda_E \sum_{j \in \hat{G}} f(j)\mathbb{P}_j(l) \tag{B.1.2}$$

is the electric Hamiltonian for a single link l, then we have to sum over all 7 links. We recall that $\mathbb{P}_j(l)$ is the projector (1.4.26) onto the subspace of the the representation j of the link l and the function $f(j)$ is defined in the equation (1.4.41) and it depends on a generating subset Γ.

Given the basis states $|i_1, i_2\rangle$ (3.4.9) consider the matrix element

$$\langle i_1, i_2| H_E^{(l)} |j_1, j_2\rangle = \lambda_E \sum_{j\in\hat{G}} f(j) \langle i_1, i_2| \mathbb{P}_j(l) |j_1, j_2\rangle . \tag{B.1.3}$$

Recall that we can write the state $|i_1, i_2\rangle$ in terms of the representation basis $|j_{mn}\rangle$ on each link except for the shared link $l = 2$, as in the expression (3.4.14). The projector operator $\mathbb{P}_j(l)$ (1.4.26) is diagonal in the representation basis $|j_{mn}\rangle$ and thus from these simple observations we can see that for $l \neq 2$ (all not-shared links):

$$\langle i_1, i_2| H_E^{(l\neq 2)} |j_1, j_2\rangle = \lambda_E f(i_l)\delta_{i_1,j_1}\delta_{i_2,j_2}, \tag{B.1.4}$$

where

$$i_l = \begin{cases} i_1 & \text{if } \ l \in p_1 \\ i_2 & \text{if } \ l \in p_2 \end{cases} . \tag{B.1.5}$$

Instead the computation for the matrix element $\langle i_1, i_2| H_E^{(2)} |j_1, j_2\rangle$ is a bit more complicated. Let's start by using the expression (3.4.6) for the multiple-plaquette character states $|i_1, i_2\rangle$:

$$\begin{aligned}\langle i_1, i_2| H_E^{(2)} |j_1, j_2\rangle =& \frac{1}{|G|^2} \sum_{g_{p_1},g_{p_2},h_{p_1},h_{p_2}\in G} \chi^*_{i_1}(h_{p_1})\chi^*_{i_2}(h_{p_2})\chi_{j_1}(g_{p_1})\chi_{j_2}(g_{p_2})\cdot \\ &\cdot \langle \tilde{h}_{p_1}, \tilde{h}_{p_2}| H_E^{(2)} |\tilde{g}_{p_1}, \tilde{g}_{p_2}\rangle .\end{aligned} \tag{B.1.6}$$

Consider the expectation value of $H_E^{(2)}$ on two multiple-plaquette states, applying the relation (3.4.7) we get

$$\begin{aligned}\langle \tilde{h}_{p_1}, \tilde{h}_{p_2}| H_E^{(2)} |\tilde{g}_{p_1}, \tilde{g}_{p_2}\rangle =& \frac{1}{|G|^5} \sum_{g_1,\dots,g_7\in G} \sum_{h_1,\dots,h_7\in G} \delta(h_{p_1}, h_1h_2h_3^{-1}h_4^{-1})\cdot \\ &\cdot \delta(h_{p_2}, h_5h_6h_7^{-1}h_2^{-1})\delta(g_{p_1}, g_1g_2g_3^{-1}g_4^{-1})\delta(g_{p_2}, g_5g_6g_7^{-1}g_2^{-1})\cdot \\ &\cdot \langle h_1, \dots, h_7| H_E^{(2)} |g_1, \dots, g_7\rangle .\end{aligned} \tag{B.1.7}$$

In the expectation value $\langle h_1, ..., h_7| H_E^{(2)} |g_1, ..., g_7\rangle$, for each link $l \neq 2$ we have the appearance of a delta $\langle h_l|g_l\rangle = \delta(g_l, h_l)$, while on the link $l = 2$ there is the action of $H_E^{(2)}$ that must be taken into account:

$$
\begin{aligned}
\langle h_2| H_E^{(2)} |g_2\rangle =&\lambda_E \sum_{j\in\hat{G}} f(j) \langle h_2| \mathbb{P}_j(2) |g_2\rangle \\
=&\lambda_E \sum_{j\in\hat{G}} \sum_{m,n=1}^{d_j} f(j) \langle h_2|j_{mn}\rangle \langle j_{mn}|g_2\rangle \\
=&\frac{\lambda_E}{|G|} \sum_{j\in\hat{G}} \sum_{m,n=1}^{d_j} d_j f(j) \rho_j(h_2)_{mn} \rho_j^*(g_2)_{mn} \\
=&\frac{\lambda_E}{|G|} \sum_{j\in\hat{G}} \sum_{m,n=1}^{d_j} d_j f(j) \rho_j(h_2)_{mn} \rho_j(g_2^{-1})_{nm} \\
=&\frac{\lambda_E}{|G|} \sum_{j\in\hat{G}} d_j f(j) \chi_j(h_2 g_2^{-1}),
\end{aligned}
\tag{B.1.8}
$$

where we used in order the equation (B.1.2) for $H_E^{(2)}$, the definition (1.4.26) of the projector $\mathbb{P}_j(2)$, the duality relation (1.3.20), the definition of the conjugate representation $\rho_j^*(g) = \rho_j(g^{-1})^T$ and finally the character $\chi_j(g) = \operatorname{Tr} \rho_j(g)$. If we insert the expression (B.1.8) that we have just obtained inside the relation (B.1.7), considering also the deltas coming from $\langle h_l|g_l\rangle = \delta(g_l, h_l)$ for $l \neq 2$, we get:

$$
\begin{aligned}
\langle \tilde{h}_{p_1}, \tilde{h}_{p_2}| H_E^{(2)} |\tilde{g}_{p_1}, \tilde{g}_{p_2}\rangle =&\frac{\lambda_E}{|G|^6} \sum_{j\in\hat{G}} \sum_{g_1,\dots,g_7\in G} \sum_{h_2\in G} \delta(h_{p_1}, g_1 h_2 g_3^{-1} g_4^{-1}) \cdot \\
&\cdot \delta(h_{p_2}, g_5 g_6 g_7^{-1} h_2^{-1}) \delta(g_{p_1}, g_1 g_2 g_3^{-1} g_4^{-1}) \delta(g_{p_2}, g_5 g_6 g_7^{-1} g_2^{-1}) \cdot \\
&\cdot d_j f(j) \chi_j(h_2 g_2^{-1}) \qquad \text{(B.1.9)} \\
=&\frac{\lambda_E}{|G|^6} \sum_{j\in\hat{G}} \sum_{g_1,g_3,\dots,g_7\in G} \delta(h_{p_2}, g_5 g_6 g_7^{-1} g_3^{-1} g_4^{-1} h_{p_1}^{-1} g_1) \cdot \\
&\cdot \delta(g_{p_2}, g_5 g_6 g_7^{-1} g_3^{-1} g_4^{-1} g_{p_1}^{-1} g_1) d_j f(j) \chi_j(h_{p_1} g_{p_1}^{-1}) \qquad \text{(B.1.10)} \\
=&\frac{\lambda_E}{|G|^6} \sum_{j\in\hat{G}} \sum_{g_1} d_j f(j) \chi_j(h_{p_1} g_{p_1}^{-1}) \delta(h_{p_2}^{-1} g_{p_2}, g_1^{-1} h_{p_1} g_{p_1}^{-1} g_1) \cdot \\
&\cdot \sum_{g_3,\dots,g_7\in G} \delta(h_{p_2}, g_5 g_6 g_7^{-1} g_3^{-1} g_4^{-1} h_{p_1}^{-1} g_1) \qquad \text{(B.1.11)} \\
=&\frac{\lambda_E}{|G|^2} \sum_{j\in\hat{G}} \sum_{g_1} d_j f(j) \chi_j(h_{p_1} g_{p_1}^{-1}) \delta(h_{p_2}^{-1} g_{p_2}, g_1^{-1} h_{p_1} g_{p_1}^{-1} g_1), \qquad \text{(B.1.12)}
\end{aligned}
$$

where we used the first delta in (B.1.9) to remove the sum over h_2 by imposing that $h_2 = g_1^{-1} h_{p_1} g_4 g_3$, while using the third delta in (B.1.9) we remove the sum over g_2, leaving as unique support $g_2 = g_1^{-1} g_{p1} g_4 g_3$. From the first delta in (B.1.10) we see that $g_5 g_6 g_7^{-1} g_3^{-1} g_4^{-1} = h_{p2} g_1^{-1} h_{p_1}$, while from the second delta in (B.1.10) we have $g_{p_2} = (g_5 g_6 g_7^{-1} g_3^{-1} g_4^{-1}) g_{p_1}^{-1} g_1$, and combining this result with the previous one we get $h_{p_2}^{-1} g_{p_2} = g_1^{-1} h_{p_1} g_{p_1}^{-1} g_1$, leading to the first delta appearing in (B.1.11). Finally in (B.1.11) we notice that the sum over $g_3, ..., g_7 \in G$ gives as result $|G|^4$ (we are summing over 5 variables but with a constraint from the delta). Now let's use the following relation:

$$\sum_{k \in G} \delta(g, k^{-1} h k) = \begin{cases} \dfrac{|G|}{|C|} & \text{if } g, h \in C \\ 0 & \text{otherwise} \end{cases}. \tag{B.1.13}$$

The relation (B.1.13) can be proved formally, but we will just give an intuitive justification for it. Clearly if $g, h \in G$ do not belong to the same conjugacy class C, the conjugation of h will never be equal to g and then the delta $\delta(g, k^{-1}hk)$ has never support and it is zero for every $k \in G$. If instead g, h belong to the same conjugacy class C, there exist some $k \in G$ that give support to the deltas $\delta(g, k^{-1}hk)$. The fact that the result is exactly $|G|/|C|$ comes from the orbit-stabilizer theorem [49]. Using the orthogonality relation for characters A.3.3, from the relation (B.1.13) we can also notice that

$$\sum_{k \in G} \delta(g, k^{-1} h k) = \sum_{i \in \hat{G}} \chi_i^*(g) \chi_i(h). \tag{B.1.14}$$

If we insert the relation (B.1.14) inside the expression (B.1.12) we get

$$\langle \tilde{h}_{p_1}, \tilde{h}_{p_2} | H_E^{(2)} | \tilde{g}_{p_1}, \tilde{g}_{p_2} \rangle = \frac{\lambda_E}{|G|^2} \sum_{i,j \in \hat{G}} d_j f(j) \chi_j(h_{p_1} g_{p_1}^{-1}) \chi_i^*(h_{p_2}^{-1} g_{p_2}) \chi_i(h_{p_1} g_{p_1}^{-1}). \tag{B.1.15}$$

Insert the expression (B.1.15) inside (B.1.6) and you will find:

$$\begin{aligned} \langle i_1, i_2 | H_E^{(2)} | j_1, j_2 \rangle = & \frac{\lambda_E}{|G|^4} \sum_{i,j \in \hat{G}} d_j f(j) \sum_{g_{p_1}, g_{p_2}, h_{p_1}, h_{p_2} \in G} \chi_{i_1}^*(h_{p_1}) \chi_{i_2}^*(h_{p_2}) \chi_{j_1}(g_{p_1}) \cdot \\ & \cdot \chi_{j_2}(g_{p_2}) \chi_j(h_{p_1} g_{p_1}^{-1}) \chi_i^*(h_{p_2}^{-1} g_{p_2}) \chi_i(h_{p_1} g_{p_1}^{-1}). \end{aligned} \tag{B.1.16}$$

One can now perform the change of variable $g_{p_1} \to k = h_{p_1} g_{p_1}^{-1}$:

$$\begin{aligned} \langle i_1, i_2 | H_E^{(2)} | j_1, j_2 \rangle = & \frac{\lambda_E}{|G|^4} \sum_{i,j \in \hat{G}} d_j f(j) \sum_{k, g_{p_2}, h_{p_1}, h_{p_2} \in G} \chi_{i_1}^*(h_{p_1}) \chi_{i_2}^*(h_{p_2}) \chi_{j_1}(k^{-1} h_{p_1}) \cdot \\ & \cdot \chi_{j_2}(g_{p_2}) \chi_j(k) \chi_i^*(h_{p_2}^{-1} g_{p_2}) \chi_i(k). \end{aligned} \tag{B.1.17}$$

In (B.1.17), in the sums over h_{p_1} and h_{p_2} we can recognize the convolution relation A.3.4, while in the sum over g_{p_2} we can recognize an orthogonality relation for characters A.3.2. In this way the expression (B.1.17) becomes

$$\begin{aligned}
\langle i_1, i_2| H_E^{(2)} |j_1, j_2\rangle =&\delta_{i_1,j_1}\delta_{i_2,j_2}\frac{\lambda_E}{d_{i_1}d_{i_2}|G|}\sum_{j\in\hat{G}}\sum_{k\in G} d_j f(j)\chi_{i_1}^*(k)\chi_j(k)\chi_{i_2}(k) && \text{(B.1.18)}\\
=&\delta_{i_1,j_1}\delta_{i_2,j_2}\frac{\lambda_E}{d_{i_1}d_{i_2}|G|}\Bigg[|\Gamma|\sum_{j\in\hat{G}}\sum_{k\in G} d_j\chi_{i_1}^*(k)\chi_j(k)\chi_{i_2}(k)- \\
&-\sum_{j\in\hat{G}}\sum_{k\in G}\sum_{g\in\Gamma}\chi_j(g)\chi_{i_1}^*(k)\chi_j(k)\chi_{i_2}(k)\Bigg] && \text{(B.1.19)}\\
=&\delta_{i_1,j_1}\delta_{i_2,j_2}\frac{\lambda_E}{d_{i_1}d_{i_2}|G|}\Bigg[|\Gamma|\sum_{k\in G}\left(\sum_{j\in\hat{G}}\chi_j^*(e)\chi_j(k)\right)\chi_{i_1}^*(k)\chi_{i_2}(k)- \\
&-\sum_{k\in G}\sum_{g\in\Gamma}\left(\sum_{j\in\hat{G}}\chi_j(g)\chi_j^*(k^{-1})\right)\chi_{i_1}^*(k)\chi_{i_2}(k)\Bigg] && \text{(B.1.20)}\\
=&\delta_{i_1,j_1}\delta_{i_2,j_2}\frac{\lambda_E}{d_{i_1}d_{i_2}}\left[|\Gamma|d_{i_1}d_{i_2}-\sum_{g\in\Gamma}\chi_{i_1}^*(g)\chi_{i_2}(g)\right] && \text{(B.1.21)}\\
=&\lambda_E\bar{f}(i_1,i_2)\delta_{i_1,j_1}\delta_{i_2,j_2}, && \text{(B.1.22)}
\end{aligned}$$

where in the expression (B.1.19) we inserted the definition (1.4.41) of $f(j)$, in the equation (B.1.20) we use $\chi_j^*(e) = d_j$, in the expression (B.1.21) using A.3.3 we performed the sum over j in the first parentheses getting $\delta(e,k)|G|$, and the sum over j in the second parentheses getting $|G|/|C|$ if g and k^{-1} are in the same conjugacy class C, otherwise 0, then we also perform the sum over k that is non zero only if $k^{-1}\in C$, thus in $|C|$ cases. Finally in (B.1.22) we defined the function $\bar{f}(i,j)$ as

$$\bar{f}(i,j) = |\Gamma| - \frac{1}{d_i d_j}\sum_{g\in\Gamma}\chi_i^*(g)\chi_j(g). \qquad \text{(B.1.23)}$$

In order to find out the matrix element of the total Hamiltonian $H_E = \sum_{l=1}^{7} H_E^{(l)}$, we have to sum over the contributions coming from all 7 links, 6 of them ($l\neq 2$) have matrix elements (B.1.4) (3 in the first plaquette p_1, 3 in the second one p_2) while one of them, $l=2$, has matrix element (B.1.22). Putting all together one finds

$$\langle i_1, i_2| H_E |j_1, j_2\rangle = \lambda_E\left[3f(i_1)+3f(i_2)+\bar{f}(i_1,i_2)\right]\delta_{i_1,j_1}\delta_{i_2,j_2}. \qquad \text{(B.1.24)}$$

Now we should also compute the matrix elements of the basis state $|i,\bar{j}\rangle$ (3.4.10) of the kind $\langle i_1,\bar{i}_2| H_E^{(l)} |j_1,\bar{j}_2\rangle$. In this case the character state $|i,\bar{j}\rangle$ is defined on the single-plaquette loop p_1 and the multiple-plaquette loop p_3; in particular we have that the link $l=2$ only belongs to the path p_1 and so it has a well defined representation i, the links $l = 5, 6, 7$ belong only to the path p_3 and so they have a well defined representation j, instead all other links $l = 1, 3, 4$ belong to both the paths. In this case we will have for the link $l = 2$

$$\langle i_1, \bar{i_2}| \, H_E^{(2)} \, |j_1, \bar{j_2}\rangle = \lambda_E f(i_1) \delta_{i_1,j_1} \delta_{i_2,j_2}, \tag{B.1.25}$$

for the links $l = 5, 6, 7$:

$$\langle i_1, \bar{i_2}| \, H_E^{(l=5,6,7)} \, |j_1, \bar{j_2}\rangle = \lambda_E f(i_2) \delta_{i_1,j_1} \delta_{i_2,j_2}, \tag{B.1.26}$$

while for the other links $l = 1, 3, 4$ we use the expression (B.1.22) computed before for a shared link:

$$\langle i_1, \bar{i_2}| \, H_E^{(l=1,3,4)} \, |j_1, \bar{j_2}\rangle = \lambda_E \bar{f}(i_1, i_2) \delta_{i_1,j_1} \delta_{i_2,j_2}. \tag{B.1.27}$$

Putting the results (B.1.25), (B.1.26) and (B.1.27) together we finally find

$$\langle i_1, \bar{i_2}| \, H_E \, |j_1, \bar{j_2}\rangle = \left[f(i_1) + 3f(i_2) + 3\bar{f}(i_1, i_2) \right] \delta_{i_1,j_1} \delta_{i_2,j_2}. \tag{B.1.28}$$

The mixed matrix elements $\langle i_1, \bar{i_2}| \, H_E \, |j_1, j_2\rangle$, or their Hermitian conjugate, are trivially zero. This concludes the computation of the matrix elements of the electric Hamiltonian H_E (B.1.1) for a two-plaquette system.

B.2 Matrix elements of the magnetic Hamiltonian

For the two-plaquette system the magnetic Hamiltonian H_B (1.4.11) reads out as

$$H_B = -2\lambda_B \left(\mathrm{Re}\, \mathrm{Tr}\, \hat{W}_{p_1} + \mathrm{Re}\, \mathrm{Tr}\, \hat{W}_{p_2} \right), \tag{B.2.1}$$

where $\hat{W}_p$ is the Wilson loop operator (1.4.10) for the plaquette p, written in terms of the position operators $\hat{g}_l$ of the link l. Explicitly they are for the first plaquette: $\mathrm{Tr}\, \hat{W}_{p_1} = \mathrm{Tr} \left(\hat{g}_1 \hat{g}_2 \hat{g}_3^\dagger \hat{g}_4^\dagger \right)$ and for the second plaquette: $\mathrm{Tr}\, \hat{W}_{p_2} = \left(\hat{g}_5 \hat{g}_6 \hat{g}_7^\dagger \hat{g}_2^\dagger \right)$. Let us first notice that the multiple-plaquette state $|\tilde{g}_{p_1}, \tilde{g}_{p_2}\rangle$ is an eigenstate of the Wilson loop operator, in particular we can see that

$$\langle \tilde{g}_{p_1}, \tilde{g}_{p_2}| H_B |\tilde{h}_{p_1}, \tilde{h}_{p_2}\rangle = -2\lambda_B \left[\mathrm{Re}\, \chi_F(g_{p_1}) + \mathrm{Re}\, \chi_F(g_{p_2}) \right] \delta(g_{p_1}, h_{p_1}) \delta(g_{p_2}, h_{p_2}), \tag{B.2.2}$$

where F is the faithful representation chosen for the magnetic piece. Now we will compute the matrix elements of H_B (B.2.1) using a basis of multiple-plaquette character states, like $|i, j\rangle$ and $|i, \bar{j}\rangle$. Consider the expression (3.4.9) of the multiple-plaquette character state $|i, j\rangle$ in terms of the multi-plaquette state $|\tilde{g}_{p_1}, \tilde{g}_{p_2}\rangle$, then we can compute

$$\begin{aligned} \langle i_1, i_2 | H_B | j_1, j_2 \rangle = &- \frac{2\lambda_B}{|G|^2} \sum_{g_{p_1}, g_{p_2} \in G} \chi_{i_1}^*(g_{p_1}) \chi_{i_2}^*(g_{p_2}) \chi_{j_1}(g_{p_1}) \chi_{j_2}(g_{p_2}) \cdot \\ &\cdot \left[\mathrm{Re}\, \chi_F(g_{p_1}) + \mathrm{Re}\, \chi_F(g_{p_2}) \right]. \end{aligned} \tag{B.2.3}$$

The same can be done for the state $|i, \bar{j}\rangle$, using the expression (3.4.10):

$$\begin{aligned}\langle i_1, \bar{i}_2|H_B|j_1, \bar{j}_2\rangle =& -\frac{2\lambda_B}{|G|^7}\sum_{g_1,\ldots,g_7\in G}\chi^*_{i_1}(g_1g_2g_3^{-1}g_4^{-1})\chi^*_{i_2}(g_1g_5g_6g_7^{-1}g_3^{-1}g_4^{-1})\chi_{j_1}(g_1g_2g_3^{-1}g_4^{-1})\cdot\\ &\cdot\chi_{j_2}(g_1g_5g_6g_7^{-1}g_3^{-1}g_4^{-1})\left[\mathrm{Re}\,\chi_F(g_1g_2g_3^{-1}g_4^{-1})+\mathrm{Re}\,\chi_F(g_5g_6g_7^{-1}g_2^{-1})\right]\\ =& -\frac{2\lambda_B}{|G|^3}\sum_{g_1,g_{p_1},g_{p_2}\in G}\chi^*_{i_1}(g_{p_1})\chi^*_{i_2}(g_1g_{p_2}g_1^{-1}g_{p_1})\chi_{j_1}(g_{p_1})\chi_{j_2}(g_1g_{p_2}g_1^{-1}g_{p_1})\cdot\\ &\cdot\left[\mathrm{Re}\,\chi_F(g_{p_1})+\mathrm{Re}\,\chi_F(g_{p_2})\right],\end{aligned} \tag{B.2.4}$$

where in the equation (B.2.4) we used the fact that given $g_{p_1} = g_1g_2g_3^{-1}g_4^{-1}$ and $g_{p_2} = g_5g_6g_7^{-1}g_2^{-1}$, we can write the group element of the two-plaquette path p_3 as $g_1g_5g_6g_7^{-1}g_3^{-1}g_4^{-1} = g_1g_{p_2}g_1^{-1}g_{p_2}$, we performed a change of variables and then we summed over the 4 variables that do not appear inside the character functions, getting a $|G|^4$ factor. Using the same trick we can compute the following mixed matrix elements:

$$\begin{aligned}\langle i_1, \bar{i}_2|H_B|j_1, j_2\rangle =& -\frac{2\lambda_B}{|G|^7}\sum_{g_1,\ldots,g_7\in G}\chi^*_{i_1}(g_1g_2g_3^{-1}g_4^{-1})\chi^*_{i_2}(g_1g_5g_6g_7^{-1}g_3^{-1}g_4^{-1})\chi_{j_1}(g_1g_2g_3^{-1}g_4^{-1})\cdot\\ &\cdot\chi_{j_2}(g_5g_6g_7^{-1}g_2^{-1})\left[\mathrm{Re}\,\chi_F(g_1g_2g_3^{-1}g_4^{-1})+\mathrm{Re}\,\chi_F(g_5g_6g_7^{-1}g_2^{-1})\right]\\ =& -\frac{2\lambda_B}{|G|^3}\sum_{g_1,g_{p_1},g_{p_2}\in G}\chi^*_{i_1}(g_{p_1})\chi^*_{i_2}(g_1g_{p_2}g_1^{-1}g_{p_1})\chi_{j_1}(g_{p_1})\chi_{j_2}(g_{p_2})\cdot\\ &\cdot\left[\mathrm{Re}\,\chi_F(g_{p_1})+\mathrm{Re}\,\chi_F(g_{p_2})\right].\end{aligned} \tag{B.2.5}$$

The matrix elements like $\langle i_1, i_2|H_B|j_1, \bar{j}_2\rangle$ are simply the complex conjugate of the expression (B.2.5). This completes the computation of all matrix elements of the magnetic Hamiltonian H_B (B.2.1).

In order to have a more explicit expression of the electric and magnetic Hamiltonian matrix elements we first have to choose a gauge group G, a generating subset Γ and a faithful representation F. This is done in section 3.4.3 for the group D_4 and in section 3.4.3 for the group D_3.

Bibliography

[1] D. S. ABRAMS AND S. LLOYD, *Quantum algorithm providing exponential speed increase for finding eigenvalues and eigenvectors*, Phys. Rev. Lett., 83 (1999), pp. 5162–5165.

[2] M. S. ALAM, S. HADFIELD, H. LAMM, AND A. C. Y. LI, *Primitive quantum gates for dihedral gauge theories*, Phys. Rev. D, 105 (2022), p. 114501.

[3] M. C. BAÑULS, R. BLATT, J. CATANI, A. CELI, J. I. CIRAC, M. DALMONTE, L. FALLANI, K. JANSEN, M. LEWENSTEIN, S. MONTANGERO, C. A. MUSCHIK, B. REZNIK, E. RICO, L. TAGLIACOZZO, K. V. ACOLEYEN, F. VERSTRAETE, U.-J. WIESE, M. WINGATE, J. ZAKRZEWSKI, AND P. ZOLLER, *Simulating lattice gauge theories within quantum technologies*, Eur. Phys. J. D, 74 (2020), p. 165.

[4] C. W. BAUER, Z. DAVOUDI, A. B. BALANTEKIN, T. BHATTACHARYA, M. CARENA, W. A. DE JONG, P. DRAPER, A. EL-KHADRA, N. GEMELKE, M. HANADA, D. KHARZEEV, H. LAMM, Y.-Y. LI, J. LIU, M. LUKIN, Y. MEURICE, C. MONROE, B. NACHMAN, G. PAGANO, J. PRESKILL, E. RINALDI, A. ROGGERO, D. I. SANTIAGO, M. J. SAVAGE, I. SIDDIQI, G. SIOPSIS, D. VAN ZANTEN, N. WIEBE, Y. YAMAUCHI, K. YETER-AYDENIZ, AND S. ZORZETTI, *Quantum simulation for high-energy physics*, PRX Quantum, 4 (2023), p. 027001.

[5] A. BAZAVOV, Y. MEURICE, S.-W. TSAI, J. UNMUTH-YOCKEY, AND J. ZHANG, *Gauge-invariant implementation of the Abelian-Higgs model on optical lattices*, Phys. Rev. D, 92 (2015), p. 076003.

[6] S. BRAVYI, I. KIM, A. KLIESCH, AND R. KOENIG, *Adaptive constant-depth circuits for manipulating non-Abelian anyons*, 2022. arXiv:2205.01933.

[7] J. W. BRITTON, B. C. SAWYER, A. C. KEITH, C.-C. J. WANG, J. K. FREERICKS, H. UYS, M. J. BIERCUK, AND J. J. BOLLINGER, *Engineered two-dimensional Ising interactions in a trapped-ion quantum simulator with hundreds of spins*, Nature, 484 (2012), pp. 489–492.

[8] T. BYRNES AND Y. YAMAMOTO, *Simulating lattice gauge theories on a quantum computer*, Phys. Rev. A, 73 (2006), p. 022328.

[9] A. CERVERA-LIERTA, *Exact Ising model simulation on a quantum computer*, Quantum, 2 (2018), p. 114.

[10] S. CHANDRASEKHARAN AND U. WIESE, *Quantum link models: a discrete approach to gauge theories*, Nucl. Phys. B., 492 (1997), pp. 455–471.

[11] S. S. CHERN AND J. SIMONS, *Characteristic forms and geometric invariants*, Ann. Math., 99 (1974), pp. 48–69.

[12] A. M. CHILDS, Y. SU, M. C. TRAN, N. WIEBE, AND S. ZHU, *Theory of Trotter error with commutator scaling*, Phys. Rev. X, 11 (2021), p. 011020.

[13] F. R. K. CHUNG, *Spectral Graph Theory*, American Mathematical Society, 1997.

[14] R. CIOLI, *Digital quantum simulations of the Z_n toric code*, Master's thesis, University of Bologna, 2022.

[15] M. CREUTZ, L. JACOBS, AND C. REBBI, *Monte Carlo computations in lattice gauge theories*, Phys. Rept., 95 (1983), pp. 201–282.

[16] S. X. CUI, D. DING, X. HAN, G. PENINGTON, D. RANARD, B. C. RAYHAUN, AND Z. SHANGNAN, *Kitaev's quantum double model as an error correcting code*, Quantum, 4 (2020), p. 331.

[17] X. CUI, Y. SHI, AND J.-C. YANG, *Circuit-based digital adiabatic quantum simulation and pseudoquantum simulation as new approaches to lattice gauge theory*, J. High Energ. Phys., 2020 (2020), p. 160.

[18] O. EZRATTY, *Perspective on superconducting qubit quantum computing*, Eur. Phys. J. A, 59 (2023), p. 94.

[19] E. FARHI, J. GOLDSTONE, S. GUTMANN, J. LAPAN, A. LUNDGREN, AND D. PREDA, *A quantum adiabatic evolution algorithm applied to random instances of an NP-complete problem*, Science, 292 (2001), pp. 472–475.

[20] R. P. FEYNMAN, *Simulating physics with computers*, International journal of theoretical physics, 21 (1982), pp. 467–488.

[21] E. FRADKIN, *General Field Theory*, Department of Physics, University of Illinois at Urbana-Champaign, 2023. Available: `https://www.damtp.cam.ac.uk/user/tong/gaugetheory.html`.

[22] D. C. HACKETT, K. HOWE, C. HUGHES, W. JAY, E. T. NEIL, AND J. N. SIMONE, *Digitizing gauge fields: Lattice monte carlo results for future quantum computers*, Phys. Rev. A, 99 (2019), p. 062341.

[23] M. IMADA, *Quantum simulation of superconductivity*, in Strongly Coupled Plasma Physics, S. Ichimaru, ed., North-Holland Delta Series, Elsevier, Amsterdam, 1990, pp. 81–91.

[24] R. IRMEJS, M. C. BANULS, AND J. I. CIRAC, *Quantum simulation of Z_2 lattice gauge theory with minimal resources*, 2023. arXiv:2206.08909.

[25] A. KIRILLOV, *An Introduction to Lie Groups and Lie Algebras*, Cambridge Studies in Advanced Mathematics, Cambridge University Press, 2008.

[26] A. KITAEV, *Fault-tolerant quantum computation by anyons*, Ann. Phys., 303 (2003), pp. 2–30.

[27] A. KNAPP, *Lie Groups Beyond an Introduction, Second edition*, vol. 140, Birkhäuser Boston, MA, 01 2002.

[28] J. KOGUT AND L. SUSSKIND, *Hamiltonian formulation of Wilson's lattice gauge theories*, Phys. Rev. D, 11 (1975), pp. 395–408.

[29] C. KOKAIL, C. MAIER, R. VAN BIJNEN, T. BRYDGES, M. K. JOSHI, P. JURCEVIC, C. A. MUSCHIK, P. SILVI, R. BLATT, C. F. ROOS, AND P. ZOLLER, *Self-verifying variational quantum simulation of lattice models*, Nature, 569 (2019), pp. 355–360.

[30] H. LAMM, S. LAWRENCE, AND Y. YAMAUCHI, *General methods for digital quantum simulation of gauge theories*, Phys. Rev. D, 100 (2019), p. 034518.

[31] N. LIGTERINK, N. WALET, AND R. BISHOP, *Toward a many-body treatment of Hamiltonian lattice SU(N) gauge theory*, Ann. Phys., 284 (2000), pp. 215–262.

[32] L. LUMIA, *Digital quantum simulations of Yang-Mills lattice gauge theories*, Master's thesis, University of Bologna, 2020.

[33] Y. MAKEENKO, *Methods of Contemporary Gauge Theory*, Cambridge Monographs on Mathematical Physics, Cambridge University Press, 2002.

[34] L. MARCHESE, *Quantum simulation of Abelian and non-Abelian gauge theories*, Master's thesis, University of Bologna, 2020.

[35] A. MARIANI, *Finite-group Yang-Mills lattice gauge theories in the Hamiltonian formalism*, Master's thesis, University of Bologna, 2020.

[36] A. MARIANI, S. PRADHAN, AND E. ERCOLESSI, *Hamiltonians and gauge-invariant Hilbert space for lattice Yang-Mills-like theories with finite gauge group*, Phys. Rev. D, 107 (2023), p. 114513.

[37] E. A. MARTINEZ, C. A. MUSCHIK, P. SCHINDLER, D. NIGG, A. ERHARD, M. HEYL, P. HAUKE, M. DALMONTE, T. MONZ, P. ZOLLER, AND R. BLATT, *Real-time dynam-*

ics of lattice gauge theories with a few-qubit quantum computer, Nature, 534 (2016), pp. 516–519.

[38] M. Nakahara, *Geometry, topology and physics*, CRC Press, 2003. Bristol, UK: Hilger (1990) 505 p. (Graduate student series in physics).

[39] S. Notarnicola, E. Ercolessi, P. Facchi, G. Marmo, S. Pascazio, and F. V. Pepe, *Discrete Abelian gauge theories for quantum simulations of QED*, J. Phys. A, 48 (2015), p. 30FT01.

[40] G. Ortiz, J. E. Gubernatis, E. Knill, and R. Laflamme, *Quantum algorithms for fermionic simulations*, Phys. Rev. A, 64 (2001), p. 022319.

[41] G. Pan and Z. Y. Meng, *Sign problem in quantum Monte Carlo simulation*, 2022. arXiv:2204.08777.

[42] G. Parisi, *Gauge theories, spin glasses and real glasses*, 1994. arXiv:cond-mat/9411115.

[43] M. E. Peskin and D. V. Schroeder, *An Introduction to Quantum Field Theory*, Westview Press, 1995.

[44] D. Poulin, A. Qarry, R. Somma, and F. Verstraete, *Quantum simulation of time-dependent Hamiltonians and the convenient illusion of Hilbert space*, Phys. Rev. Lett., 106 (2011), p. 170501.

[45] Qiskit contributors, *Qiskit: An open-source framework for quantum computing*, 2023. `https://qiskit.org`.

[46] G. Roumpos, C. P. Master, and Y. Yamamoto, *Quantum simulation of spin ordering with nuclear spins in a solid-state lattice*, Phys. Rev. B, 75 (2007), p. 094415.

[47] G. Schaller, S. Mostame, and R. Schützhold, *General error estimate for adiabatic quantum computing*, Phys. Rev. A, 73 (2006), p. 062307.

[48] F. Schäfer, T. Fukuhara, S. Sugawa, Y. Takasu, and Y. Takahashi, *Tools for quantum simulation with ultracold atoms in optical lattices*, Nat. Rev. Phys., 2 (2020), pp. 411–425.

[49] J.-P. Serre, *Linear representations of finite groups*, vol. 42 of Graduate texts in mathematics, Springer, 1977.

[50] J. Steinhauer, *Observation of quantum Hawking radiation and its entanglement in an analogue black hole*, Nat. Phys., 12 (2016), pp. 959–965.

[51] S. Sternberg, *Lie Algebras*, Orange Grove Books, 2004. Available: `https://people.math.harvard.edu/~shlomo/docs/lie_algebras.pdf`.

[52] F. TACCHINO, A. CHIESA, S. CARRETTA, AND D. GERACE, *Quantum computers as universal quantum simulators: State-of-the-art and perspectives*, Adv. Quantum Technol., 3 (2019), p. 1900052.

[53] D. TONG, *Gauge theory*, 2018. Available: `https://www.damtp.cam.ac.uk/user/tong/gaugetheory.html`.

[54] M. TROYER AND U.-J. WIESE, *Computational complexity and fundamental limitations to fermionic quantum monte carlo simulations*, Phys. Rev. Lett., 94 (2005), p. 170201.

[55] K. G. WILSON, *Confinement of quarks*, Phys. Rev. D, 10 (1974), pp. 2445–2459.

[56] X. WU, X. LIANG, Y. TIAN, F. YANG, C. CHEN, Y.-C. LIU, M. K. TEY, AND L. YOU, *A concise review of Rydberg atom based quantum computation and quantum simulation*, Chinese Physics B, 30 (2021), p. 020305.

[57] A. ZIMMERMAN, *Representation theory of finite groups and Burnside's theorem*, 2015. Available: `http://math.uchicago.edu/~may/REU2015/REUPapers/Zimmerman.pdf`.

[58] E. ZOHAR AND M. BURRELLO, *Formulation of lattice gauge theories for quantum simulations*, Phys. Rev. D, 91 (2015), p. 054506.